GEO-3900

MASTER'S THESIS IN GEOLOGY

The Tromsø Nappe Contact with the Nakkedal Nappe Complex NE of Tromsdalstind: Shear kinematics and relationship with metamorphism.

Kjetil Indrevær

Mai, 2011

FACULTY OF SCIENCE AND TECHNOLOGY
Department of Geology

University of Tromsø

GEO-3900

MASTER'S THESIS IN GEOLOGY

The Tromsø Nappe Contact with the Nakkedal Nappe Complex NE of Tromsdalstind: Shear kinematics and relationship with metamorphism.

Kjetil Indrevær

Mai, 2011

ACKNOWLEDGEMENTS

I would like to thank my advisors Holger Stünitz and Erling J. Krogh Ravna for great guidance through this work. I feel honoured to have been a part of your research.

I also wish to sincerely thank Luca Menegon and Pritam Nasipuri for all their patience and good advice. Your great skills and passion for geology has been a real inspiration for me. My thesis wouldn't have been the same without you!

Tusen takk til Odd-Arne Mikkelsen for trivelig feltarbeid og alle de produktive diskusjonene vi har hatt om temaet. Takk til Jan Petter Holm for all hjelp med GIS-relaterte problemer og til Kåre Kullerud og Steffen Bergh for å være tilgjengelige når veilederene mine var ute og jaktet på reinsdyr. Takk til Edel Ellingsen for prepareringen av tynnslipene og til Øystein Indrevær for gjennomlesning av oppgaven.

Mange takk til Gard, Kristina og Maria for koselige stunder på kontoret og til Heidi, Morten og Henrik for gale stunder i passivhuset. En spesiell takk til Henrik for bildet til forsiden. Takk til mine medstudenter Phillip, Isac, Elisabeth, Lene, Kristine, Kenneth, David, Julia, Sandra, Petter, Brigit, Håkon, Torgeir, Arne, Audun, Emil og David G. for å ha spritet opp hverdagen.

Og Heidi, tusen takk for at du har hold ut med meg gjennom dette året. Jeg gleder meg til resten av livet vårt!

Tromsø, Mai 2011

Kjetil Indrevær

ABSTRACT

The tectonic contact between the Nakkedal Nappe Complex and the Tromsø Nappe crops out NE of Tromsdalstind, 5 km E of Tromsø, Norway. Petrological- and structural analysis of the contact have been undertaken in order to contribute to a better understanding of the tectonometamorphic history of the Uppermost Allochton in the Scandianavian Caledonides. Methods such as P-T pseudosection analysis, Computer-Integrated Polarization microscopy (CIP) and quartz grain size and -shape analysis have been combined with classic polarizing microscopy to obtain shear sense, P-T-conditions, flow stress and strain rate of deformation. A minimum P-T condition of a Scandian prograde metamorphism is obtained from a metapelite in the Tromsø Nappe at 0.9 GPa and 680°C. A widespread distribution of quartz deformation microstructures indicate that deformation was continuous and took place over a large span of temperatures during final retrograde conditions from more than 700°C to less than 400°C. Flow stress and strain rate during deformation are estimated to ~30 MPa and 10^{-11} s^{-1}. Chessboard patterns in quartz are observed locally and c-axis orientation images and pole figures of a quartz vein within the Tromsø Nappe show prism [c]- and basal <a>-slip indicative c-axis preferred orientions (CPOs) in completely recrystallized grains. Prism [c]- and basal <a>-slip pole figures from the same microstructure have previously only been reported in large submagmatic quartz grains. The implications of the new findings for the current theories on the development of prism [c]-slip are discussed. A new unit within the Skattøra Migmatite Complex (SMC) is identified and evidence of retro-eclogites and partial melting in the Tromsø Nappe is presented. A switch in the direction of nappe translation during a late- to post-Scandian retrograde metamorphism from either SW or NE to SSE is identified in the Tromsø Nappe.

The results are set into context with previous work in the area and it is concluded that the Tromsø Nappe was subjected to at least two major prograde metamorphic events followed by uplift, partial melting and retrogradation interpreted to reflect the Taconian- and the Scandian phase, respectively. The SMC suffered extensive partial melting in connection with the Taconian phase, was relatively unaffected by Scandian deformation and did not come into contact with the Tromsø Nappe until late in the Scandian phase.

Keywords: Scandianavian Orogeny, Uppermost Allochthon, shear kinematics, partial melting, CIP, prism [c]-slip.

TABLE OF CONTENT

1. INTRODUCTION

1.1 AIM

The aim of this thesis has been to contribute to a better understanding of the tectonometamorphic history of the Uppermost Allochton of the Scandianavian Caledonides. This should be done through the investigation of a tectonic contact between the Nakkedal Nappe Complex and the Tromsø Nappe.

The aim is reached through:

1. A geological mapping of the contact and its associated lithologies and their structures.
2. A determination of kinematic properties such as shear sense, flow stress, P-T conditions and strain rate of deformation.

The results from this work are to be set into context with previous work in the area.

1.2 GEOGRAPHICAL LOCATION OF STUDY AREA

The area of investigation is located NE of Tromsdalstind, about 5 km E of Tromsø (fig. 1.2-1). The area is reached by fot from Tromsdalen and lies in the range of altitude from about 500-700m above sea level. The terrain is easily accessible and the abundance of outcrops is mainly good. Mid-valley, substantial amounts of surface rubble make investigation more difficult.

The area was divided into a northeastern and southwestern part, where detailed studies of the northeastern part are undertaken in this thesis and detailed studies in the southwestern part was done by Mikkelsen (2011).

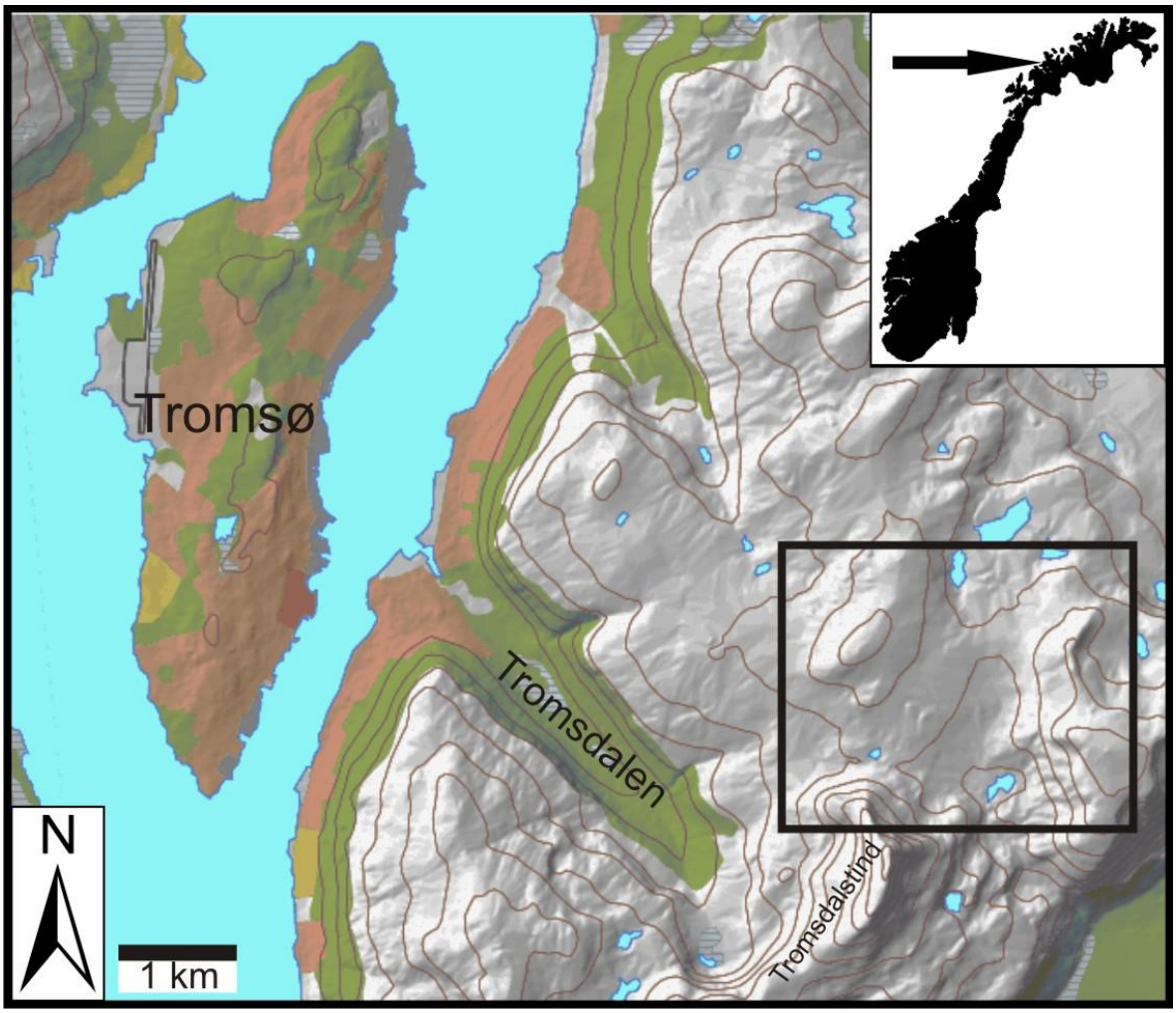

Figure 1.2-1: Topographical map illustrating the location of the studied area (box).

1.3 ABBREVIATIONS

The following abbreviations are used in this thesis:

Minerals:

Aln = allanite
Amph = amphibole
Bt = biotite
Cal = calcite
Cpx = clinopyroxene
Czo = clinozoisite
Di = diopside
Ep = epidote
Grt = garnet
Hbl = hornblende
Ilm = ilmenite
Kfs = K-feldspar
Pl = plagioclase
Qtz = quartz
Rt = rutile
Sph = sphene
Ttn = titanite
Zo = zoisite

Other

BLG = grain boundary bulging
CIP = computer-integrated polarization microscopy
COI = c-axis orientation image
CPO = c-axis preferred orientation
GBM = grain boundary migration
LMC = Lyngen Magmatic Complex
LREE = light rare earth element
MORB = mid-ocean-ridge basalt
P = pressure
REE = rare earth element
SGR = subgrain rotation
SMC = Skattøra Migmatite Complex
T = temperature
UHP = ultra high pressure

1.4 REGIONAL GEOLOGY

The units of the studied area have undergone metamorphism during the Scandianavian Caledonian Orogeny (e.g. Zwaan et al., 1998). In this chapter, an introduction to this orogeny will be presented.

1.4.1 THE SCANDINAVIAN CALEDONIAN OROGENY

In the Palaeozoic, the two continental plates Baltica and Laurentia where positioned south of the equator, separated by a large ocean called the Iapetus Ocean (Torsvik et al., 1996). The Iapetus Ocean closed through a gradual convergence of Laurentia and Baltica (Roberts, 2003). This eventually led to a collision involving subduction of the margin of Baltica beneath Laurentia in Silurian to Early Devonian time. Several subduction zones had earlier been active and caused a complex accretion of exotic terrains, sediments and island arcs,

together with slivers of Laurentian, Baltican and oceanic crust making up the Caledonian Orogen (Roberts & Gee, 1985). A general southeast- and eastwards translation of these units has resulted in a distinctive tectonostratigraphy comprising of the Lower-, Middle-, Upper- and Uppermost Allochthons with translation of nappes up to several hundreds of kilometers (Roberts and Gee, 1985), (fig. 1.4-1).

Underlying these major allochthons are parauthochthonous units and an autochthonous sediment cover deposited unconformly on top of Pre-Cambrian crystalline basement. This sediment cover can be traced along the entire front of the exposed orogen (Roberts and Gee, 1985).

The Lower- and Middle Allochthons are composed of rocks derived from the shelf and continental rise from the Baltoscandian margin, whereas the Upper Allochthon consists of ophiolites, magmatic arcs and marginal basins previously located outboard in the now closed Iapetus ocean (Roberts, 2003 and references therein). The Uppermost Allochthon's lithological assemblages and magmatic units are quite different from those in underlying allochthons. Supracrustal rocks originate mainly from platform, shelf-edge and basin-slope environments with extensive developments of carbonate rock units that range in age from late Riphean to early Silurian. Metasedimentary iron ore formations, Ordovician granitoid plutons and batholiths are also present. The Uppermost Allochthon shows an Ordovician tectonothermal record and early Caledonian, NW-vergent folds and thrusts that are unique in Norway and is therefore believed to be of a Laurentian origin (Roberts et al., 2007).

The Scandinavian Orogeny is divided into three major tectonothermal events; the Trondheimian (early Ordovician), the Taconian (mid to late Ordovician) and the Scandian (mid Silurian to early Devonian) phase (Roberts, 2003; Corfu et al., 2007). An extensional collapse, partly by gravity, followed the orgenesis (Roberts, 2003).

The Trondheimian phase, dating to about 475 Ma, marks a distinct event of deformation and metamorphism, including ophiolite obduction and blueschist facies metamorphism. (Eide and Lardeaux, 2002) The obducted ophiolites were deposited on continental rocks, interpreted to be an inferred microcontinental fragment that had previously been rifted off Baltica (Roberts, 2003).

Evidence for **the Taconian phase**, dating to about 452 Ma, is largely confined to the Uppermost Allochthon, but can also be found in several locations currently placed in the

uppermost parts of Upper Allochthon (e.g. Smøla, Fauske and Karmøy-Bergen district). The Taconian phase is recognized by the previously mentioned, early NW-vergent internal thrusts and folds, a structural setting which is very similar to the Taconian in the Appalachians of eastern North America. The early structures are overprinted by SE-vergent thrusts, cleavages and folds which are related to the Scandian event. On this basis, it is argued that the units from the Uppermost Allochthon are considered to have been a part of the Taconian phase and accretionary wedge on the margin of Laurentia, and later being detached from Laurentia and placed high in the tectonostratigraphy of the Scandinavian Caledonides during the Scandian phase (Roberts, 2003).

The Scandian phase, dating to about 425 Ma, is considered to be the main tectonometamorphic event that shaped the appearance of Caledonian Allochthons in Norway and Sweden as present today (Gee, 1975). This orogenesis was caused by a collision between Baltica and Laurentia, together with the subduction of Baltica beneath Laurentia. Biostratigraphic and geochronological evidence from different areas and nappes clearly show that the timing of the Scandian phase varies greatly, both transversely and laterally. All allochthons, including those involved in the earlier phases were more or less affected by the Scandian phase, including the Uppermost Allochthon that where detached from Laurentia as mentioned above (Roberts, 2003).

A late- to post Scandian extensional deformation, partly due to gravitational collapse of the orogen, involved major low angle detachment faults and caused the creation of early to mid Devonian sediment basins, especially in western and central Norway. This early phase of extension may have been syn-tectonic with convergent deformation at lower levels of the crust and at the surface in the foreland (e.g. Andersen, 1993; Roberts, 2003).

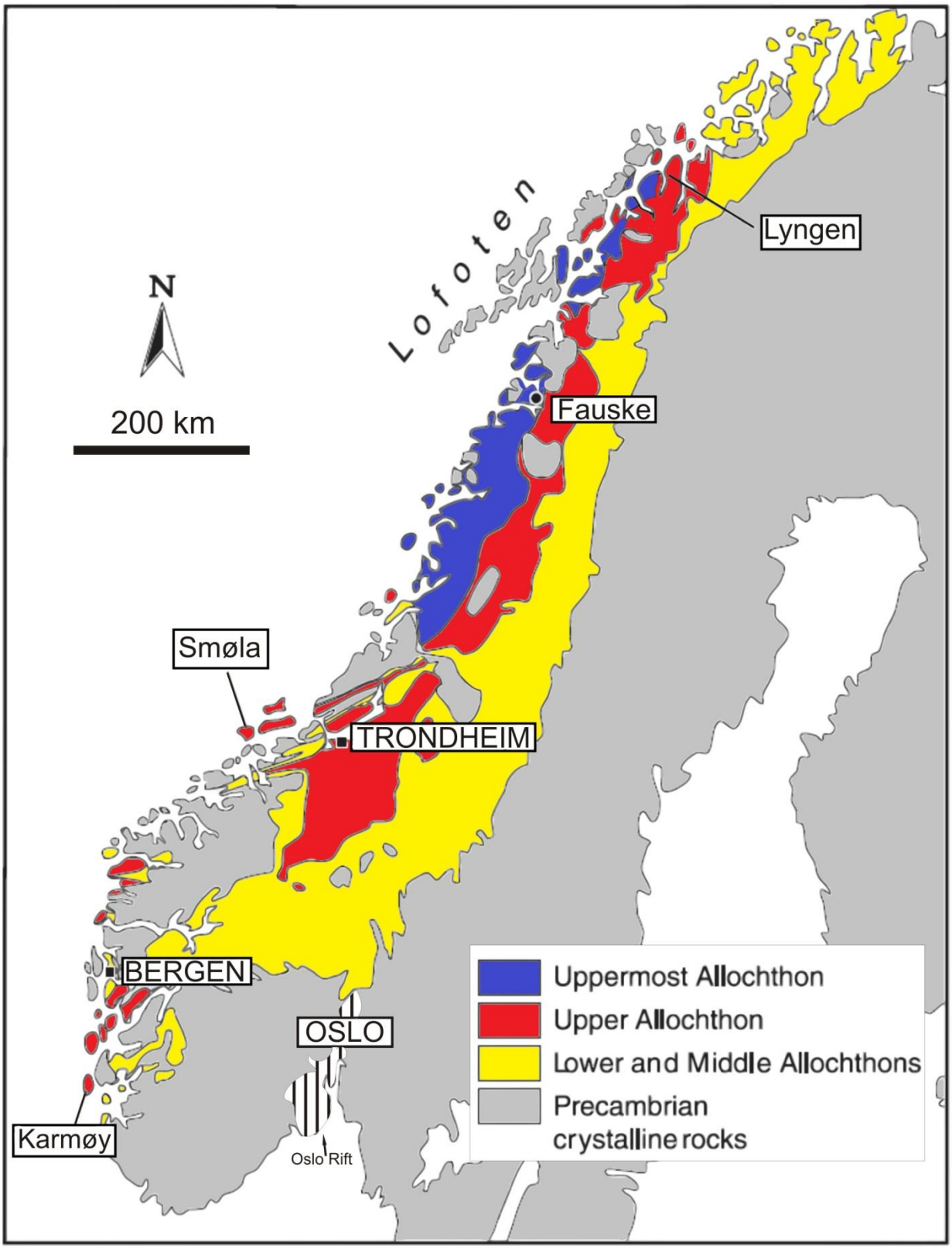

Figure 1.4-1: Simplified tectonostratigraphical subdivisions of the Scandinavian Caledonides, with place names and regions mentioned in the text. Based on Roberts (2003), modified from Roberts & Gee (1985) and Ravna et al. (2007).

1.4.2 Scandinavian Caledonides in Troms

In Troms, the Scandinavian Caledonides can be traced as rather flat-lying NE-SW striking allochthons which are comprised of nappes and thrust sheets. The Lower Allochthon is not present in Troms. The Middle Allochthon rests on a thin layer of parautochthonous and autochthonous late Precambrian to Cambrian sediments, called the Dividal group (Binns, 1978). The sediments crop out along the eastern margin of the Caledonides and can be traced, together with Precambrian basement rocks, in several tectonic windows further to the west. The sediment layer is missing far to the west, where Caledonian nappes are resting directly on top of the basement (Andresen et al., 1985). The outer islands of Troms consist mainly of Pre-Cambrian basement and it is generally accepted that the eastern and western basement rocks are connected, forming the Baltica basement. The Caledonian Allochthons were emplaced on top of the Baltica basement from WNW with a translation of up to 600 km (Binns, 1978; Zwaan et al., 1998). It is argued that there is no evidence for pre-Scandian tectonothermal activity in Troms, except for in the Uppermost Allochton which has recorded Taconian tectonothermal activity as well (Barker, 1989; Roberts 2003). Even so, it is suggested that an early Caledonian metamorphism occurred in the Nordmannvik Nappe of the Upper Allochthon (e.g. Binns, 1978; Berg & Andresen, 1985; Dallmeyer & Andresen, 1992).

The main nappes and nappe complexes in the region are the Vaddas Nappe, Kåfjord Nappe, Normannvik Nappe and Lyngen Nappe Complex (Upper Allochthon), and Nakkedal Nappe Complex and Tromsø Nappe (Uppermost Allochthon), (fig. 1.4-2).

The **Vaddas Nappe** consists of meta-greywacke, marbles and garnet-mica schists with lenses and layers of quartzites and amphibolite (Zwaan et al., 1998). The amphibolite, interpreted as originally basaltic pillow lavas and gabbros, are constrained to the upper part of the nappe, the Oksfjord Group, deposited within metasedimentary rocks (Lindahl et al., 2005). The lower part, Kvænangen Group, is a metasedimentary succession which shows large differences in thickness, composition and metamorphic facies along strike (Lindahl et al., 2005). A granitic gneiss in the lower part of the group has been given an age of 602 ± 5 Ma (Corfu et al., 2007). The nappe as a whole shows most commonly amphibolite facies, locally up to kyanite grade. The Vaddas Nappe has a two part origin. The Kvænangen Group is interpreted to represent a continental shallow-water sequence (Lindahl et al., 2005). The Oksfjord Group lies unconformly om top of the Kvænangen Group and is interpreted to represent the development of a short-lived transtensional- or marginal basin, with lava flows and continental slope sediments intruded by gabbros during the Silurian (Lindahl et al., 2005; Corfu et al., 2007).

Resent data from Corfu et al. (2007) indicates that the Vaddas nappe and the underlying Kalak Nappe originates from an exotic terrain that developed outboard of Baltica and were accreted to Baltica during the Scandian phase. This places the Vaddas Nappe within the Upper Allochthon.

The **Kåfjord Nappe** truncates the subjacent Vaddas Nappe and consists of metamorphosed granite and pegmatites, together with metasedimentary and metamagmatic rocks like garnet-mica schists, marbles, quartzites and hornblendites of presumably Ordovician age (Zwaan et al., 1998). The metamorphic grade is typically amphibolite facies throughout the Kåfjord Nappe (Dallmeyer & Andresen, 1992). The Kåfjord Nappe shows similarities with the Vaddas Nappe both lithologically and metamorphically. It is suggested that more than one exotic terrain may have been involved in the Caledonian origin in the Troms-Ofoten area (Andresen & Steltenpohl, 1994). It is therefore assumed that the Kåfjord Nappe has a similar tectonometamorphic evolution as the Vaddas Nappe, originating from either the same or a different exotic terrain.

The **Nordmannvik Nappe** consists of mylonitic mica schists, amphibolite-bearing gneisses, marbles and local ultramafic lenses (Dallmeyer & Andresen, 1992). The nappe is distinguished from neighboring tectonic units on the basis that it shows a polyphase metamorphic evolution and a high metamorphic grade reaching granulite facies. The Nordmannvik Nappe may represent a metamorphic basement during a Scandian deposition of overlying tectonic units (Bergh and Andresen, 1985). Lindstrøm & Andresen (1992) have dated a metadiorite to 492 ± 5 Ma, inferred to represent an early Caledonian tectonic event. This early event is overprinted by records of the Scandian phase (Dallmeyer & Andresen, 1992).

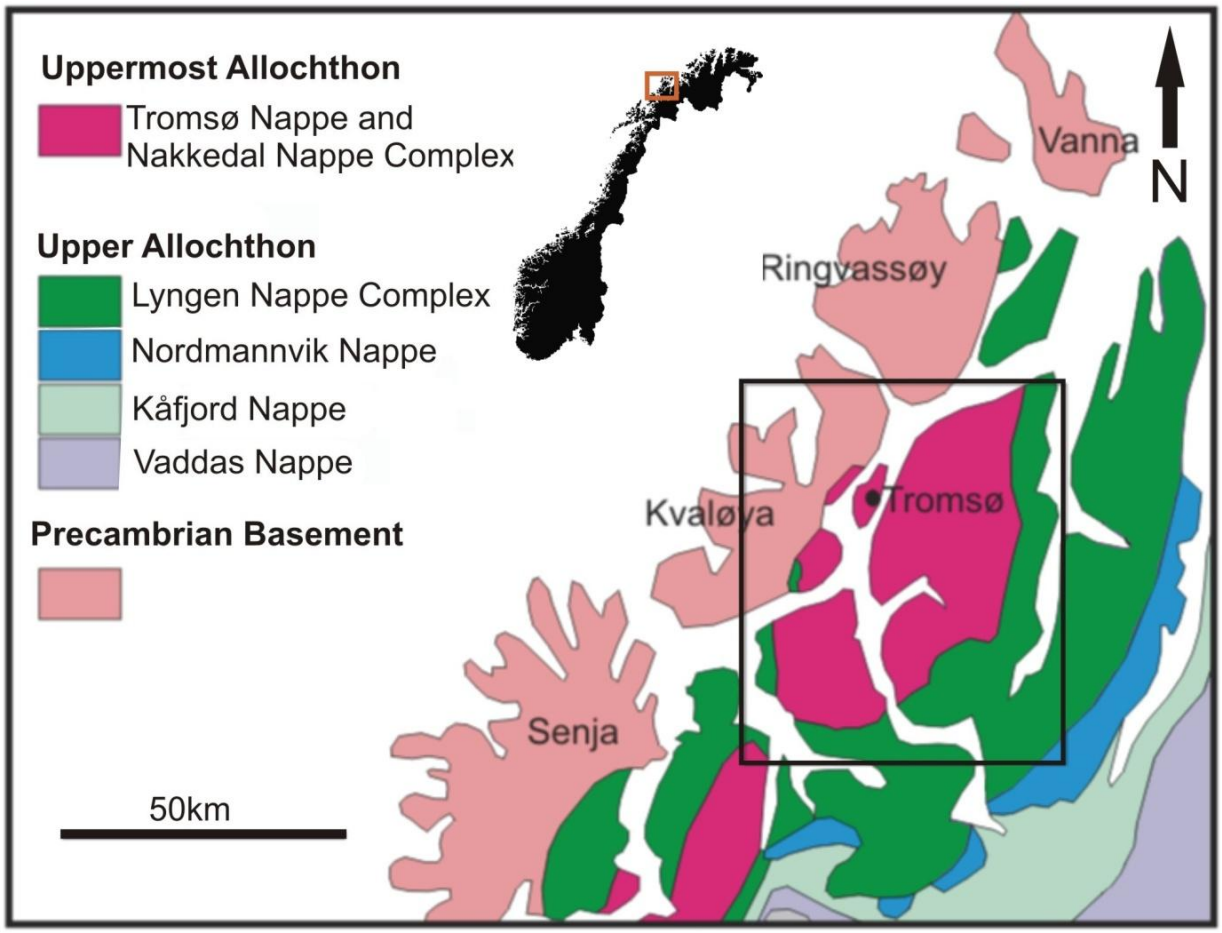

Figure 1.4-2: Simplified tectonostratigraphical map of the Scandinavian Caledonides in Troms. Modified after Ravna et al. (2007). See figure 1.5-1 for details within the outlined area.

The **Lyngen Nappe Complex** is located in the upper part of the Upper Allochthon and is divided into the Lyngen Magmatic Complex (LMC) and the Balsfjord group.

The LMC is again subdivided into an eastern and a western suite by a large N-S trending ductile shear zone, the Rypedal shear zone. The western suite is comprised of layered ultramafics and layered and massive gabbro with both MORB and calc-alkaline affinities. The eastern suite shows metabasaltic greenschists, pillow lavas with island arc thoelitic affinities. Minor volcanoclastic and sedimentary rocks are also present (Selbekk et al., 1998). The Lyngen Gabbro has been dated to a minimum age of 469 ± 5 Ma (Oliver & Krogh, 1995).

The Balsfjord group lies uncomformly on top of the LMC and consists mainly of supracrustal rocks, including calcareous units containing late Ordovician to Silurian fossils (Bjørlykke & Olaussen, 1981). In addition, pillow lavas, calcareous schists, conglomerates and quartzites are also present.

The LMC has been interpreted to be of metavolcanic and MORB origin (Selbekk et al., 1998). The Balsfjord Group is interpreted as a pre-Scandian sedimentary basin, deposited on top of the obducted ophiolites of the LMC which later were subjected to Scandian transportation and metamorphism (Andresen & Steltenpohl, 1994).

The **Nakkedal Nappe Complex** marks the lower border of the Uppermost Allochthon and is divided into the lower quartzo-feldspathic gneisses and the overlying Skattøra Migmatite Complex (SMC). The nappe is tectonically separated from the overlying **Tromsø Nappe** by a major thrust fault (Zwaan et al., 1998; Selbekk et al., 2000). The two nappes make up the Uppermost Allochthon in the region and will be described in detail in chapter 1.6.

1.5 Previous work in the Tromsø Nappe and the SMC

The Tromsø Nappe has been the target of extensive research for over a century**.** The pioneer **Karl Pettersen** mapped parts of western Troms in the period 1865-1890 which resulted in several publications (e.g. Pettersen, 1868, 1870, 1873). Pettersen referred to the Tromsø Nappe as "Tromsø glimmerskiferavdeling" and thoroughly described the occurrence of eclogites within the nappe. He also referred to the SMC as "Syenittgneissen i Tromsøsund" and indicated that the gneiss has a composition between syenite and diorite. Today it is clear that the SMC does not have a syenitic composition (e.g. Selbekk et al., 2000).

Landmark (e.g. 1951, 1973) remapped the area and introduced the idea of dividing the region into allochthons. He named the allochthons Lower-, Middle-, and Upper Allochthon, placing the Tromsø Nappe and the Nakkedal Nappe Complex of today's terminology in the Upper Allochthon. Landmark (1973) described eclogites, amphibolites, mica schist gneisses, the "Tromsøkalken", calc-silicates and the "Skulgam gneiss", known as the SMC today. He claimed that a proper detailed mapping of these units is nearly impossible, due the common appearance of transitional rock types, the varying orientation of fold axes and the lack of outcrops giving a complete stratigraphic overview.

The Skulgam gneiss became renamed "Skattøra gneiss" by **Binns (1978).** Binns (1978) argued that the Skattøra gneiss is a lens of basement rock, partly affected by Caledonian deformation.

Andresen et al. **(1985)** introduced the term "Tromsø Nappe Complex" as the name for what today is known as the Tromsø Nappe and the Nakkedal Nappe Complex. The Tromsø Nappe

Complex was divided into three major lithotectonic units: The lower, quartzo-feldspathic gneisses, the middle, Skattøra Gneiss and the top, supracrustal Tromsdalstind sequence.

Broks (1985) undertook petrological and structural investigations in the area and concluded that both the Tromsdalstind sequence and the Skattøra gneiss have undergone several deformation events. Broks also concluded that both the Skattøra gneiss and a major amphibolite body within the Tromsdalstind sequence were of magmatic origin.

Krogh et al. (1990) performed thermobarometry on eclogites and associated metabasalts and metapelites in the Tromsø area, and determined high pressure metamorphic conditions.

Zwaan et al. **(1998)** refined the geological mapping of the Tromsø area in 1: 250 000. The Tromsø Nappe Complex was divided into two different units and renamed the two lower units from Andresen et al. (1985) as the Nakkedal Nappe Complex and the upper one as the Tromsø Nappe. The name "Skattøra Migmatite Complex" was introduced by **Selbekk et al**. **(2000)** on the basis that it mainly consists of migmatites together with associated anorthositic dykes. Selbekk et al. (2000) refers to leucosomes within the SMC as anorthositic, but the leucosomes will in this text be refered to as oligoclasic on the basis that the Ca-content in the plagioclase defines it as oligoclasic.

The area of investigation in this thesis was mapped in 1:50 000 by **Zwaan (2001).**

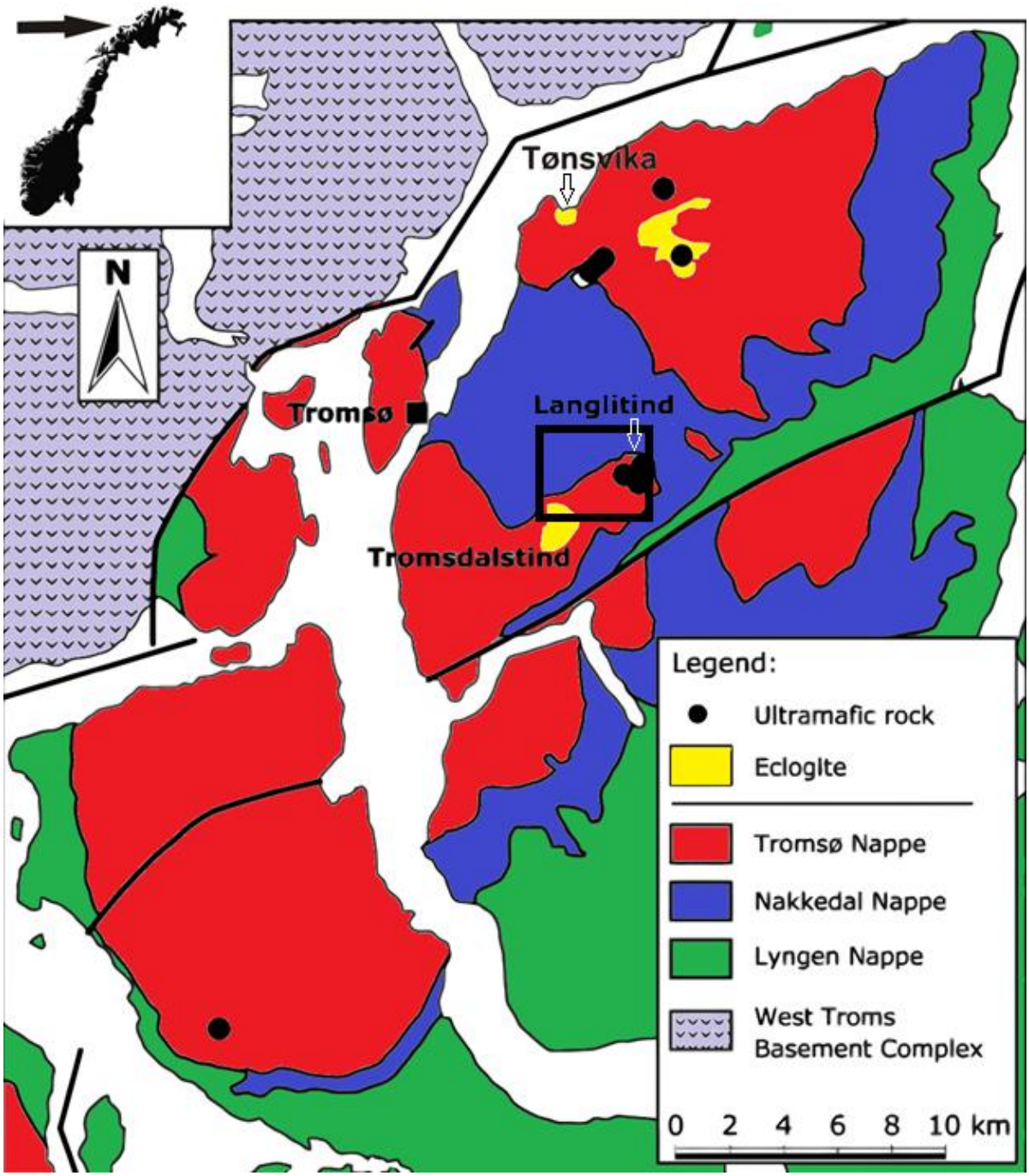

Figure 1.5-1: Tectonostratigraphical map of the Tromsø region showing the location of major bodies of eclogite and ultramafic rocks. Area of map is outlined in fig. 1.4-2. The area of investigation in this thesis is outlined (box). Modified after Ravna et al. (2006).

1.6 General description of lithologies from previous work

The lithology of the units in both Nakkedal Nappe Complex and Tromsø Nappe will in this section be described in detail based on previous work. This is done in order to properly set the results from this thesis into context. A tectonometamorphic evolution based on this work will follow.

1.6.1 Quartzo-feldspathic gneisses of the Nakkedal Nappe Complex

The quartzo-feldspathic gneisses form the lower unit in the Nakkedal Nappe Complex. They are garnet-bearing and folded, locally occuring as augen gneisses or schists. They are locally migmatized. Minor bodies of amphibolite and gabbroic intrusions occur (Zwaan et al., 1998; Krogh et al., 1990; Andresen et al., 1985). Towards its top, they show a gradual transition into the overlying SMC (Andresen et al., 1985).

1.6.2 Skattøra Migmatite Complex (Nakkedal Nappe Complex)

The SMC consists of migmatitic mafic rocks with oligoclase-bearing dioritic leucosomes and foliated amphibolitic melanosomes. The complex has an areal extent of about 200 km^2. Draining structures with thin leucosomes connecting to dykes indicate that the leucosomes are the source of the dykes. Dyke thickness varies from a few centimeters to several meters. The dykes usually cross-cut the foliation, but can also be parallel to foliation. In general, the dykes have sharp, subplanar contacts with the country rock, but the contacts can also be anastomosing, irregular and more diffuse. The dykes consist of 85 – 100% plagioclase and 0-15% irregularly distributed amphibole. The dykes vary from fine grained to pegmatitic. Accessory minerals in dykes are iron oxides or sulphides and titanite. Muscovite, biotite, apatite, epidote and clinozoisite occur as secondary phases (Selbekk et al, 2000). The dykes show little or no evidence of ductile deformation except towards the overlying Tromsø Nappe where they are locally mylonitized. None of the dykes cut the tectonic contact (Krogh et al., 1990; Andresen et al., 1985).

The amphibolite consists of 70-100% amphibole, 0-30 % plagioclase and 0-5% Fe-Ti oxide. They are usually medium to coarse grained and amphibole grains are subhedral to anhedral. The amphibolites are interpreted to be restites, although most amphibolites, especially those parallel to dyke margins are hydration products caused by late dewatering of the anorthositic melt during crystallization (Selbekk and Skjerlie, 2002).

Lenses of metagabbro, meta-anorthosite and metasedimentary rocks occur locally within the SMC. The metagabbro is medium-grained to pegmatitc and consists of 40-65% plagiclase and 35-60% amphibole. The metagabbro shows no preferred crystal orientation, but layering, interpreted to be magmatic, does occur locally, indicating that it originally was a layered igneous intrusion (Rindstad, 1992; Selbekk & Skjerlie, 2002). The meta-anorthosite occurs as fairly bright, fine-grained layers of nearly pure anorthosite (< 10 % amphibole). The layers are locally foliated. The foliation is defined by dark mm-thick layers of banded amphibole locally retrograded to white mica (Rindstad, 1992). The metasedimentary lenses occur as two types. The most common type is a garnet-biotite schist consisting of biotite, garnet, feldspar and accessory zircon. The other type is a skarn-like epidote-garnet-calcite mineral assemblage. The metasedimentary lenses are interpreted to be xenoliths in the original gabbro intrusion.

The SMC is dated by the U/Pb method on titanite to 456 ± 4 Ma and believed to be formed through anatexis of gabbro (Selbekk et al, 2000). Experiments done by Selbekk and Skjerlie (2001) shows that the Skattøra type dykes can be produced at ~1.0 GPa and ~900°C.

1.6.3 Mafic rocks within the Tromsø Nappe

Eclogite

The eclogites of the Tromsø nappe occur as large bodies and smaller lenses enclosed in supracrustal rocks. The eclogite is fine- to coarse grained with a granoblastic microstructure and comprised of the primary phases garnet (30-40%) + omphacite (50-60%) ± quartz, kyanite, zoisite, high-Si phengite, high-Al titanite, rutile and calcite. Secondary minerals are plagioclase, augite, amphibole, garnet, orthopyroxene, biotite, magnetite, low-Al titanite and epidote. The amphibole is gradually recrystallized to granular clinopyroxene (Krogh et al., 1990; Ravna & Roux, 2006). The largest occurrence of eclogite in the Tromsø Nappe is found at Tromsdalstind, where a ~0.4km^3 large body occupies a whole mountain top. The eclogite is interpreted as metamorphosed mafic layered intrusions with a minimum intrusion age of 493 +5/-2 Ma (Corfu et al., 2003). The eclogitization has reached Ultra High Pressure (UHP) metamorphic conditions with pressure and temperature peaking at 3.36 GPa and 735°C (Ravna & Roux, 2006) and been dated by zircon U/Pb to 452.1 ±1.7 Ma (Corfu et al., 2003). Partial melting of eclogites within the Tromsø Nappe is common (Krogh et al., 1990). Stevenson (2005; 2006) has identified two episodes of partial melting; an early episode producing peritectic garnet + melt at 2.0-2.2 GPa and 762-844°C and a later one producing

peritectic hornblende + melt at 1.0-1.3 GPa and 743-950°C. The partial melting is believed to be caused by uplift. The second episode of partial melting is believed to be caused by both uplift and the emplacement onto the neighboring SMC (Stevenson, 2006).

Tromsø Nappe amphibolite

The amphibolite of the Tromsø Nappe consists of hornblende, plagioclase and garnet, with quartz and rutile as accessory minerals. Biotite, clinozoisite and titanite occur as secondary minerals (Ravna & Roux, 2006). The amphibolite occurs as either recrystallized margins of larger eclogite bodies or as smaller fine-grained lenses and bands associated with metapelites. They are locally strongly aligned with the foliation in the metapelites. The amphibolite is presumed to have the same meta-volcanic origin as the eclogite (Zwaan et al., 1998).

1.6.4 Ultramafic rocks within the Tromsø Nappe

Peridotite

Garnet-bearing peridotitic rocks can be found within the Tromsø nappe. Their composition varies from Ca- and Al-rich, olivine-poor garnet peridotite (type 1) to Ca- and Al-poor, dunitic peridotite (type 2). Garnets have only been found in type 1 rocks (Ravna et al, 2006).

On Langlitind, one large (350 x 100 m) and several smaller irregular bodies of type 2 peridotites have been found. Foliation within the country rock wraps around the larger ultramafic body which is mainly composed of medium to coarse grained granoblastic dunite and porphyroblastic harzburgite. Common minerals are olivine and orthopyroxene, with minor constituents of hornblende in the harzburgite. The smaller bodies have cores of dunite/harzburgite, which grade outwards to hydrated varieties composed of orthopyroxene, amphibole, talc, chlorite and minor carbonite. Olivine occurs as anhedral grains up to 6 cm across in dunite and comprises up to 90-92% of the rock. Orthopyroxene appear as dark green to golden brown prismatic crystals in harzburgite with up to 20 % of its composition. Smaller fractions of spinel, chromite, serpentinite and tremolite are also present as a result of retrograde mineral reactions. P-T estimates apparently peak at 2.40 GPa at 740°C, but may have been higher, matching the associated eclogites (Ravna et al, 2006).

The peridotites are interpreted to represent hydrated slices of an overlying sub-continental mantle wedge which became incorporated in the subducting continental crust early in the Caledonian orogeny (Ravna et al, 2006; Brueckner and Medaris, 2000; Medaris 2000).

1.6.5 METASEDIMENTS OF THE TROMSØ NAPPE

Garnet-mica schist

Garnet-mica schists of the Tromsø nappe have been described to consist of biotite, phengite, quartz, plagioclase and garnet. Hornblende, kyanite, rutile, ilmenite, calcite and pyrite occur as minor constituents. The banded mica schist is fine- to medium grained with a grayish color. Rusty spots after pyrite are common (Ravna & Roux, 2006). Biotite-free garnet phengite schists (Krogh et al., 1990), gneiss- and augen structures (Zwaan et al., 1998) occur locally. Inclusions in garnets from a kyanite-bearing metapelite indicate a prograde evolution from about 636°C and 1.25 GPa to about 720°C and 1.4-1.5 GPa (Krogh et al., 1990). A garnet-phengite schist with Si- and Ti-rich phengite indicate a P-T peak at 3.36 GPa and 735°C (Ravna & Roux, 2006).

Calc-silicate rock

Marbles and calc-silicate rocks have been described from the Tromsø Nappe by e. g. Binns (1985) and Krogh et al. (1990). Only recently has a thorough analysis of these units been undertaken. Ravna et al. (2008) identified two types of calc-silicate rocks – a massive carbonitic rock and a calc-silicate marble. The massive carbonitic rock is comprised of Sr-bearing Fe-Mg-calcite, exsolved lamellae and recrystallized grains of Fe-dolomite, garnet, sodic clinopyroxene, Ti- and Ba-rich biotite, F-rich apatite and rutile. Secondary hornblende occurs after clinopyroxene and light Rare Earth Elements (LREE)-rich allanite grows on biotite-garnet and calcite-garnet interfaces. Low-Al titanite after rutile occurs as well. Garnets contain inclusions of apatite, calcite biotite and clinopyroxene. An isotropic fabric and evenly distributed silicate minerals in a matrix of calcite gives it an igneous appearance (Ravna et al., 2008).

The calc-silicate marble contains calcite, Ca-rich garnet, clinopyroxene, zoisite, K-feldspar and Al-rich titanite. Secondary minerals are diopside and plagioclase after Na-rich clinopyroxene (Ravna et al., 2008). The calc-silicates in general seem to be common along the tectonic contact to the SMC (Zwaan et al., 1998). Biotite, locally present in substantial amounts and phengite has also been reported (Ravna & Roux, 2006).

Based on the differences in mineralogy and in REE-patterns it is suggested that the massive carbonate is a meta-carbonatite, while the calc-silicate marble is of metasedimentary origin (Ravna et al., 2008).

1.7 TECTONOMETAMORPHIC EVOLUTION

Through the investigation within the Tromsø Nappe and Nakkedal Nappe Complex, the tectonometamorphic evolution of the Uppermost Allochton in Troms is relatively well constrained (e.g. Krogh et al., 1990; Corfu et al., 2003; Ravna & Roux, 2006; Selbekk et al, 2000; Selbekk & Skjerlie, 2002; Rindstad, 1992).

1.7.1 PRE-OROGENIC ORIGIN

The Tromsø Nappe sequence has been interpreted to have a platform sedimentary origin based on the presence of carbonates and metapelites (Krogh et al., 1990). The occurrence of mafic rocks, interpreted to be metabasalts and gabbros, together with meta-carbonatites indicates an active magmatic setting, possibly rift-related. Where eclogite occurs as small lenses within marbles (e.g. Tønsvika) they are interpreted as originally basaltic flows, whereas larger eclogite bodies (e. g. Tromsdalstind) are interpreted to be gabbroic massifs (Corfu et al., 2003; Krogh et al., 1990). The SMC is also interpreted as a metagabbro (e.g. Rindstad, 1992) although its connection to the gabbroic intrusions in the Tromsø Nappe is poorly understood.

The original tectonic setting of the Uppermost Allochton has been suggested to be a rifted margin, based on the association of alkaline gabbroic rocks (SMC protolith) and the surrounding quartzo-feldspathic metasedimentary rocks of Nakkedal Nappe Complex (Selbekk et al., 2000). The discovery of carbonatites supports this (Ravna et al., 2008). Dating has given an U/Pb intrusion age of 493 +5/-2 Ma of an eclogite protolith in Tromsø Nappe (Corfu et al., 2003).

1.7.2 OROGENIC EVOLUTION

P-T determinations show that the supracrustal rocks were subjected to at least two major metamorphic events during the Caledonian Orogeny (Krogh et al., 1990; Corfu et al., 2003; Ravna & Roux, 2006; Ravna et al., 2006). Stevenson (2005; 2006) has identified two episodes of partial melting believed to be associated with uplift (Ravna & Roux, 2006) in the Tromsø Nappe. In addition, the SMC has also been subjected to an event of extensive anatexis, but in a separate tectonic setting.

The first event has been dated with zircons within the eclogite from Tønsvika and gave a Taconian age of 452 ± 1.7 Ma (Corfu et al., 2003). It is believed that this marks the age of the formation of eclogite together with the maximum reached, UHP-conditions attained at

pressures of 3.36 GPa at 735°C (Ravna & Roux, 2006). Ravna et al. (2006) suggests a prograde, subduction-related metamorphic evolution as the cause of eclogitization, followed by uplift on the basis of spinel- and garnet- bearing assemblages in peridotites. High-Al titanite from an eclogite and a calc-silicate rock yielded ages of 451-450 Ma (Corfu et al, 2003). These ages can either correspond to the eclogitization or the subsequent uplift. A post eclogite, hornblende-bearing leucosome gave an age of 450.3 ± 0.9 Ma (Corfu et al., 2003) for which pressure estimates indicated 1.0-1.3 GPa (Stevenson, 2005; 2006). The almost identical ages of two different metamorphic conditions indicate that the high pressure event lasted for a very limited period of time and that the uplift was rapid and occurred over only a few million years (Corfu et al., 2003). Thermobarometry indicates a moderate increase in temperature to >800°C during initial phases of uplift, from 3.36 GPa to ~1.4 GPa, causing partial melting followed by further uplift and cooling (Ravna & Roux, 2006). A mean exhumation rate of 36 km/Ma is calculated by Ravna & Roux (2006).

The event of partial melting in the SMC yields an age of 456 ± 4 Ma (Selbekk et al, 2000).

The second metamorphic event is, among others, recorded in rutile fragments from eclogites in Tønsvika and yielded an age of 428.4 ± 0.8 Ma (Corfu et al., 2003), reaching 1.0-1.3 GPa and 743-950°C with subsequent uplift and partial melting (Stevenson, 2005; 2006). Corfu et al. (2003) interpreted this event to reflect tectonic activity during the Scandian phase where the Tromsø Nappe and Nakkedal Nappe Complex were thrusted on top of the Balsfjord group of Lyngen Nappe Complex. Ravna & Roux (2006) interprets this event as the tectonic emplacement of the Tromsø Nappe onto the SMC.

2. METHODS OF ANALYSIS

2.1 MAPPING

An area of ~4 x 5 km^2 NE of Tromsdalstind was mapped in the scale 1:5000. The mapping was done in cooperation with Odd-Arne Mikkelsen (Mikkelsen, 2011) and with special emphasis on the relationship of different lithologies and their structures.

A considerable amount of rock samples and structural data were gathered with the intention to properly describe the different lithologies and to construct the kinematic evolution of the area in conjunction with pressure and temperature estimate for the deformation.

2.2 POLARIZING MICROSCOPY

14 thin sections were prepared, cut normal to foliation and parallel to lineation. The thin sections were examined in a "Leitz Laborlux 11 pol s" polarization microscope with emphasis on both petrology and deformation microstructures. The petrologic investigation is based on the text books from Shelley (1993), Bucher and Frey (1994), Winter (2001) and Vernon (2004). The examination of deformational microstructures were done based on Passchier & Trouw (2006) and Stünitz (1989 and references therein), looking for shear sense indicators, partial melting and quartz recrystallization structures for use in temperature and deformation mechanism determinations.

2.3 X-RAY- AND PSEUDOSECTION ANALYSIS

A P-T pseudosection analysis (Holland & Powell, 1998; Connolly, 2005; White et al., 2001) has been undertaken to understand the phase topological and compositional relations for the bulk composition of a garnet-mica schist in the Tromsø Nappe.

In order to obtain the bulk composition of the rock, the sample was crushed in a "Retsch® type BB2/A" jaw crusher and ground to powder in a ball mill. The powder was then mixed with flux (Li-tetraborate) in a weight ratio of 1:7 and melted over a gas burner at ~1200°C and left to cool in a mold. The cooled bead was analyzed for major elements in a Bruker AXS S8 Tiger wavelength dispersive X-ray fluorescence machine.

The calculation of the P-T pseudosection, biotite- and melt isopleths were performed in Perple_X 07 (Connolly, 2005) using hp02ver.dat as thermodynamic database and solut_08.dat as solution model file (software and solution models available at [1]: 'www.perplex.ethz.ch').

2.4 Computer-Integrated Polarization Microscopy (CIP)

CIP (software available at [2]: Panozzo Heilbronner & Paulie, 1993; Heilbronner, 2000a) was applied to a quartz vein from the garnet-mica schist of the Tromsø Nappe to reveal the quartz CPO. The CPO was used for determination of strain geometry (Schmid and Casey, 1986; Law, 1990), shear sense (Simpson & Schmid, 1983) and temperature of deformation (Stipp et al., 2002a and b).

A thin section of the vein was prepared, cut parallel to L^T_2-lineation (ch. 3.1) and normal to foliation. In all, 8 sites within the quartz vein were selected for CIP analysis. A set of images from each selected site were acquired with an "Optronics® MicroFire®" monochrome digital camera on a "Zeiss-Jena" polarization microscope using a 3.2x magnification. The images were processed using the current version of the freeware Image SXM (Barrett, 2002), producing input images for the CIP method [2].

Area-weighted c-axis pole figures and c-axis orientation images (COIs) were produced, showing (1) the c-axis orientation at any given pixel of the image and (2) the average orientation of complete grains so that the lateral distribution of grains with similar c-axis orientation are easy to identify.

The size, aspect ratio (long axis/short axis) and long axis orientation of the best fit ellipses of the individual grains were measured using the Lazy Grain Boundary method (Heilbronner, 2000b) in combination with Image SXM. The individual grain sizes were calculated as both the radius and diameter of a circle with an equivalent area as the grain (r equ and D equ, respectively).

The distribution of grain volumes was calculated from the numerical densities of equivalent radius'. This 2-D to 3-D conversion was done by using the software StripStar [2], which is based on the Schwartz-Saltykov approach (Underwood, 1970).

Grain shape orientations were determined by digitizing grain boundaries using Image SXM and processing the data using SCASMO, PAROR and SURFOR methods ([2]; Panozzo,

1983, 1984). The obtained data of grain long axes and grain boundary orientations were plotted in rose diagrams.

2.5 Strength of CPO, stress- and strain rate estimation

The strength of CPO was calculated by the use of the mean vector strength ($\bar{a}$) defined by the equation (Cladouhos, 1999):

$$\bar{a} = \frac{1}{N}\left\{\left(\sum \sin 2\theta_i\right)^2 + \left(\sum \cos 2\theta_i\right)^2\right\}^{\frac{1}{2}} \qquad (1)$$

where N is the number of measured grains and θ_i is the angle between the grain long axis and the foliation, measured in an anticlockwise sense. The magnitude of ā varies from zero for a perfectly random distribution to one for a population of parallel lines. The angles were obtained using Image SXM.

The paleostress has been calculated using three different paleopiezometers; one empirically derived paleopiezometer (Stipp & Tullis, 2003) and two theoretically derived paleopiezometers, one for α- and one for β-quartz (Shimizu, 2008). The use of both α- and β-quartz paleopiezometers is necessary because of the locally developed chessboard subgrain patterns in quartz (ch. 3.4). These subgrain patterns may indicate the presence of both α- and β-quartz (Kruhl, 1996). In addition, temperature estimates (Ch. 3.3 and 3.4) suggest that the quartz should lie close to the α- and β-quartz transition zone.

The paleopiezometers are given as:

$$\sigma = \sqrt[1.26]{\frac{3631}{D}} \qquad (2)$$

From Stipp & Tullis (2003), where σ is the flow stress [MPa] and D is the recrystallized grain size [μm].

$$\sigma = 217 * D^{-0.8} exp^{\left(\frac{1190}{T}\right)} \qquad (3)$$

for α-quartz (Shimizu, 2008), where T is the temperature [K].

$$\sigma = 352 * D^{-0.8} exp^{\left(\frac{698}{T}\right)} \qquad (4)$$

for β-quartz (Shimizu, 2008).

Recrystallized grain size used in equation (2) and temperature used in the equations (2), (3) and (4) are taken from the CIP- (ch. 3.5) and pseudosection analysis (ch. 3.3), respectively.

Finally, the strain rate ($\dot{\varepsilon}$) was calculated using the flow law for dislocation creep (e.g. Weertman, 1978):

$$\dot{\varepsilon} = A\sigma^n e^{-Q/RT} \qquad (5)$$

where A is a material constant, σ is the flow stress [MPa], n is an empirical exponent typically set as 3-5 (e.g. Poirier, 1985) , Q is the activation energy [$Jmol^{-1}$], R is the gas constant [$J\ K^{-1}\ mol^{-1}$] and T is the absolute temperature [K].

Two sets of values for the material constant, the empirical exponent and the activation energy are used: (a) $A = 1.1*10^{-4}\ MPa^{-n}s^{-1}$, n = 4 and Q = 223 kJ mol^{-1} (Gleason & Tullis, 1995) and (b) $A = 300*10^{-4.93}\ MPa^{-n}s^{-1}$, n = 2.97 and Q = 242 kJ mol^{-1} (Rutter & Brodie, 2004).

3. RESULTS

3.1 GEOLOGICAL MAP AND DESCRIPTION OF LITHOLOGIES IN FIELD

In this chapter, a geological map produced of the area of the study area will be presented. The macro- and mesoscopic characteristics of the different lithologies and their associated structural elements will be described and divided into different deformational events.

The structural data gathered have been divided into the following deformation events and structural elements:

D^S_1 - The earliest recorded deformation event in the SMC.

D^T_1 - The earliest recorded deformation event in the Tromsø Nappe found in residual clinopyroxene in bodies of amphibolite.

D^T_2 - The main deformation event of the Tromsø Nappe producing foliation with the same orientation as D^T_1, but with different orientation of stretching lineation.

D_3 - A later deformation event recorded close to the major thrust fault, affecting older structures in both the upper 10-15m of the SMC and the lower part of the Tromsø Nappe.

S^S_0 - Primary magmatic layering in the SMC.

S^S_1 - Foliation connected to D^S_1.

$S_{T1\ \&\ T2}$ - Foliation connected to D^T_1 and D^T_2.

S_3 - Deflection of $S_{T1\ \&\ T2}$ connected to D_3 and locally mylonitization of the upper 10-15m of the SMC.

L^S_1 - SW-NE trending stretching lineation connected to S_3.

L^S_2 - SE-NW trending stretching lineation connected to S_3.

L^T_1 - SW-NE trending stretching lineation connected to $S_{T1\ \&\ T2}$.

L^T_2 - SE-NW trending stretching lineation connected to $S_{T1\ \&\ T2}$.

F^T_1 - Asymmetric, upright- to moderately inclined and horizontal- to moderately plunging open folding connected with D^T_1. The fold axes are ~SW-NE trending. The fold phase is interpreted to be syntectonic with the formation of L^T_1based on its orientation and therefore older than F^T_2. The axial planes and fold axes are perpendicular to L^T_1.

F^T_2 - Asymmetric, upright- to moderately inclined and horizontal- to moderately plunging open folding interpreted to be connected to D^T_2 based on its orientation with respect to L^T_2. The fold axes and axial planes are ~SE-NW trending and hence, approximately perpendicular to L^T_2.

F_3 - Asymmetric tight- to isoclinal folding connected to D_3. Found close to the contact, commonly in marbles. F^T_2 and F_3 folds have similar orientations and are difficult to differentiate between in the Tromsø Nappe.

It is believed that many of the deformation events are a part of the same continuous movement so that they form structural elements with similar orientations.

3.1.1 GEOLOGICAL MAP

The geological map produced during the field work is presented in figure 3.1-1.

The tectonic contact has not been observed directly, but been possible to trace because of the frequent number of outcrops and the increasing amount of mylonitization in the top 10-15m of the SMC. In the less saturated area, the tectonic contact is mapped on the basis of the major constituent of surface rubble rock type; the transition between SMC- and Tromsø Nappe dominated surface rubble could be traced within a ~20m wide zone along the inferred contact path. Other lithological boundaries within this area are only an interpretation. The northern parts of the non-layered SMC (dashed lines) are plotted from a distance on the basis of weathering colors. Tromsø Nappe units are found within the SMC in the western parts of the mapped area. They are interpreted as an imbrication.

Figure 3.1-1: (Next page) Geological map with plotted structural data produced during field work. Less saturated area indicates areas where the amount of surface rubble is extensive. The mapped boundaries occurring within this area are only an interpretation. The northern parts of the non-layered SMC (dashed lines) are plotted from a distance on the basis of weathering colors. The part of the tectonic contact within the less saturated area is mapped on the basis of the major constitute of surface rubble rock type. The transition between SMC- and Tromsø Nappe dominated surface rubble could be traced within a ~20m wide zone along the inferred contact path.

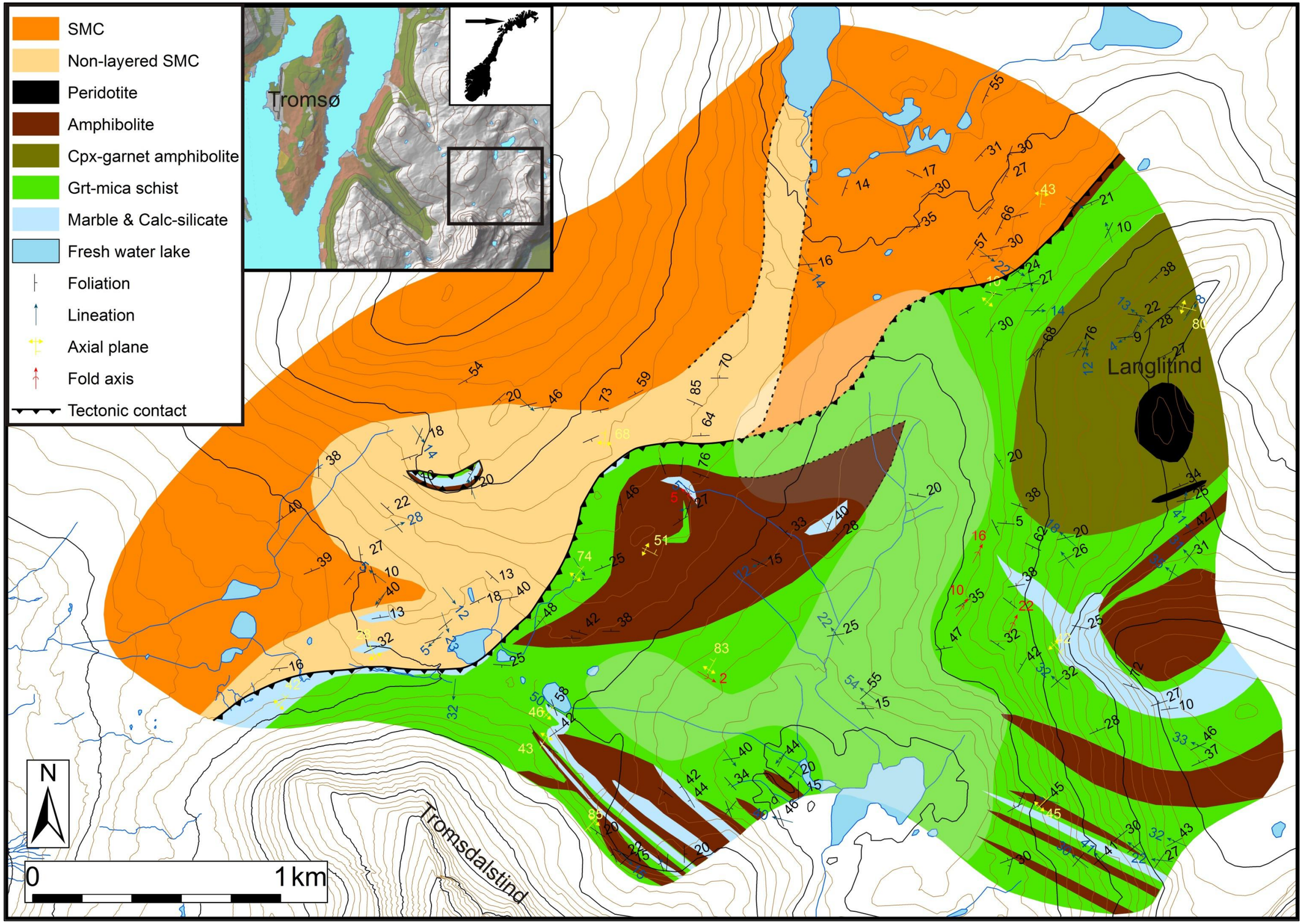
SMC
Non-layered SMC
Peridotite
Amphibolite
Cpx-garnet amphibolite
Grt-mica schist
Marble & Calc-silicate
Fresh water lake
Foliation
Lineation
Axial plane
Fold axis
Tectonic contact
Tromsø
Langlitind
Tromsdalstind
N
0
1 km

The structural data is presented in Lambert equal area projection stereonets in fig 3.1-2.

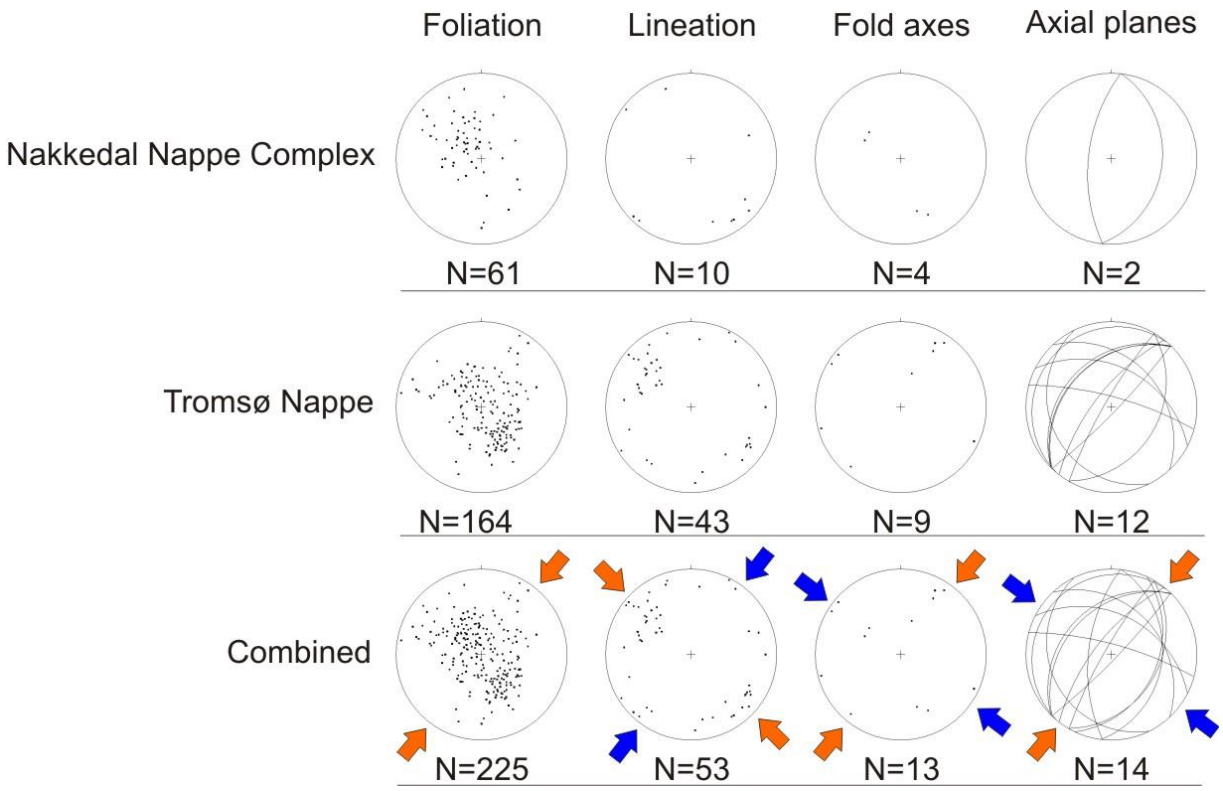

Figure 3.1-2: Lambert equal area projection stereonets with plotted structural data for each nappe and combined. Foliation is plotted as poles to planes. The structural elements within the two nappes have rather similar orientations. The different structures interpreted to be originating from the same kinematic event are grouped by arrows with the same color in the combined plots. Both nappes indicate two populations of lineations, consistent with L^S_1/L^T_1 and L^S_2/L^T_2. The orientation of L^S_1/L^T_1 and L^S_2/L^T_2 is indicated in the combined plot with blue and red arrows, respectively. Orientations of folds within the Tromsø Nappe fall into two population, consistent with F^T_1 and F^T_2/F_3. The fold orientations from the Nakkedal Nappe Complex is insufficient, but fold orientations consistent with F_3 is present. In the combined plots, the foliation shows a folding pattern consistent with F^T_2/F_3 (fold axis orientation indicated by red arrows).

Both the lineations and folds in the Tromsø Nappe show at least two populations believed to coincide with D^T_1 and D^T_2/D_3. L^T_1 and F^T_1 are weak and overprinted by the more pervasive structures of L^T_2 and F^T_2/F_3. Lineations close to the contact in the Nakkedal Nappe Complex show similar orientation as the lineations in the Tromsø Nappe and group into the two populations as well. Folds within the Nakkedal Nappe Complex are SW-NE trending and are only found close to the tectonic contact. They are thereby defined as F_3-folds. The plotted foliation shows an elongation pattern consistent with SW-NE trending fold axes, believed to be a product of D^T_2. Close to the tectonic contact, this orientation of foliation may reflect D_3.

3.1.2 SKATTØRA MIGMATITE COMPLEX

Petrology

The SMC is a very hetrogenous rock (e.g. Rindstad, 1992). The following description is only valid for the mapped part of the SMC.

The SMC occurs mainly as dark amphibolitic melanosomes cut by felsic leucosomes. The distribution between these lithologies is about 1:1. The amphibole is fine- to coarse grained, locally pegmatitic. Draining structures feeding larger leucosome dykes are common. The leucosomes are medium- to coarse grained with an olgiclasic to dioritic composition, locally pegmatitic. Large amphibole crystals within the dykes occur locally. The leucosomes vary in thickness from millimeter- to meter scale. The SMC is grey in color when weathered.

Close to the contact, a second type of felsic dykes within the amphibolite is occurring. It is characterized as a relatively soft clinozoisite- and chlorite-bearing unit and is both conform and unconform to foliation.

In addition, a major unit within the SMC shows a different texture within its melanosome. The melanosomes of this unit have a random distribution of plagioclase and amphibole grains. This random fabric is termed “salt and pepper”-texture. The mix of amphibole and plagioclase gives the rock a non-layered, magmatic appearance. This texture tends to occur where anatexis only has reached an initial phase. Locally, this unit has a high Ca-content, making it heavily weathered. The Ca-content is locally so high that it has been defined as a calc-silicate rock (fig 3.1-1). The weathering color is rusty brown and thereby different from the common SMC, which weathers in grey colors.

Structures

Primary layering, S^S_0, in the melanosomes is believed to be observed in areas that has only reached initial phase of partial melting. More or less mafic- to utramafic layers show different degree of anatexis, which make the different layers easy to distinguish from each other (fig. 3.1-1). This has to be confirmed through a more extensive analysis.

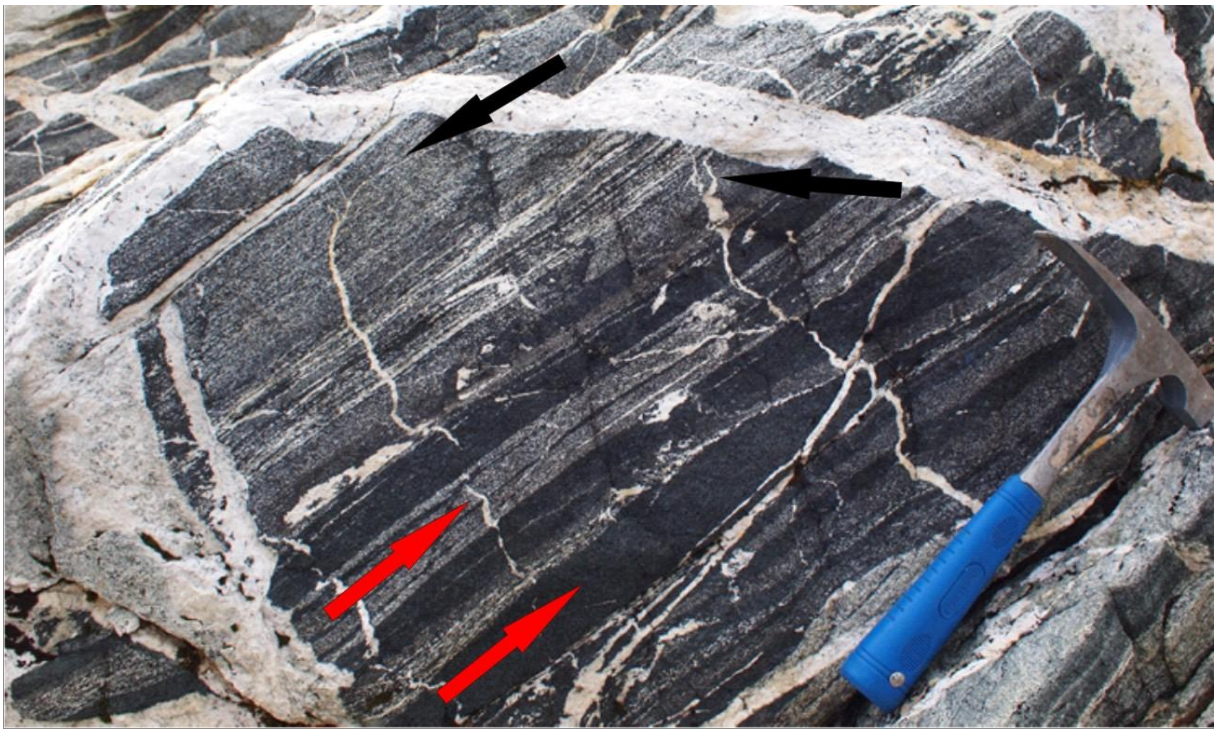

Figure 3.1-3: Image of the SMC interpreted to show primary layering in the form of more or less anatexic layers (red arrows) reflecting differences in protolith composition. Some layers show "salt and pepper"-texture. Note how drain-out structures feed larger dykes (black arrows).

The melanosomes show a moderate foliation, S^S_1. Dykes are both conform and unconform to S^S_1. Older dykes cut by younger dykes are common as well as apparent metasomatosis of host rock along dyke boundaries. No dykes from the SMC are observed to cut the contact.

S^S_1 seems to be bent into parallelism with the tectonic boundary towards the contact to the Tromsø Nappe. This new orientation of the foliation is named S_3. In the SW part of the mapped area, S_3 is deflected underneath the Tromsdalstind eclogite body. The SMC gets locally mylonitic in the top 10-15 m of the unit. Close to the contact, two populations of lineations, $L^S_1$and L^S_2, are present. The two populations of lineation are defined by amphibole and at ~90 degrees to each other.

F_3-folds are observed along the contact (fig. 3.1-4). Little or no deformation connected to D_3 is observed in the SMC away from the contact.

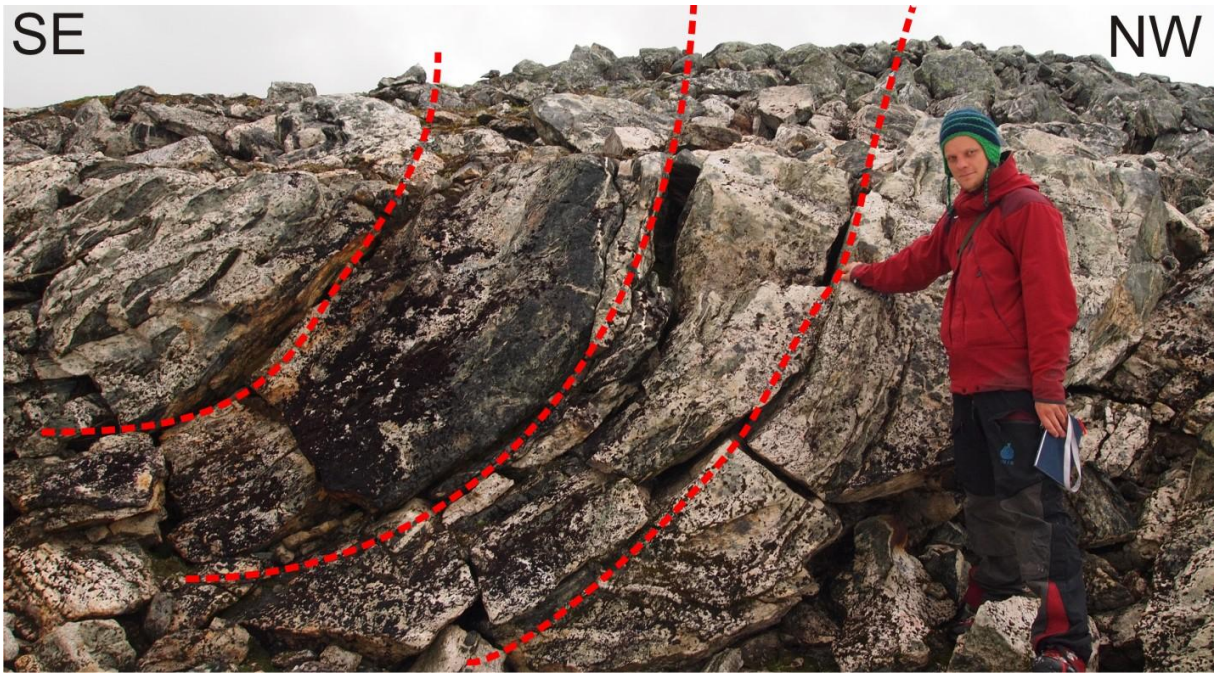

Figure 3.1-4: Image of a F_3 – fold (red dashed lines) in the SMC close to the tectonic contact. Fold axis is SW-NE trending.

3.1.3 Cpx-garnet amphibolite

Petrology

The cpx-garnet amphibolite occurs as a mafic, garnet- and cpx-bearing, commonly fine grained, rock. Felsic dykes that are unconform with foliation occur frequently, giving it an appearance very similar to the SMC. The cpx-garnet amphibolite can be locally coarse grained and is commonly strongly weathered, giving it a rusty color. Although its field appearance is very similar to both the SMC and the amphibolite of the Tromsø Nappe, it is characterized from these units on the basis of commonly being fine grained and having a low coherence.

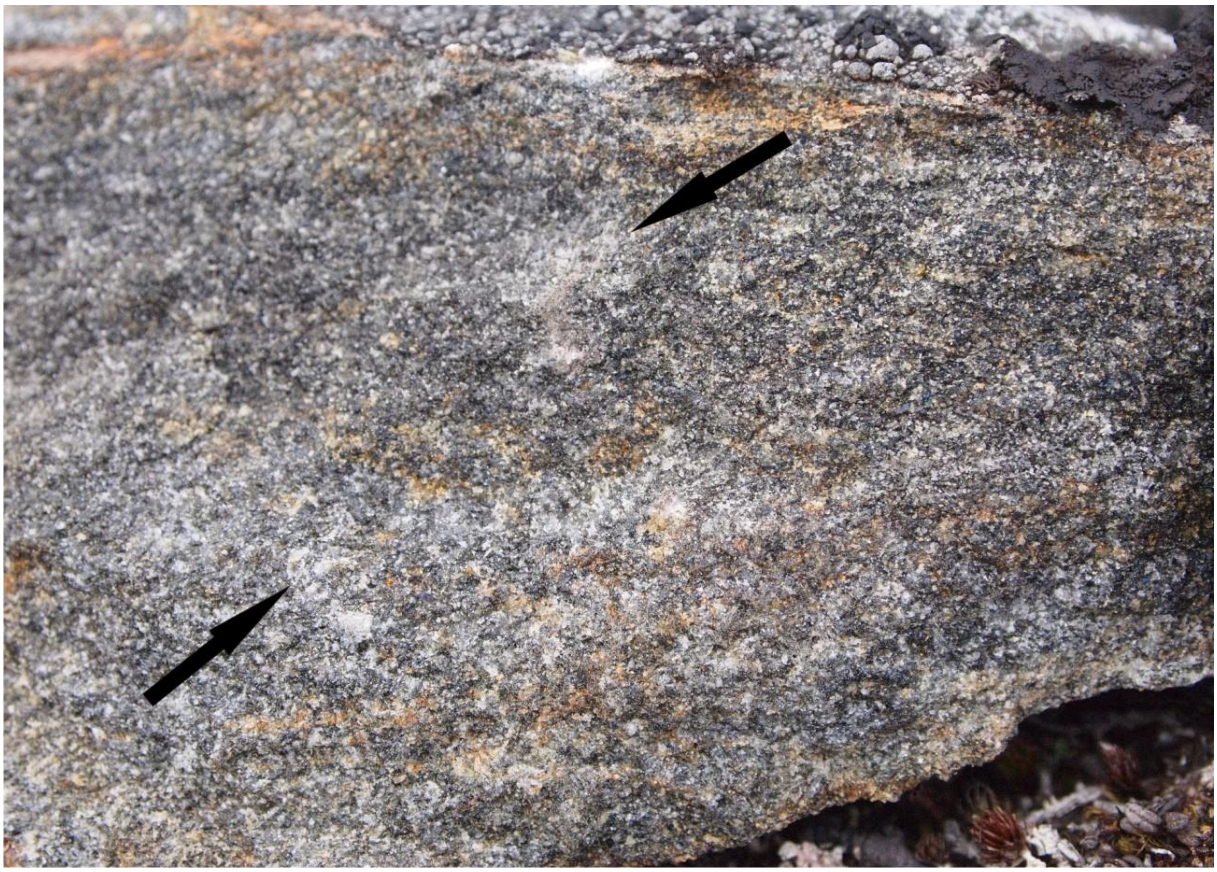

Figure 3.1-5: Image of the cpx-garnet amphibolite. Note the fine grain size and low coherence. Arrows mark examples of residual cpx which are light green in color. Base of image: ~10cm.

Structures

The unit has a pervasive $S_{T1\ \&\ T2}$ - foliation bent symmetrically around a peridotite body within. Both L^T_1 and L^T_2 are present. L^T_1 is locally strong and is defined by clinopyroxene or in secondary hornblende after clinopyroxene. In other areas, the L^T_1 is either partially overprinted or completely wiped out by L^T_2. F^T_1 - folding has been observed.

3.1.4 Tromsø Nappe amphibolite

Petrology

The amphibolite of the Tromsø Nappe occurs as layers (from centimeter to tens of meters thick) and lenses (from centimeter to 100's of meters in extent) in close association with marbles/calc-silicates and garnet-mica schist. Thinner layers are locally boudinaged. It is medium- to coarse grained and is locally garnet- and mica- bearing. Pure amphibolite does also occur. Residual clinopyroxene is present and quartzo-feldspathic bands which are both parallel and unconform to foliation are common. The latter locally gives the amphibolite a very similar appearance to the SMC and cpx-garnet amphibolite. The color is rusty when weathered and black with bluish tint when fresh.

Figure 3.1-6: Close-up of the amphibolite of the Tromsø Nappe. Note the bluish tint of the fresh sample. Base of image: 5cm.

Structures

The foliation is pervasive and reflects the foliation in the garnet-mica schist, even inside amphibolite bodies, where the foliation within the garnet-mica schist is bent around the body. It is therefore defined as $S_{T1\ \&\ T2}$. The foliation is defined by elongated amphibole grains. Strong L^{T}_{2} - lineation defined by amphibole is common. Weak L^{T}_{1} is observed with a hand lens in residual clinopyroxene. F^{T}_{1} and F^{T}_{2}/F_{3} is observed within the unit.

3.1.5 GARNET-MICA SCHIST

Petrology

The garnet-mica schist occurs as a host rock closely associated with layers and bodies of amphibolite and marble/calc-silicates. Micro- and mesostructures vary from schist to gneiss and weathered surfaces show a rusty color. Garnets are always present, but size (from centimeter to microscopic) and frequency varies. Amphibole-rich bands and irregular centimeter-thick, quartzo-feldspathic leucosomes occur locally.

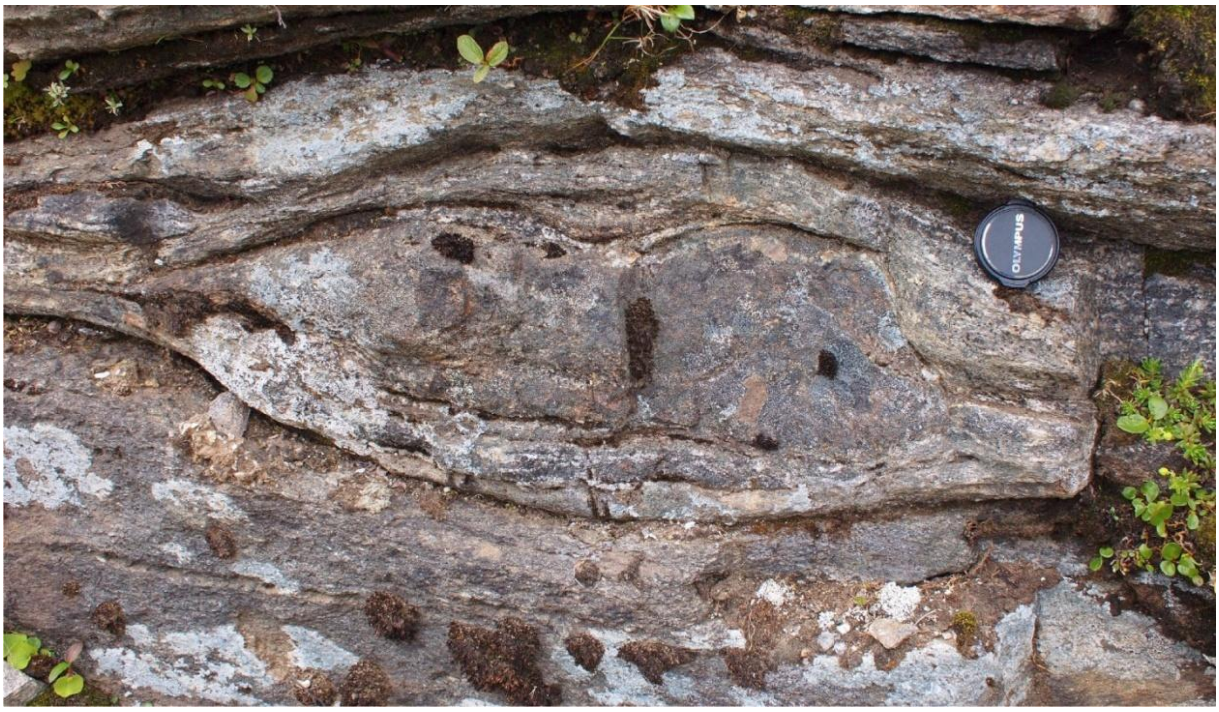

Figure 3.1-7: Image of boudinaged amphibolite within a grt-mica schist. Note the rusty weathering color of the grt-mica schist. Lens cap is 4cm in diameter.

Structures

Primary layering is not observed. The rock is strongly foliated by $S_{T1\ \&\ T2}$ and SE -trending stretching lineations, L^{T}_{2}, are commonly observed. Locally, L^{T}_{1} is present. Foliation is defined by fine- to coarse grained mica, mostly biotite, but locally also white mica.

$S_{T1\ \&\ T2}$ is bent around larger bodies of amphibolite and a body of cpx-garnet amphibolite. In areas distant from such bodies a NE-SW trending foliation that dips moderately towards NW is common. S_3 is present along the tectonic contact.

The unit shows both the NE-SW-trending folds (F^{T}_{2} and F_3) and the NW-SE-trending folds (F^{T}_{1}). Locally, interference between the the fold populations form “dome-and-basin” structures (Ramsay, 1962).

3.1.6 MARBLES AND CALC-SILICATES

Petrology

The marbles and calc-silicates occur as layers closely associated with amphibolite and garnet-mica schist. They appear either as pure, medium- to coarse grained, white layers of marble, or as dark colored calc-silicates. The marble is heavily deformed and abundant along the tectonic contact. The marble is commonly weathered and has a low coherence. The calc-silicate shows

less weathering.

Figure 3.1-8: Image of heavily folded marble in a block.

Structures

The marble and calc-silicate is believed to show S^T_2 defined in the marble as < 1 mm thin, darker layers of biotite within thicker carboniferous layers. The foliation in the calc-silicate is defined by elongated grains of pyroxene. Strong L^T_2-lineation together with curtain folding with fold axis parallel to L^T_2 occurs commonly in the marble. The marble and calc-silicate along the contact are believed to be deformed by D_3.

3.1.7 PERIDOTITE

The peridotite consists of centimeter long tremolite crystals which cover the heavily weathered surface. The weathering gives the peridotite a characteristic yellow-brown color making it easy to point out in the landscape.

Figure 3.1-9: Image of the weathered surface of peridotite showing large tremolite crystals and the characteristic yellow-brown weathering color. The lens cap is 4cm in diameter.

Other than mapping its extent, no analytic work was done to this unit.

3.2 Description of lithologies in thin sections

3.2.1 Skattøra Migmatite Complex

One thin section has been available for the microscopical analysis of this unit. The available thin section is comprised of amphibolite cut by felsic dykes. The dykes are both parallel and oblique to the foliation. Both, the amphibolite and dykes, are cut by late veins filled with calcite.

Amphibolite

Hornblende (95%)

Occurs as anhedral, 2-<0.05mm large grains. The mineral is biaxial (+), yellow-green to brown in color with inclined extinction. The mineral is elongated along foliation and shows a zonation, from brown in the center to greenish towards its rims (see fig 3.2-1). This

observation indicates that the Ti-fraction decreases towards the rim, suggesting a lowering of temperature during growth of hornblende (Winter, 2001). The hornblende grains are locally rimmed by secondary fine grained clinozoisite and epidote.

Opaque mineral (3%)

Occurs as sub- to euhedral, 0.45-<0.05mm large grains. Some grains show a cubic shape. The mineral is most likely a Fe-Ti oxide as identified in Selbekk & Skjerlie, (2002).

Plagioclase (2%)

Occurs as intergranular, 0.3mm - <0.05mm large grains in vacancies among hornblende. The mineral is colorless, biaxial, with 1st order birefringence and low relief. It shows inclined extinction and the development of subgrains.

Titanite

Occurs as sub- to euhedral, 0.2mm - <0.05mm large grains. The mineral is pale brown in color and shows no pleochroism. The grains are biaxial, elongated rhomb-shaped crystals with a single cleavage, extreme birefringence and a very high relief. The mineral is found as inclusions in hornblende (fig. 3.2-1).

Carbonate is present in very small amount. Chlorite, epidote and clinozoisite occur as secondary minerals.

Felsic dykes

The felsic dykes were believed to be of oligoclase composition in field, but have shown quite different characteristics in thin sections. The dykes are 1-3 mm thick (see fig 3.2-1) and show the following mineral assemblage:

Clinozoisitt (30%)

Occurs as colorless, subhedral, 0.8mm – 0.1mm large grains. The mineral is biaxial and shows a single cleavage, medium relief, inclined extinction and 2nd order birefringence. The mineral is interpreted to be in equilibrium with epidote, plagioclase and chlorite.

Epidote (30%)

Occurs as sub- to euhedral, 0.5 – 0.05mm large grains. The mineral is biaxial (-) and appears as pale green in color with low pleochroism and one very good cleavage. It has patchy texture, high birefringence colors and a medium relief with well developed zonation.

Chlorite (20%)

Occurs as euhedral, sub-sperulitic, 0.5-<0.05mm large aggregates. The mineral is biaxial (+), pale green to brown with a micasous cleavage and straight extinction.

Plagioclase (10%)

Occurs as 0.3- <0.05mm large grains. The mineral is colorless, biaxial, with 1st order birefringence and low relief. It shows inclined extinction and the development of subgrains.

Rutile

Occurs as anhedral blebs, < 0.05mm in size. The mineral has a dirty yellow color and occurs isolated in felsic dykes (see fig 3.2-1).

Metamorphic facies

Due to the zonation within the hornblende, the amphibolite of the SMC shows upper amphibolite facies. The felsic dykes are later and show greenschist facies.

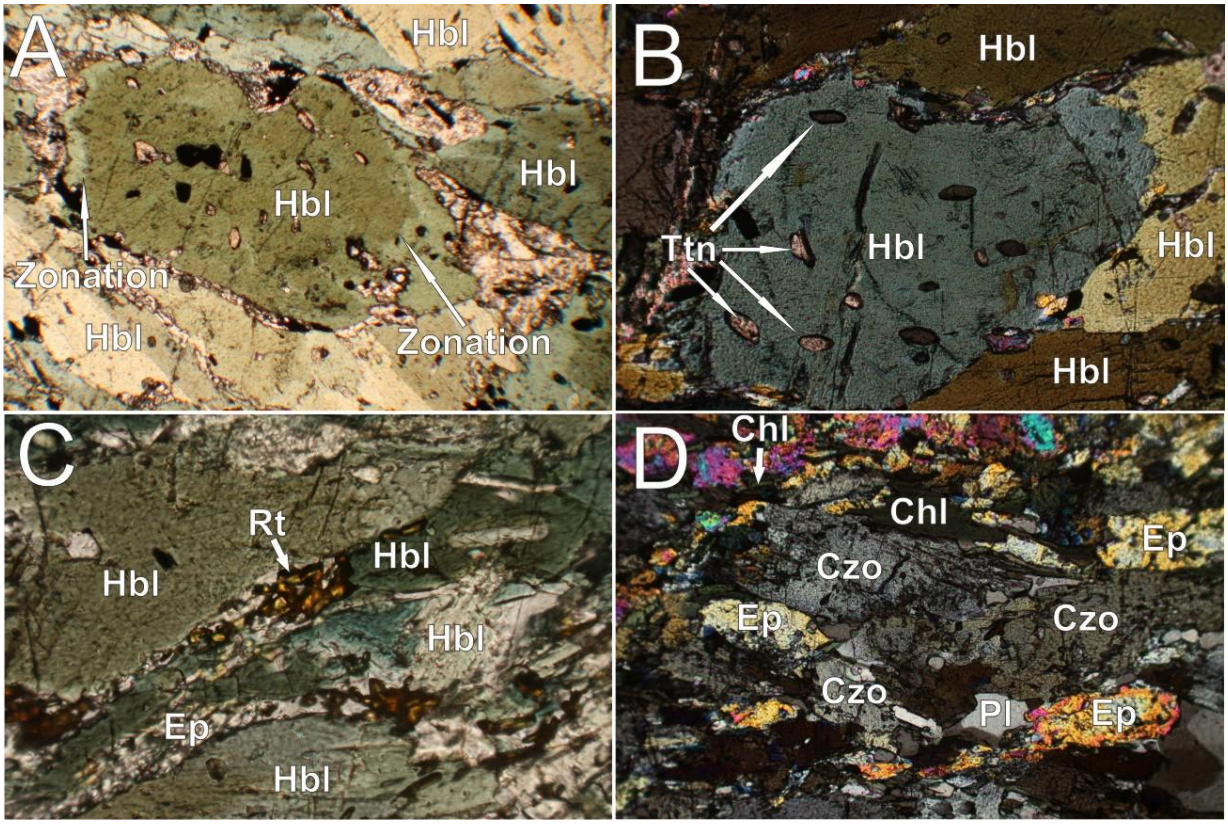

Figure 3.2-1: Images from thin section. (A) Zonation in hornblende. Base of image: 2.5mm. (B) Inclusions of titanite in hornblende. Crossed polars; base of image: 1.6mm. (C) Rutile in felsic vein. Base of image: 0.8mm. (D) Felsic vein showing greenschist facies. Crossed polars; base of image: 1.6mm.

3.2.2 CPX-GARNET AMPHIBOLITE

Two thin sections have been prepared from the cpx-garnet amphibolite of the Langlidtinden body. The thin sections show a well developed foliation defined by mm thick layers of more or less diopside/hornblende- and clinozoisite-rich domains. The different minerals in the rock are well mixed and probably indicate a diffusion creep dominated deformation.

Hornblende (40-70%)

Occurs as euhedral, 1-<0.05mm large grains. The mineral is biaxial (+), yellow-green to brown in color with inclined extinction and constitutes the main fabric. It also occurs as rims around equigranular symplectites with finer grained hornblende, diopside and plagioclase, both in fine- and medium grained aggregates (see fig 3.2-2).

Diopside (10-30%)

Occurs as 2.5-<0.05mm large grains in equigranular symplectites with plagioclase, both in fine- and medium grained aggregates. The mineral is brownish green in color and has a low pleochroism. The mineral shows two cleavages at ~90 degrees and a 45° extinction angle.

Plagioclase (5-20%)

Occurs as colorless, 1-<0.5mm large grains. The mineral is biaxial with 1st order birefringence, low relief, two cleavages at ~90° and inclined extinction. It occurs in two textural different settings:

(1) in equigranular symplectites with hornblende and diopside, both in fine- and medium grained aggregates,
(2) as retrograded rims around garnets,
(3) as worms in symplectite with clinozoisite, commonly around relicts of garnet, often as garnet pseudomorphs.

Clinozoisite (3-15%)

Occurs as colorless, 1.2-<0.05mm large grains. The mineral is biaxial and shows a single cleavage, medium relief, inclined extinction and 2nd order birefringence. The mineral occurs in three texturally different settings:

(1) in bands, closely associated with plagioclase and hornblende, often with an inclined orientation compared to main fabric (fig. 3.2-2),
(2) as inclusions in garnets,

(3) As symplectite with plagioclase worms growing around relicts of garnet, often as garnet pseudomorphs.

Garnet

Occur as colorless, anhedral, 0.5-0.3mm large grains. The mineral is isotropic, with no cleavage and has a high relief. The garnets appear as relicts, rimmed with zones of plagioclase and sumplectite of clinozoisite and plagioclase worms (see fig 3.2-2). Inclusions of clinozoisite are common.

Titanite with inclusions of rutile, quartz and carbonate occur as accessory minerals.

Metamorphic facies

The presence of rutile as inclusions in titanite indicates high pressure metamorphism overprinted by amphibolite facies. In addition, the origin of equigranular symplectites may indicate a retrograde overprinting of an earlier high pressure metamorphism. This is discussed in chapter 4.1.2).

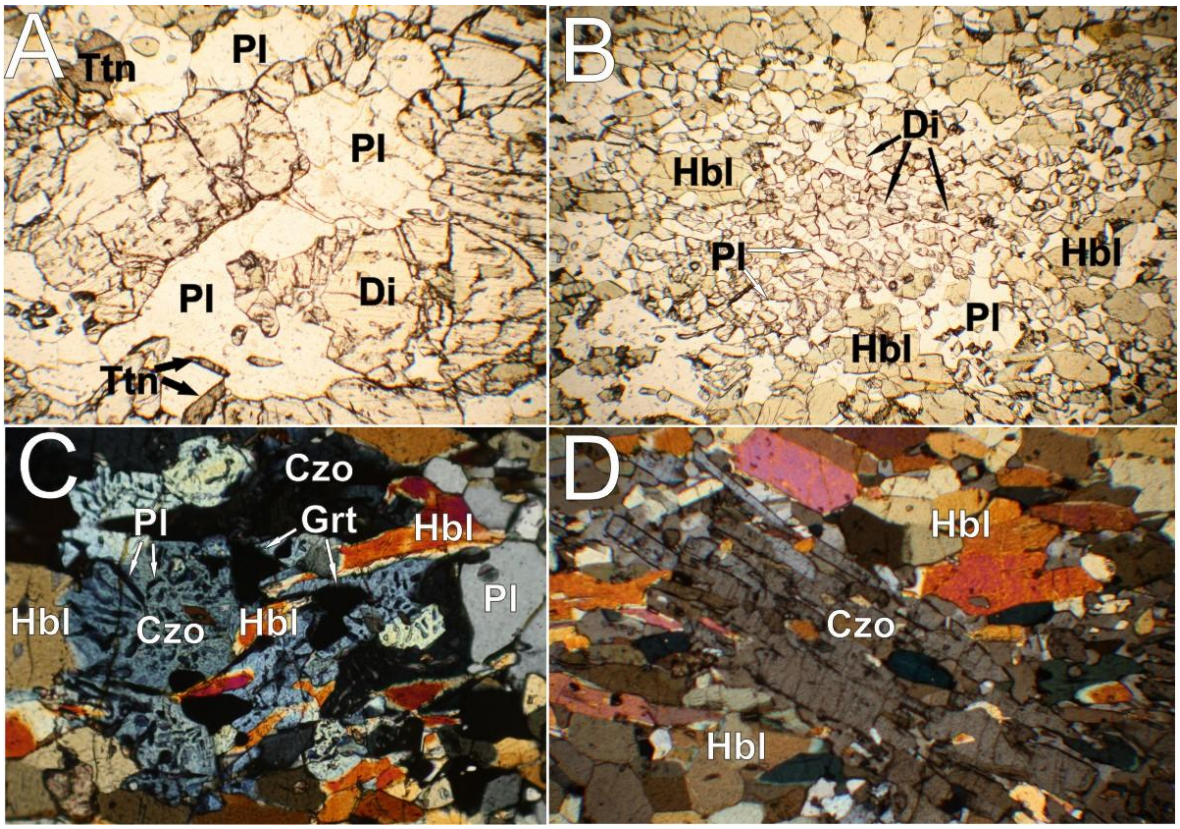

Figure 3.2-2: Images from thin section. (A) Medium grained symplectite with diopside and plagioclase. Base of image: 2.5mm. (B) Fine grained symplectite with diopside, hornblende and plagioclase. Base of image: 3.5mm. (C) Symplectite. Plagioclase worms in clinozoisite, probably as a reaction product involving residual garnet. Crossed polars; Base of image: 1.2mm. (D) Clinozoisite with long axis in an angle in relation to main foliation defined by hornblende (parallel to base of image). Crossed polars; base of image: 2.5mm.

3.2.3 TROMSØ NAPPE AMPHIBOLITE

In all, 5 thin sections from this lithology have been available. The amphibolite of the Tromsø nappe show often great similarities with the amphibolite of the SMC and to differentiate between the two can therefore be difficult in hand specimen as well as in thin section. Qualitatively, the strain varies greatly, from relatively undeformed to deformed with well developed foliation. Felsic veins occur locally.

Amphibole (30-95%)

Occurs locally as actinolite, but most commonly as hornblende. Both minerals are biaxial (+), with inclined extinction. Actinolite shows a pale brown color, while hornblende is browner in color. Hornblende locally shows zonation where the color changes to green towards the rims. This indicates retrograde conditions during growth of the mineral (Winter, 2001). Grain size varies from 4-< 0.05mm. The less deformed samples show larger euhedral grains, whereas more deformed samples show smaller, sub- to anhedral grains which are elongated along foliation.

Plagioclase (1-40%)

The mineral is colorless, biaxial, with 1st order birefringence and low relief. It shows inclined extinction and occurs in four texturally different settings:

(1) as intergranular, 1 - <0,05mm large grains in vacancies among hornblende,
(2) as larger (5 - <0.05mm) grains in quartzo-feldspathic veins,
(3) in myrmekites with quartz worms (see fig 3.2-3),
(4) as retrograded rims around amphibole,
(5) as albite in veins of epidote, clinozoisite and chlorite.

Quartz (1-40%)

Occurs as colourless, 1-0.05mm large grains. The mineral is uniaxial (+), with low relief, low birefringence, and no cleavage planes. The mineral has a straight, but often undulating extinction with development of subgrains, locally showing c-axis parallel subgrain boundaries or chessboard pattern.

Quartz occurs in two textural different settings:

(1) as relatively large grained aggregates in quartzo-feldspathic veins,
(2) as worms in myrmekites with plagioclase in leucosomes (see fig 3.2-3).

Quartz acts as a weak phase and appears in bands indicating that deformation was dislocation creep dominated. Microstructures show evidence of subgrain rotation recrystallization (SGR) and grain boundary migration (GBM).

Clinopyroxene (0-10%)

Occurs as anhedral, 1-0.5mm large grains with a brownish green color and low pleochroism. The mineral shows two cleavages at ~90 degrees and a 45° extinction angle. Appear as residuals with rims of plagioclase and inclusions of amphibole (fig. 3.2-3).

Clinozoisite (0-5%)

Occurs as colorless, euhedral, 1-<0,5mm large grains along longest axis. The mineral is biaxial and shows a single cleavage, medium relief, inclined extinction and 2nd order birefringence.

The mineral appears in three textural different settings:

(1) in equilibrium with epidote, plagioclase and chlorite in late felsic dyke that is parallel to foliation,
(2) as needles in plagioclase or as poles in quartz.

Opaque mineral (0-3%)

Occurs as anhedral, 0.6-<0.05mm large grains. Interpreted to be sulphides, presumably pyrite.

Titanite (0-1%)

Occurs as sub- to euhedral, 0.8-<0.05mm large grains. The mineral is pale brown in color and shows no pleochroism. The mineral is biaxial with an extreme birefringence and a very high relief. The grains are elongated, rhomb-shaped crystals with a single cleavage.

The mineral occurs in two different textural settings:

(1) as inclusions in hornblende,
(2) with inclusions of rutile.

Epidote

Occurs as sub- to euhedral, 0,5mm –< 0,05mm large grains. The mineral is biaxial (-), pale green with low pleochroism. It has a patchy appearance with high birefringence colors and medium relief. The mineral occurs in two textural different settings:

(1) in association with clinozoisite, plagioclase and chlorite in felsic veins,
(2) in association with residual clinopyroxene within the amphibolite.

Rutile

Occurs as anhedral blebs, 0.1-<0.05mm large. The mineral has a dirty yellow color and sits as inclusions in titanite (fig. 3.2-3).

Carbonate, zircon, K-feldspar and garnet occur as accessory minerals. Clinozoisite, epidote, titanite, chlorite, biotite, white mica and apatite occur as secondary minerals in the amphibolite.

Metamorphic facies

The amphibolite of the Tromsø Nappe shows upper amphibolite- to granulite facies due to zonation in hornblende (Winter, 2001) and the presence of clinopyroxene, respectively. The amphibolite is locally cut by felsic veins of greenschist facies mineral assemblage.

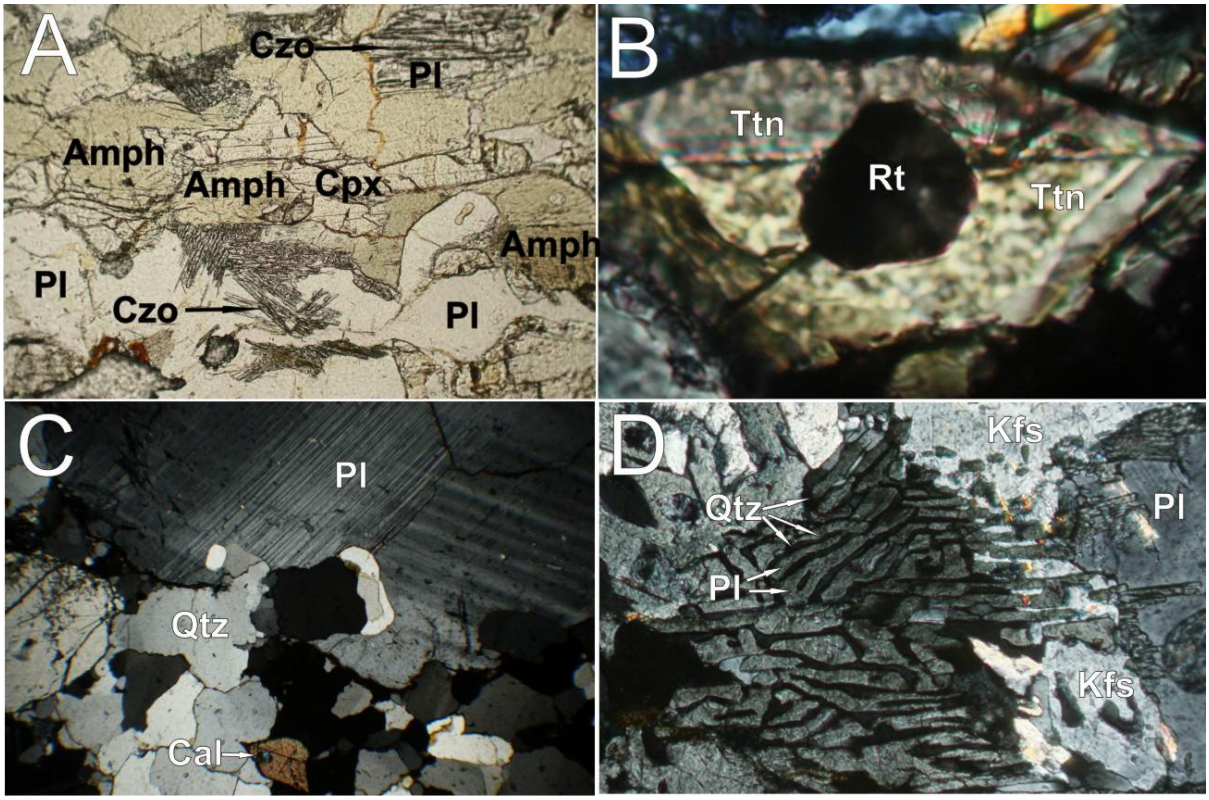

Figure 3.2-3: Images from thin sections. (A) Residual clinopyroxene in association with amphibole and plagioclase. Clinozoisite grows as needles in plagioclase. Base of image: 1.6mm. (B) Rutile as inclusion in titanite. Crossed polars; base of image: 0.15mm. (C) Quartzo-feldspathic vein showing coarse grained feldspar and recrystallized quartz. Crossed polars; base of image: 3.6mm. (D) Myrmekites. Quartz worms in plagioclase were precipitated as K-feldspar reacted to form albite and anorthite during cooling (Shelley, 1993).

3.2.4 GARNET-MICA SCHIST

Five thin section of this unit has been prepared. The garnet-mica schist is closely associated with amphibolites and the transition between the two can be very gradual. All thin sections show more or less deformation. Quartz veins are common and the amount of quartz increases with deformation. Quartzo-feldspathic veins occur locally.

Quartz (40-70%)

Occurs as subhedral, 3.5-<0.05mm large grains in bands. The mineral is colorless, has no cleavage and low relief. It is uniaxial (+), with low birefringence. Well developed triple junctions as well as lobate grain boundaries occur locally. The extinction is straight, but undulating with development of subgrains. The subgrains boundaries are often c-axis parallel, with local development of chessboard patterns. These and other microstructures indicate deformation through GBB-, SGR- and GBM recrystallization.

Quartz does also occur as inclusions in garnets and in symplectite with clinozoisite as a product after reaction between plagioclase and garnet.

Biotite (15-30%)

Occurs as pale brown to reddish brown, subhedral, 1.5-<0.05mm large grains. The mineral is biaxial(-) with a single cleavage along its longest axis which is parallel to foliation. The biotite shows straight extinction, 'birds eye' texture when extinct and 3rd or 4th order birefringence. The biotite is locally foliated around garnets and appears commonly as 'mica fish'. Inclusions of zircon are common.

Plagioclase (1-40%)

Occurs as colorless and sub- to anhedral, 3-<0,05mm large grains. The mineral is biaxial and shows two cleavages at ~90 degrees, 1st order birefringence, low relief, inclined extinction and twinning.

The mineral occurs in two textural different settings:

(1) as coarse grains, commonly zoned in association with quartzo-feldspathic veins,
(2) as retrograded rims around garnets.

Garnet (3-10%)

Occurs as colorless, an- to euhedral, 3-0.3mm large grains. The mineral is isotropic, with no cleavage and has a high relief. Anhedral garnets are often occurring within zones of plagioclase and biotite. Quartz, plagioclase and biotite inclusions are common, locally

showing rotation during syndeformational growth. The mineral is often found in association with amphibole.

Clinozoisite (0-10%)

Occurs as colorless, an- to subhedral, 2.5-<0.05mm large grains. The mineral is biaxial (+) and shows a single cleavage, medium relief, inclined extinction and 2nd order birefringence. The mineral is found in association with biotite and garnet, commonly as symplectite with plagioclase. The mineral is locally growing around allanite showing radial fraction. This is because allanite often contain radioactive elements which break down the crystal structure within the allanite (fig. 3.2-4).

Amphibole (0-10%)

The amphibole occurs as anhedral, 1.5-0.1mm large grains. The mineral occurs locally as actinolite, but most commonly as hornblende. Both minerals are biaxial (+), with inclined extinction. Actinolite shows a pale brown color, while hornblende is more yellow-green to brown in color. Both minerals have a high relief. Inclusions of quartz and biotite are common.

Titanite (0-2%)

Occurs as sub- to euhedral, 1.5-<0.05mm large grains. The mineral is pale brown in color and shows no pleochroism. The mineral is biaxial with an extreme birefringence and a very high relief. The grains are elongated, rhomb-shaped crystals with a single cleavage. Titanite can be found as inclusions in hornblende and in association with biotite bands.

Rutile

Occurs as anhedral blebs, <0.05mm large. The mineral has a dirty yellow color and forms inclusions in titanite.

Allanite, zircon and opaque minerals occur as accessory minerals. Titanite, epidote and white mica occur as secondary phases.

Metamorphic facies

The presence of rutile as inclusions in titanite indicates high pressure metamorphism overprinted by amphibolite facies. White mica from biotite is present in the S-fabrics, which indicates a retrogradation during deformation.

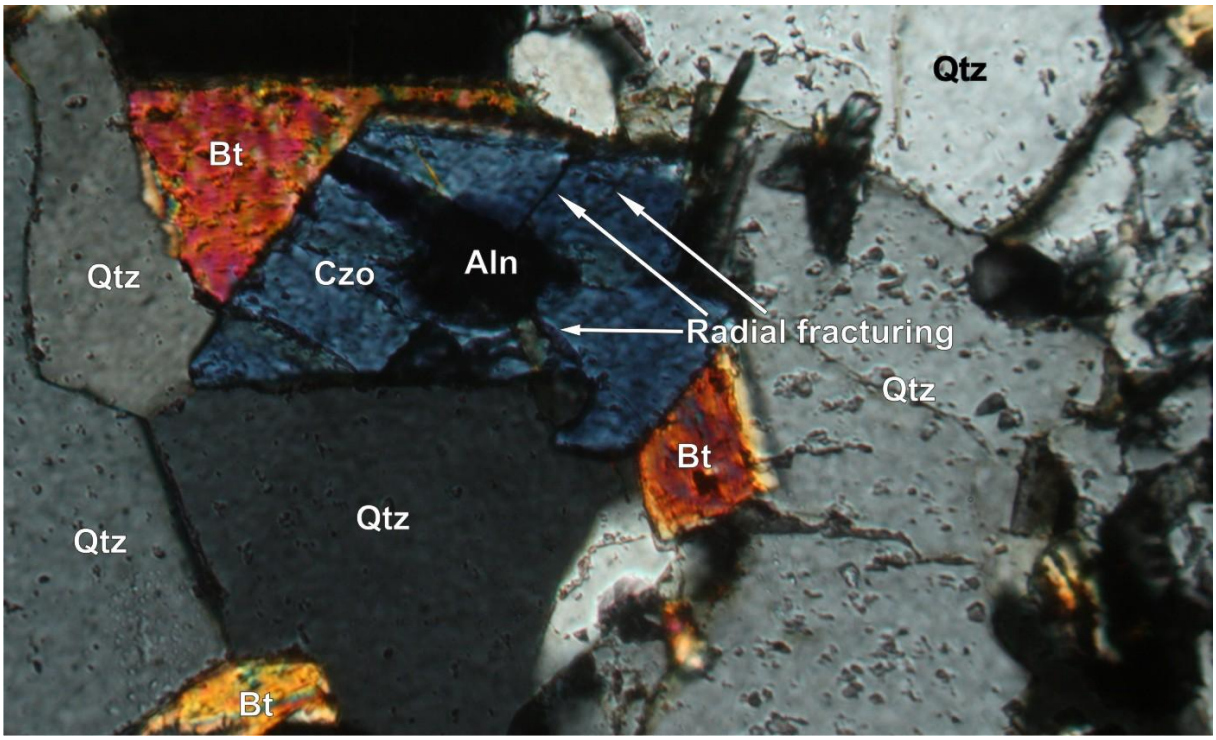

Figure 3.2-4: Image from thin section of allanite overgrown by secondary clinozoisite. Allanite contains radioactive elements which breaks down the crystal structure so that the mineral expands, causing radial fracturing in the clinozoiste.

3.2.5 CALC-SILICATE ROCKS

One thin section has been produced from this unit. The unit is dark in color and is easily mistaken for amphibolites in hand specimen. Quartz-rich bands occur.

Clinopyroxene (40%)

Occur as an- to subhedral, 1,5mm – 0,05mm large grains. The mineral has a brownish green color and low pleochroism. The mineral is biaxial and shows two cleavages at ~90 degrees and a 45° extinction angle. The mineral is most likely diopside and occurs in equilibrium with clinozoisite and epidote.

Clinozoisite (40%)

Occurs as anhedral, 2-0,1mm large grains. The mineral is colorless and biaxial, with a single cleavage, medium relief, inclined extinction and 2nd order birefringence. The mineral occurs in two textural different settings:

(1) as larger, zonated, euhedral grains in association with clinopyroxene, epidote and quartz,

(2) as 0.5-0.05mm long needles in quartz.

Epidote (10%)

Occurs as sub- to anhedral, 1,5mm –< 0,05mm large grains. The mineral is colorless, biaxial (-) and pale green with low pleochroism. It has a patchy appearance with high birefringence colors and medium relief. The mineral can be found in association clinozoisite and clinopyroxene.

Quartz (10%)

Occurs as 1.3-<0,05mm large grains. The mineral is colorless and uniaxial (+), with low relief, low birefringence and no cleavage planes. The mineral has a straight, but often undulating extinction with development of subgrains. Grain boundaries are either straight or lobate. Quartz occurs in veins and is in equilibrium with both clinopyroxene and clinozoisite.

Microstructures indicate that dislocation creep is the dominating process with clear indication of both SGR and GBM.

Titanite

Occurs as sub- to euhedral, 0.5-<0.05mm large grains. The mineral is pale brown in color and shows no pleochroism. The mineral is biaxial with an extreme birefringence and a very high relief. The grains are elongated, rhomb-shaped crystals with a single cleavage.

The mineral occurs in close association with clinopyroxene and with or without inclusions of rutile.

Rutile

Occurs as anhedral blebs, <0.05mm large. The mineral has a dirty yellow color and sits as inclusions in titanite.

A few grains of kyanite are present as accessory mineral in association with garnet and the current foliation.

Metamorphic facies

The presence of rutile as inclusions in titanite indicates high pressure metamorphism overprinted by amphibolite facies, up to kyanite grade. Secondary white mica from biotite is present in the S-fabrics, which indicates a retrograde temperature conditions during deformation.

3.3 X-RAY- AND PSEUDOSECTION ANALYSIS

This section presents the results from the X-ray and pseudosection analysis. P-T pseudosection analysis (Holland & Powell, 1998; Connolly, 2005; White et al., 2001) is a convenient tool for understanding phase topological and compositional relations for a bulk composition of a rock.

The minerals Bt + Grt + Qtz + Pl + Rt + melt have been recognized as a prograde mineral assemblage in the garnet-mica schist. The mineral assemblage has been identified on the basis of being present as inclusions in (1) syn-deformational garnets (Bt, Qtz and Pl) and (2) secondary titanite (Rt) (ch. 3.2.4). In addition, evidence of partial melting is convincing (ch. 3.4.3).

An attempt was made to determine the TiNCKFMASH phase topological relation to explain the reaction textures using the bulk rock composition of the selected sample. The phase diagram involves the following minerals and solution models: garnet (Gt, HP), biotite (TiBio, TCC), plagioclase (Pl, h) and melt (HP). All calculations were performed in Perple_X 07 (Connolly, 2005) using hp02ver.dat as thermodynamic database and solut_08.dat as solution model file.

3.3.1 X-RAY FLUORESCENCE ANALYSIS

The chemical composition of the bulk rock was determined through an X-ray diffraction analysis done according to the procedure described in ch. 2.3.

The results from the X-ray diffraction analysis is presented in table 3.3-1:

Sample: T8.4B	SiO2	Al2O3	TiO2	Cr2O3	Fe2O3	FeO	MnO	MgO	CaO	Na2O	K2O	P2O5	H2O	Total
wt %	69,44	11,42	0,83	0,07	6,31	-	0,12	2,86	2,51	1,97	2,08	0,12	2,27	100
Norm. Mol. Prop	69,82	6,77	0,63	-	-	4,77	0,10	4,29	2,70	1,92	1,33	0,05	7,61	100

Table 3.3-1: Results from the X-ray diffraction analysis in wt % and calculated normalized molar proportions. Fe_2O_3 is calculated from stoichiometry. $H_2O = \Sigma$ wt %

3.3.2 PSEUDOSECTION ANALYSIS

The topological relations of different phases in the TiNCKFMASH system for the garnet-mica schist are shown in fig. 3.3-1 for the temperature range 600-1000°C and pressure of 0.5 – 1.2 Gpa. It is assumed that the composition represents equilibrium mineral assemblage and reflects the equilibrium reaction volume. Krogh et al. (1990) describes a convergence of P-T

data from different thermobarometric methods which indicates that a high degree of equilibrium was reached for different assemblages within the Tromsø Nappe.

The prograde mineral assemblage Bt + Grt + Qtz + Pl + Rt + melt occurs within a temperature range of 700-850°C at a pressure range from 0.9 to 1.2 GPa (fig. 3.3-1).

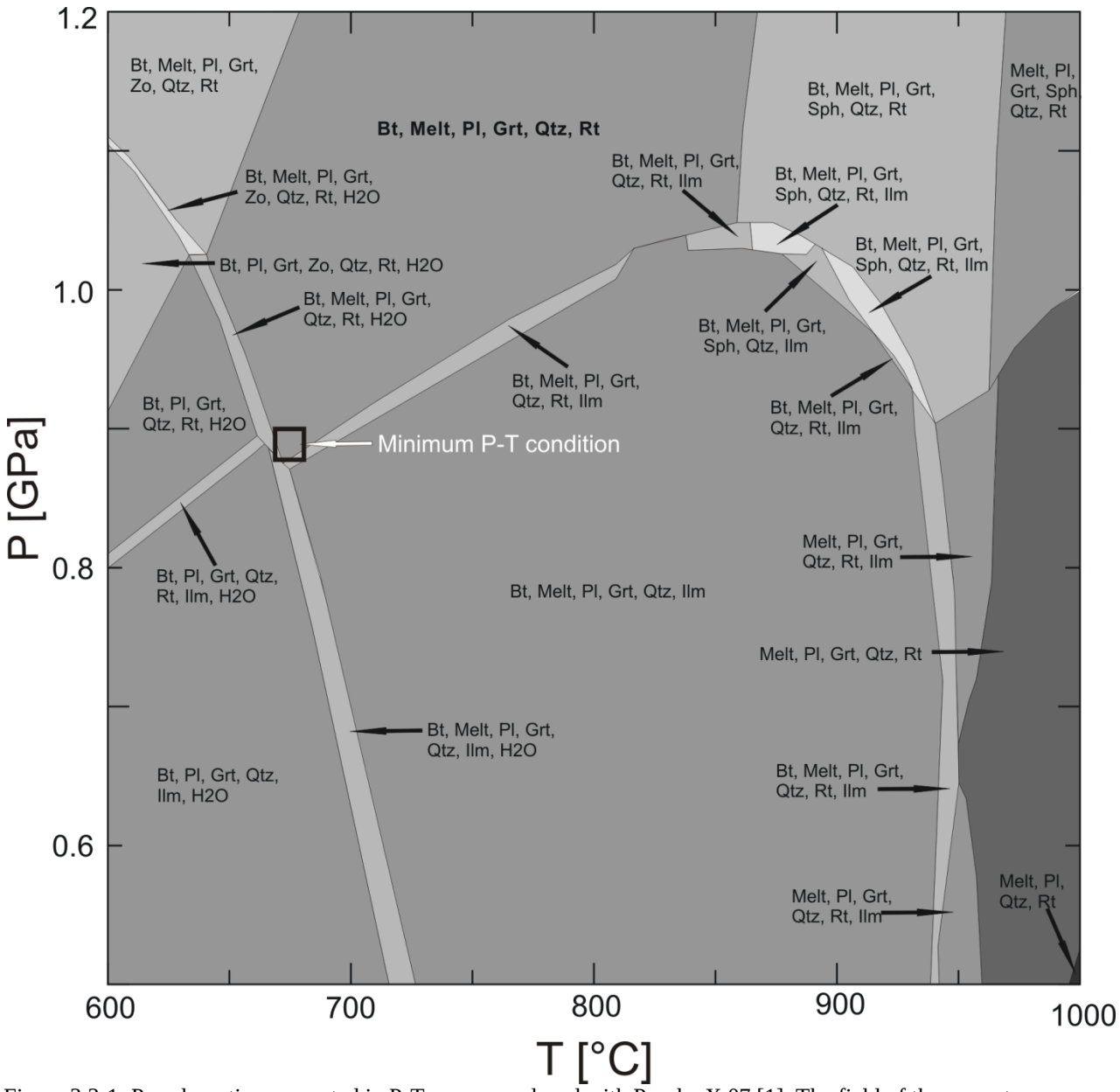

Figure 3.3-1: Pseudosection presented in P-T space, produced with Perple_X 07 [1]. The field of the correct phase assemblage is indicated by bold letters. Minimum P-T condition is marked (box).

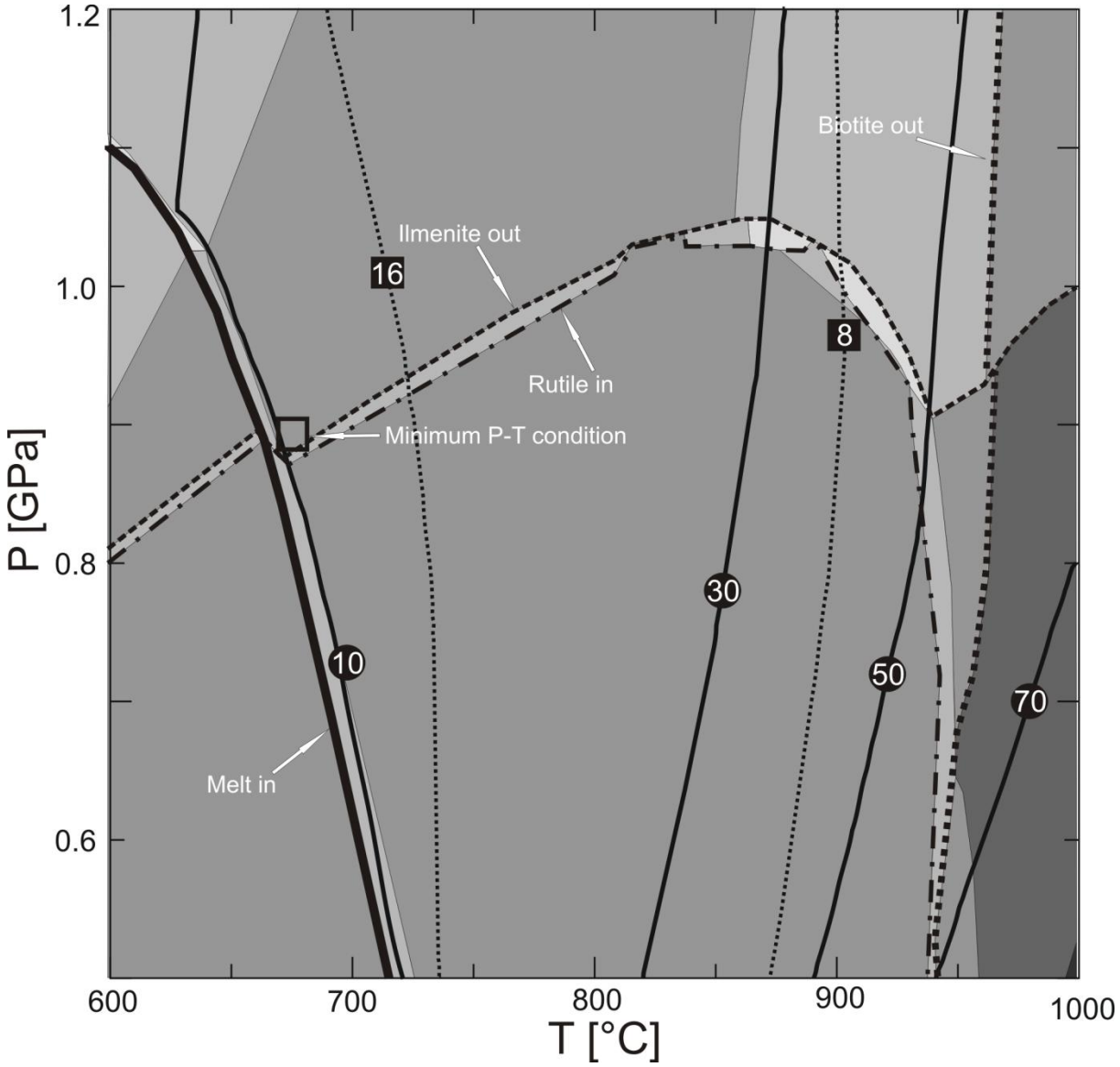

Figure 3.3-2: Same pseudosection as in fig. 3.3-1 with plotted biotite and melt isopleths giving the volume fraction (biotite: black squares with numbers, melt: black circles with numbers). The isopleths indicate that towards higher temperatures, melt fraction is increasing on the expense of biotite. The phase transition between ilmenite and rutile has been used as a minimum pressure criterion. The isopleths are calculated using Perple_X 07 [1].

Determination of modal isopleths of melt and biotite indicates that the melt fraction increases towards higher temperatures at the expense of biotite (fig. 3.3-2). The 'melt in' line should therefore indicate the minimum temperature of which the rock will experience biotite melting. As the 'melt in' line has a steep slope in relation with the temperature axis, the biotite-melt reaction could not be used to constrain the minimum pressure of the reaction. The minimum pressure assemblage is estimated using the phase transformation between ilmenite and rutile. Rutile is the only Ti-bearing phase in the rock and is stable at minimum pressure of 0.9 GPa in the obtained field. The minimum P-T window is marked as a black box in the diagrams and

gives a minimum P-T condition for the prograde mineral assemblage at 0.9 GPa and 680°C. The calculated melt fraction at the minimum P-T condition is 13 vol %.

3.4 EVIDENCE OF PARTIAL MELTING

Partial melting has been reported from eclogites within the Tromsø Nappe (Stevenson, 2005 and 2006). In the field, the presence of irregular, quartzo-feldspathic veins within the garnet-mica schist and amphibolite of the Tromsø Nappe were indicative of partial melting taking place outside the eclogites.

In addition to the presence of mesoscale leucosomes, the criteria to establish the former presence of melt include P-T estimation and microstructures inferred to record metamorphic reactions and mineral paragenesis consistent with melting (Marchildon & Brown, 2002). Furthermore, the recognition of mineral pseudomorphs after melt-films, -envelopes and -pools (Sawyer, 2001) is looked upon as firm evidence for partial melting.

Microstructural evidence for partial melting

Several thin sections have been prepared of the quartzo-feldspathic veins. The veins consist of coarse grained quartz with chessboard structures, plagioclase and K-feldspar together with finer grained quartz. Myrmekites indicate that K-feldspar has reacted with fluids to form albite, anorthite and quartz during cooling (Shelley, 1993). The veins show evidence of post-crystallization deformation in the form of BLG and SGR in quartz. As a result, the recognition of microstructural evidence for partial melting as mentioned above is difficult. Still, possible pseudomorphs after melt (fig 3.4-1 A, C), cuspate and unlike grain boundaries (fig 3.4-1 B, C) and inclusions of rounded blebs of quartz within feldspar and larger quartz grains (fig. 3.4-1 B,D) occur. The latter is interpreted as melt reactant residuals.

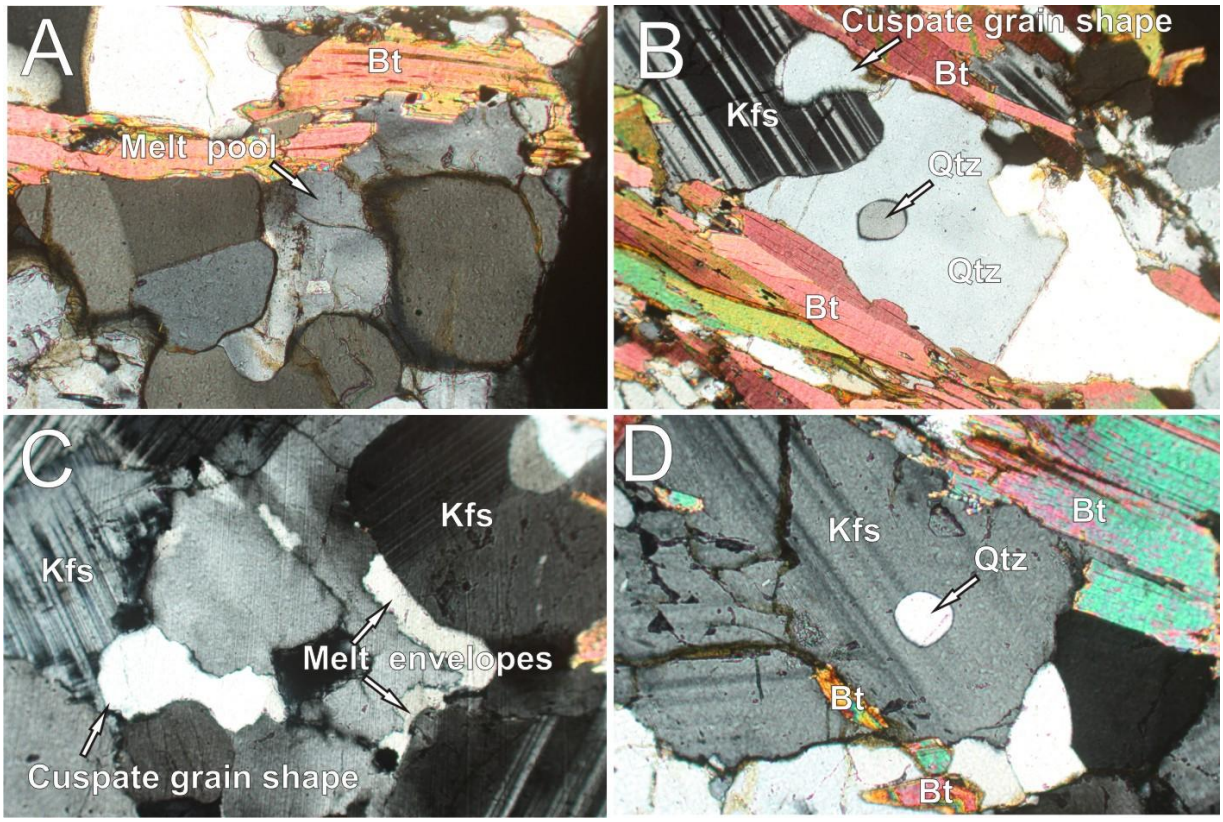

Figure 3.4-1: Images of possible evidence of partial melting. (A) Melt pool following grain boundaries. Melt is forming from the biotite. Crossed polars; base of image: 1.2mm. (B) Highly cuspate grain shapes and a xenolith of qtz interpreted as melt reactant residual. Crossed polars; base of image: 1.6mm. (C) Cuspate grain shapes and melt envelopes along grain boundaries. Crossed polars; base of image: 1.6 mm. (D) Xenolith of quartz in K-feldspar interpreted to be melt reactant residuals.

Although the microstructural evidence of partial melting is indicative, it is not conclusive. The lack of clear evidence may be due to a syn- to post-melting deformation event recrystallizing and overprinting the partial melt microstructures.

Melt ratio estimation from P-T conditions

In chapter 3.3, minimum P-T conditions were obtained at 0.9 GPa and 680°C. The melt fraction calculated at minimum P-T condition was calculated using Perple_X 07 [1] to 13%. This confirms the rather widespread occurrence of leucosomes in field, both in meso- and micro scale.

3.5 DEFORMATION MICROSTRUCTURES

This section contains a description of deformation related microstructures. The identification and interpretation of different microstructures is used as a part of the shear sense- and deformation mechanism determination.

3.5.1 SHEAR SENSE INDICATORS

In thin section, many reliable shear sense indicators can occur, helping to establish movement directions. Of 14 thin sections in total, 8 thin sections have been found to give reliable shear senses. A short description of the different shear sense indicators found in the thin sections will now follow.

S-C fabrics (described in Berthé et al., 1979) occur in both the garnet-mica schist and the amphibolite. In the garnet-mica schist, the S-C fabrics are found in aggregates of biotite, giving the individual grains a 'mica fish' appearance (fig. 3.5-1 A). The same fabrics are also found in aggregates of quartz and biotite, were the S-direction is marked by relatively competent quartz grains, while the C-direction or slip plane is defined by the long axis of biotite. In the amphibolite, the fabrics occur in association with aggregates of ~80% hornblende and ~20% quartz, were quartz acts as a weak phase and S-direction is defined by the long axis of hornblende grains which locally inhabit σ-clast shape. C-direction is defined by the deflection of σ-clast tails.

Shear bands represent local ductile faults with a synthetic normal fault displacement sense (Stünitz, 1989). Such features occur in the amphibolite of the SMC (fig. 3.5-1 E).

σ-clasts are unrotated clasts of material that develop σ-shaped tails by either pressure solution followed by precipitation, or dynamic recrystallization of clast material (Simpson & Schmid, 1983). Such shapes occur in (1) hornblende (fig. 3.5-1 B), (2) in quartz clasts which has undergone recrystallization, (3) as tails of quartz around garnets or (4) as σ-shaped symplectites of fine grained hornblende, biotite, quartz, titanite and garnet.

Rotated porphyroblasts are syndeformational blasts that have rotated during growth, leaving rotated inclusion trails. Such inclusion trails are found in garnets within the garnet-mica schist. The inclusions are comprised of biotite in the center and quartz towards the rims. This shear sense indicator reflects a late stage of deformation because the inclusions in the garnets are of the same minerals as those defining the present foliation (fig. 3.5-1 C).

Quartz shape fabrics are commonly used as shear sense indicator (e.g. Simpson & Schmid, 1983; Lister & Snoke, 1984). The quartz shape fabrics are asymmetric, with inclined grain long axes in relation to foliation. An appearent anticlockwise rotation of the grain long axes in relation to foliation is indicative of a dextral shear sense and vice versa. This type of asymmetric fabrics has been found in quartz veins in both the garnet-mica schist and the Tromsø Nappe amphibolite (fig. 3.5-1 D).

Mica fish (described in Lister and Snoke, 1984) are produced by the bending of mica grain edges so that they are given the shape of σ-clasts (fig. 3.5-1 F).

Quartz CPO is believed to be one of the most reliable shear sense indicators (e.g. Simpson & Schmid, 1983) and is commonly closely associated with quartz shape fabrics. The CPO has been investigated in a quartz vein within the garnet-mica schist using CIP microscopy. The results from this investigation are presented in chapter 3.6.

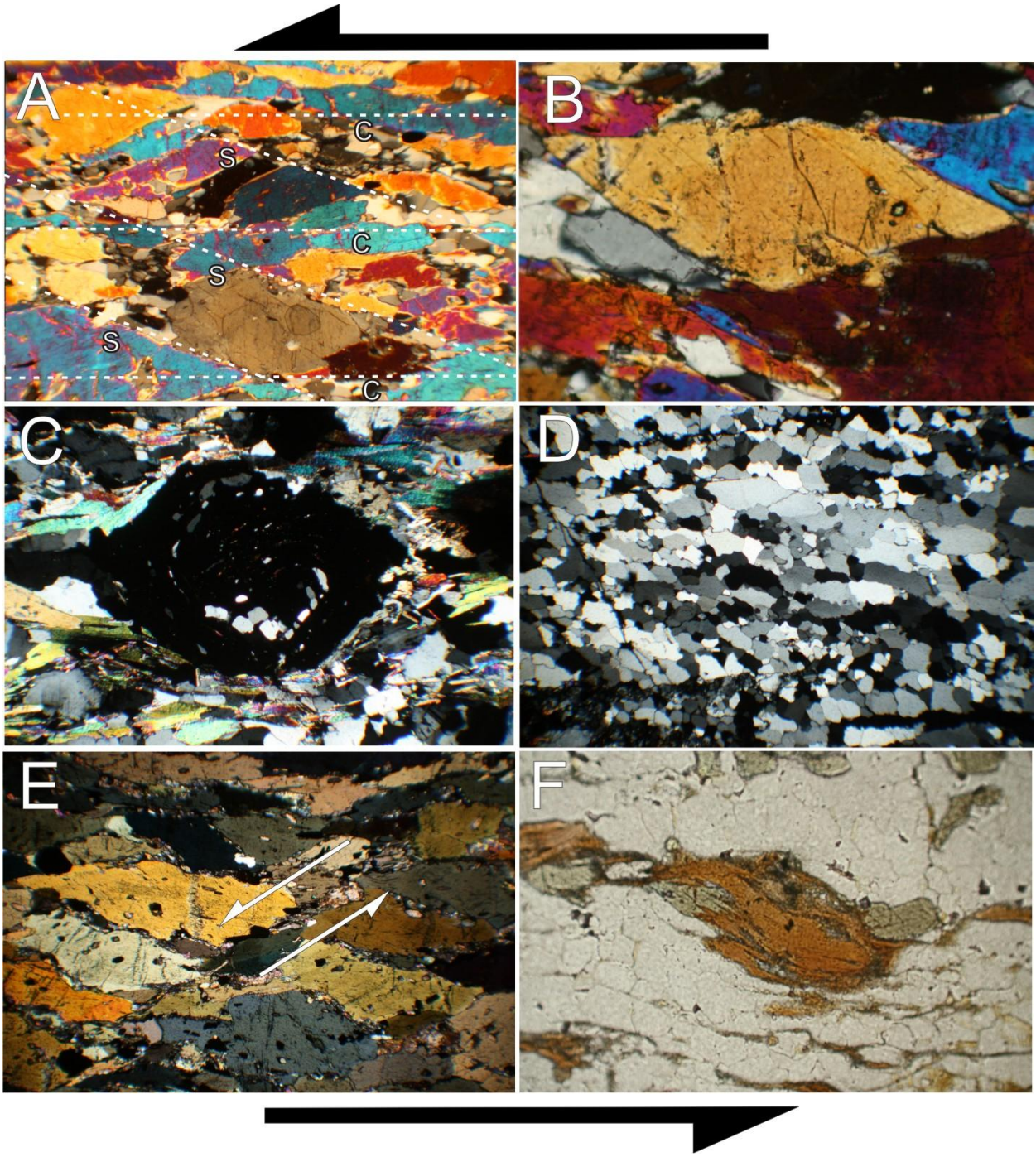

Figure 3.5-1: Images of shear sense indicators used to determine movement of upper block. Shear sense is sinistral. (A) S-C fabrics in an amphibolite. Crossed polars; base of image: 3.mm. (B) σ-clast comprised of hornblende in an amphibolite. Crossed polars; base of image: 1mm. (C) Rotated porphyroblast in a garnet-mica schist. The syndeformational garnet has rotated during growth, leaving rotated inclusion trails. Crossed polars; base of image: 2mm. (D) Quartz shape fabric in a quartz vein from a garnet-mica schist. Crossed polars; base of image: 3.6mm. (E) Shear band (parallel with white arrow) in an amphibolite from the SMC. Crossed polars; base of image: 3.6mm. (F) Mica fish in a garnet-mica schist. Base of image: 1.6mm.

The occurrence of shear sense indicators and the inferred movement direction of the upper block are given in table 3.5-1.

Sample No	Lithology	S-C fabrics	Sigma-clasts	Rotated porphyro-blasts	Qtz Shape fabric	Qtz CPO	Shear bands	Mica Fish	Movement of upper block
T8.4B	Garnet-mica schist	*	*				*		SW 210
T12.2	Garnet-mica schist	*	*		*	*		*	S 172
T12.1	Garnet-mica schist	*		*					SE 149
T8.5	Garnet-mica schist		*					*	S 180
T12.22[$]	Garnet-mica schist								S 113
T12.3	Amphibolite TN	*	*		*		*		SE 160
T1.8	Amphibolite Sk.		*				*		SE 164
T2.11	Cpx-grt amph.	*							NE 028

Table 3.5-1: The occurrence of shear sense indicators and the inferred movement direction of the upper block. ([$]): From Mikkelsen (2011).

The obtained movement directions of the upper block are presented on a geological map in fig. 3.5-2. 6 of the 8 obtained movement directions indicate movement to SSE. The remaining directions (sample T8.4B and T2.11) indicate movement directions in a SW- and NE direction, respectively. The implications of these results will be discussed in chapter 4.2.2.

Figure 3.5-2: (Next page) Geological map with the determined shear senses from table 3.5-1. Arrows indicate the movement of the upper block.

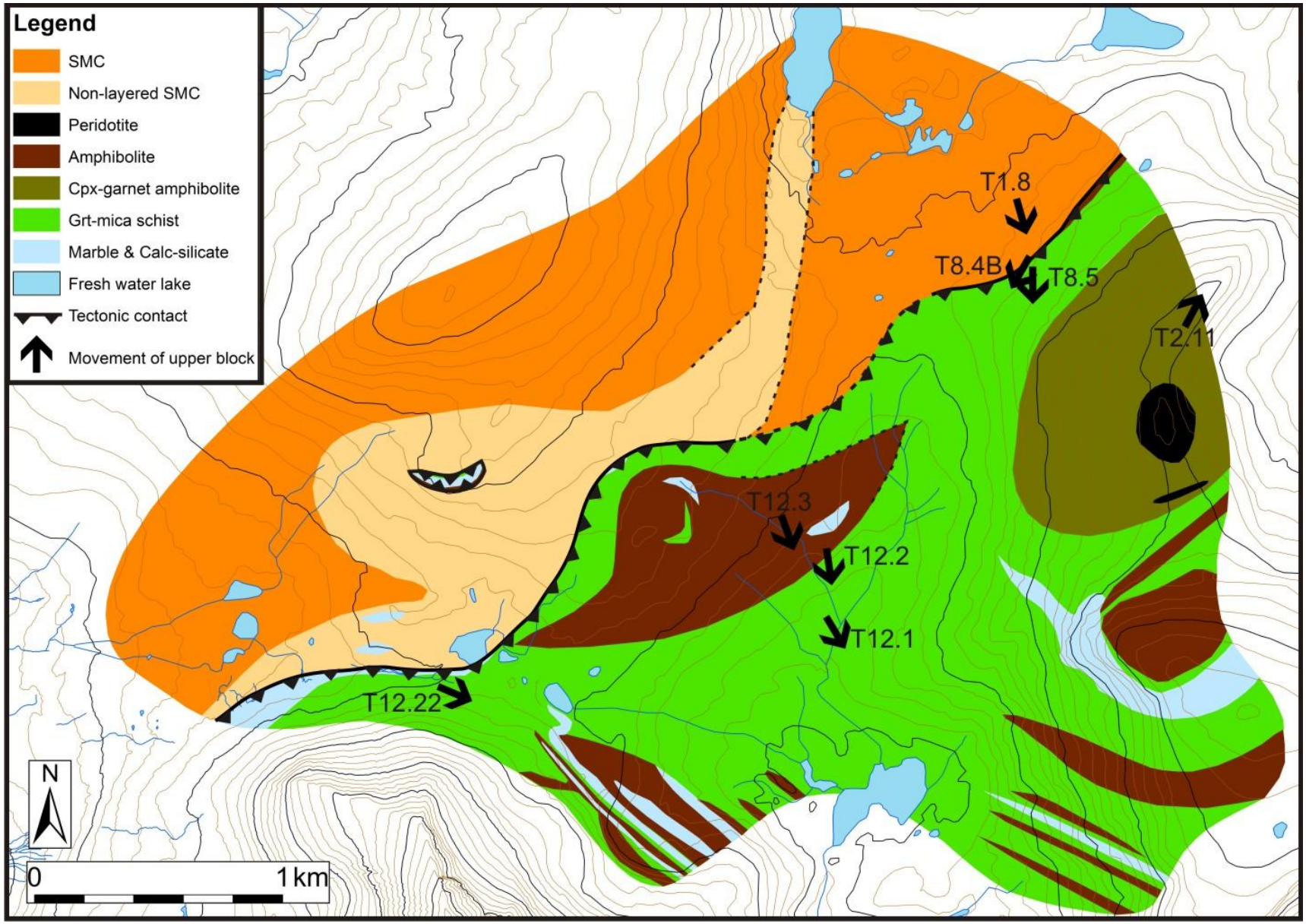
Legend
SMC
Non-layered SMC
Peridotite
Amphibolite
Cpx-garnet amphibolite
Grt-mica schist
Marble & Calc-silicate
Fresh water lake
Tectonic contact
Movement of upper block
T1.8
T8.4B
T8.5
T2.11
T12.3
T12.2
T12.1
T12.22
N
0
1 km

3.5.2 QUARTZ RECRYSTALLIZATION

Several types of dynamic recrystallization microstructures have been identified in thin sections. The microstructures are useful for estimating temperature and pressure conditions during deformation. A short description of the different microstructures will now follow.

Dynamic recrystallization in quartz occurs through the process of dislocation creep. The process is divided into three mechanisms: **grain boundary bulging**- (GBL), **subgrain rotation**- (SGR) and **grain boundary migration** (GBM) recrystallization (fig. 3.5-3). The mechanism of which is dominating is dependent on temperature and strain rate and can therefore be used as an approximate geothermometer if the strain rate is known (Stipp et al., 2002a) (fig. 3.5-4). In addition, the formation and orientation of subgrain boundaries varies with temperature and pressure. At low temperatures, if basal <a> slip is activated (Trépied et al., 1980), subgrain boundaries tend to be prism-plane parallel. At higher temperatures, if prism <c> slip is activated (Trépied et al., 1980), basal-parallel subgrain boundaries accompany the prism-parallel subgrain boundaries, creating **chessboard** patterns. The onset of chessboard pattern with increasing temperature is believed to coincide with the α-β quartz transition and may be used for thermobarometry (Kruhl, 1996; 1998) (fig. 3.5-4). Mainprice et al. (1986) suggest that the onset of chessboard patterns is controlled by partial melting and wet conditions rather than the α-β quartz transition.

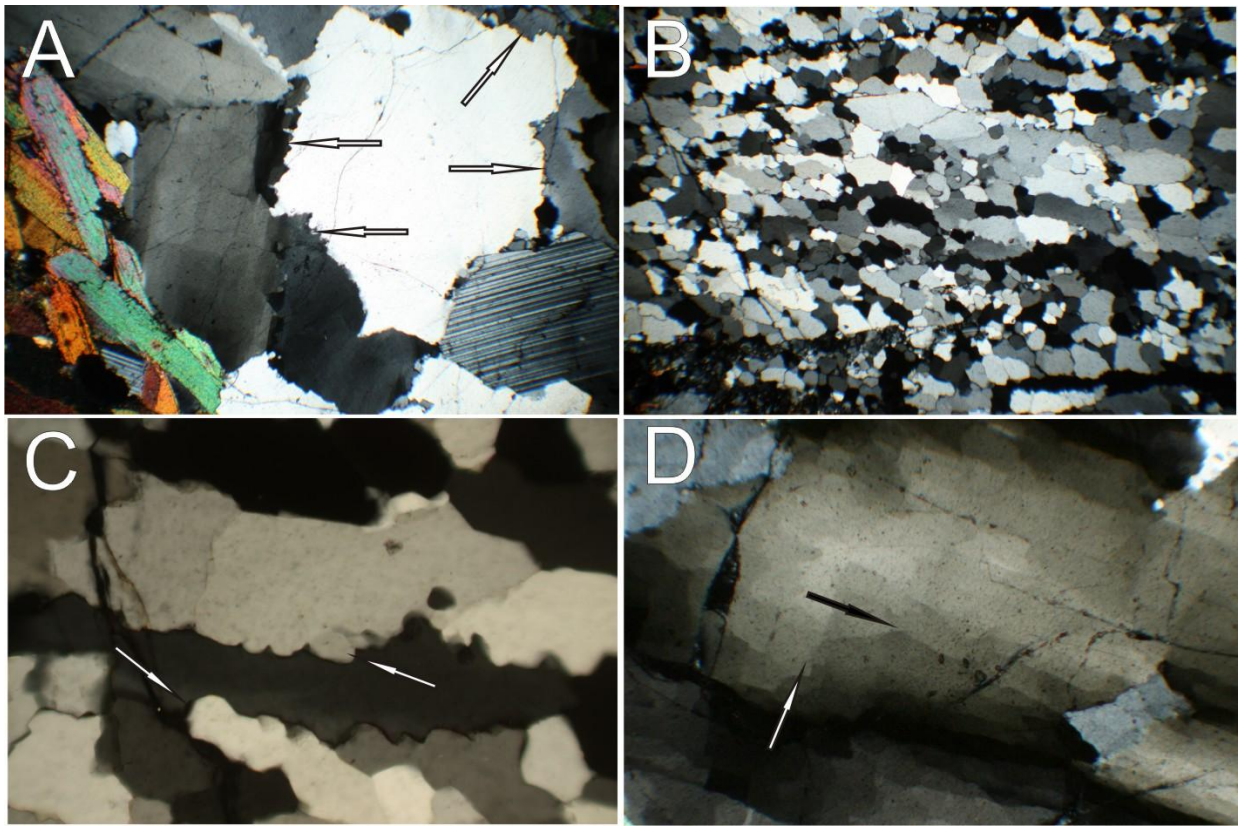

Figure 3.5-3: Images of dynamic recrystallization mechanisms found in thin sections. (A) BLG (arrows) in a leucosome. Crossed polars; base of image: 3.6mm. (B) SGR (and GBM) in a quartz vein from a garnet-mica schist. Crossed polars; base of image: 3.6mm. (C) GBM (arrows) in a quartz vein from a garnet-mica schist. Crossed polars; base of image: 0.4mm. (D) Chessboard pattern in quartz. The black arrow indicates the orientation of prism-parallel subgrain boundaries while the white arrow indicates the orientation of basal-parallel subgrain boundaries. Crossed polars; base of image: 1.8mm.

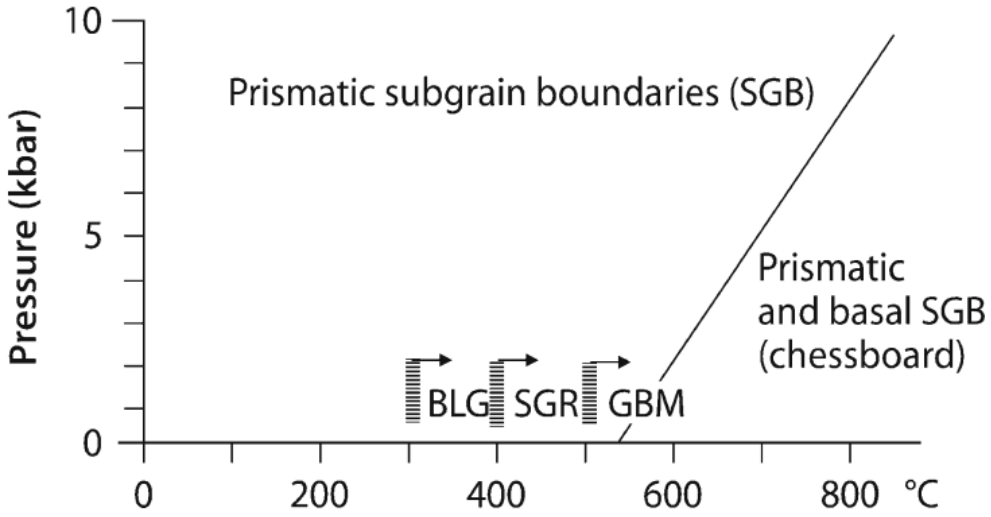

Figure 3.5-4: Fields of dynamic recrystallization and the appearance of chessboard subgrains in quartz in a P-T diagram. Arrows indicate the effect of a decrease in strain rate and bars indicate transition zones. From Passchier & Trouw (2006), based on Stipp et al. (2002a) and Kruhl (1996; 1998).

The distribution of observed dynamic recrystallization microstructures in quartz from thin sections is shown in table 3.5-2.

Sample No.	Lithology	BLG	SGR	GBM	Chessboard
T8.4B	G-m schist	-	medium	weak	weak
T12.1	G-m schist	weak	medium	strong	-
T12.2	G-m schist	-	strong	medium	weak
T8.5	G-m schist	-	weak	weak	-
T8.6	G-m schist	strong	strong	strong	medium
T8.4A	Amphibolite TN	-	medium	weak	-
T12.3	Amphibolite TN	-	strong	-	-
T4.10	Calc-silicate TN	-	medium	strong	weak

Table 3.5-2: Overview of the distribution of observed dynamic recrystallization microstructures in quartz from thin sections. TN = Tromsø Nappe.

All of the dislocation creep mechanisms in addition to chessboard patterns are represented in the thin sections. SGR and GBM are the most common types of microstructures.

3.6 C-AXIS PREFERRED ORIENTATION, GRAIN SIZE AND GRAIN SHAPE

In this section, the results from the CIP-, grain size- and grain shape analysis of quartz in a vein from the garnet-mica schist will be presented. The COIs and c-axis pole figures calculated using the CIP-method [2] is useful for determination of strain geometry (Schmid and Casey, 1986; Law, 1990), shear sense (Simpson & Schmid, 1983) and temperature of deformation (Stipp et al., 2002a and b). The grain size- and grain shape analysis is used to give a kvantitative estimation of grain- size and shape fabrics and how they may vary with changing deformation processes. The data is produced as described in chapter 2.4.

The quartz vein could visually be divided into two domains by grains size; one relatively coarse grained domain (~30%) and one finer grained domain (~70%). The domains are commonly separated by <0.03mm thin bands of biotite, but transitional changes between the two domains occur as well.

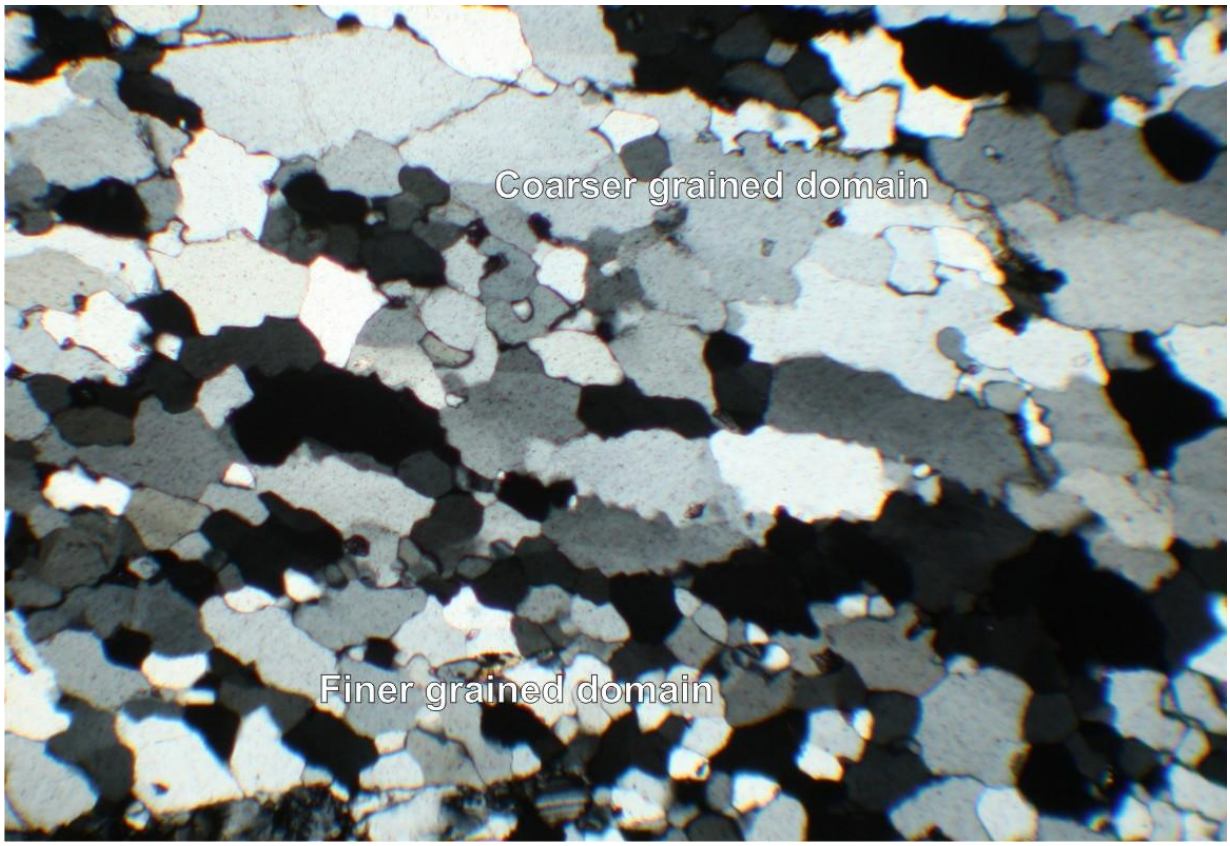

Fig. 3.6-1: Image of parts of the quartz vein used for the CIP-method showing the occurrence of finer- and coarser grained domains. Sinistral shear sense. Crossed polars; base of image: 2mm.

3.6.1 C-AXIS PREFERRED ORIENTATION

C-axis pole figures (fig. 3.6-2) show that the CPO is not randomly orientated, but clustered in certain areas of the pole figures. Using fig. 3.6-2, the different areas can be categorized into three main populations: (1) grains with the c-axis in the clusters rotated around an axis parallel to Y with an angle -10/+30° in relation to the the X-direction, measured in an anticlockwise sense (population referred to as X-maxima from here on), (2) grains with the c-axis in the clusters sub-parallel to the Y-direction (population referred to as Y-maxima from here on) and (3) grains with the c-axis in the clusters rotated around an axis parallel to Y with an angle of 20-45° to the Z-direction, measured in an anticlockwise sense (population referred to as Z-maxima from here on). In general, an anticlockwise rotation of the X- and Z maximas are consistent with a sinistral shear sense (Simpson & Schmid, 1983).The three main populations have been treated separately in the grain size and grain shape analysis.

The lateral distribution of grains within different populations (fig. 3.6-2) are well scattered. Some sites show a slight layered distribution with the angle of the layers in relation to the foliation similar to the grain shape fabric. In the finer grained domains, the X-maxima is

dominating (site 06 and 07) while in coarser grained domains the contributions from the different populations seems to be more or less equal (site 01 and 08) Figure 3.6-3 indicates that the X- and Y-populations are more widespread than the Z-population.

The grain long axis orientation (PAROR) indicates a strong grain shape fabric. The shape fabric has a slightly steeper orientation in relation to foliation in coarser grained domains (site 01 and 08) compared to finer grained domains (site 02, 06 and 07) (see fig 3.6-2). The grain boundary orientations (SURFOR) indicate that grain shapes are preferably rhomb like with orientations at a small angle to the foliation and a sub-maxima at a high angle to the foliation.

The COIs and c-axis pole figures from the remaining sites can be found in the appendix.

Figure 3.6-2: (Next page) C-axis orientation images presented with two different look-up tables (bottom) so that the distribution of the different populations are clearly shown. Four representative sites are presented with pole figures, grain long axes- (PAROR) and grain boundary orientations (SURFOR) for all grains within each site. Grains touching the edge is not considered in the COIs to the right or in the PAROR and SURFOR analysis. The COIs and c-axis pole figures from the remaining sites are shown in the appendix.

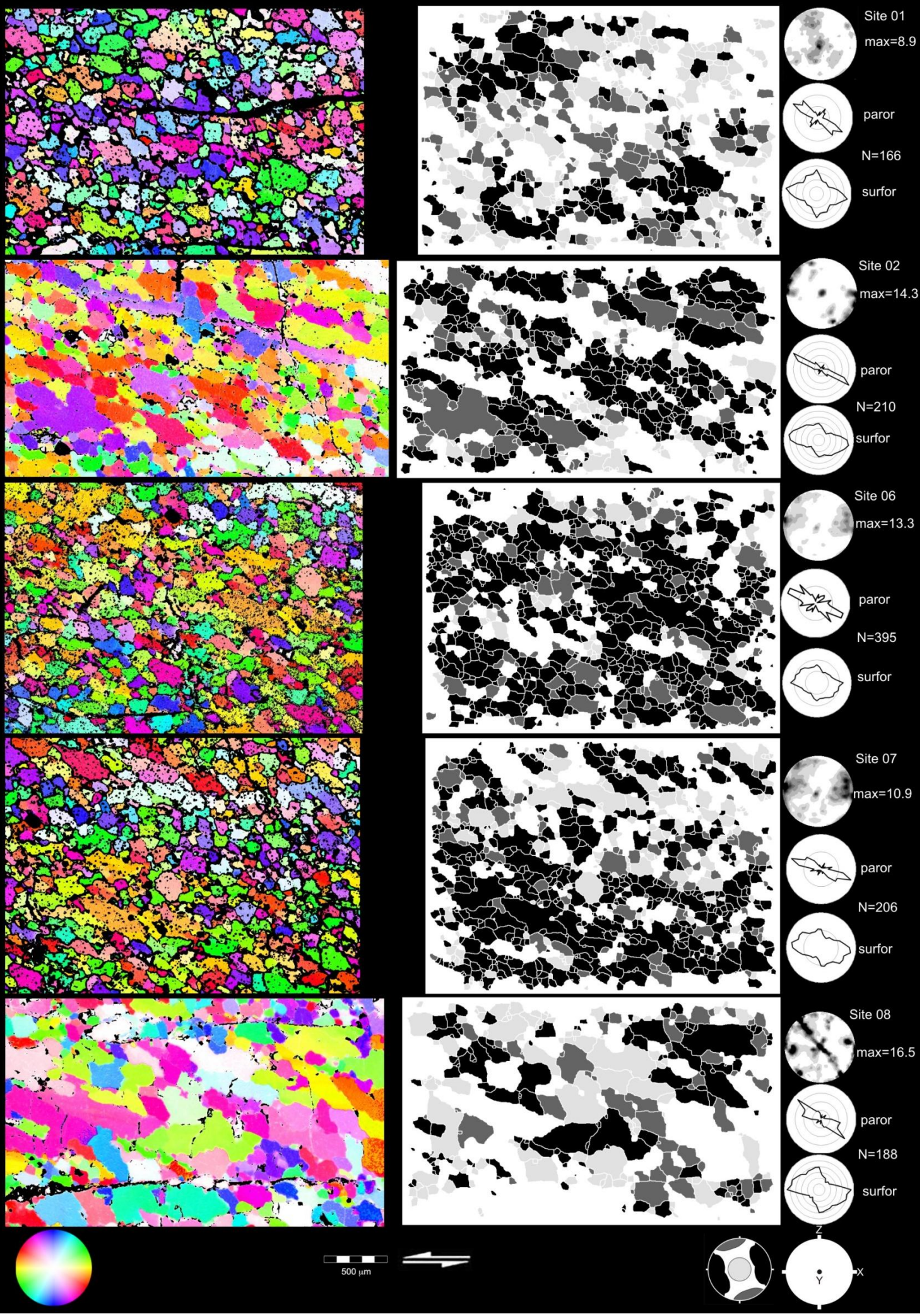
Site 01
max=8.9
paror
N=166
surfor
Site 02
max=14.3
paror
N=210
surfor
Site 06
max=13.3
paror
N=395
surfor
Site 07
max=10.9
paror
N=206
surfor
Site 08
max=16.5
paror
N=188
surfor
500 μm
Z
X
Y

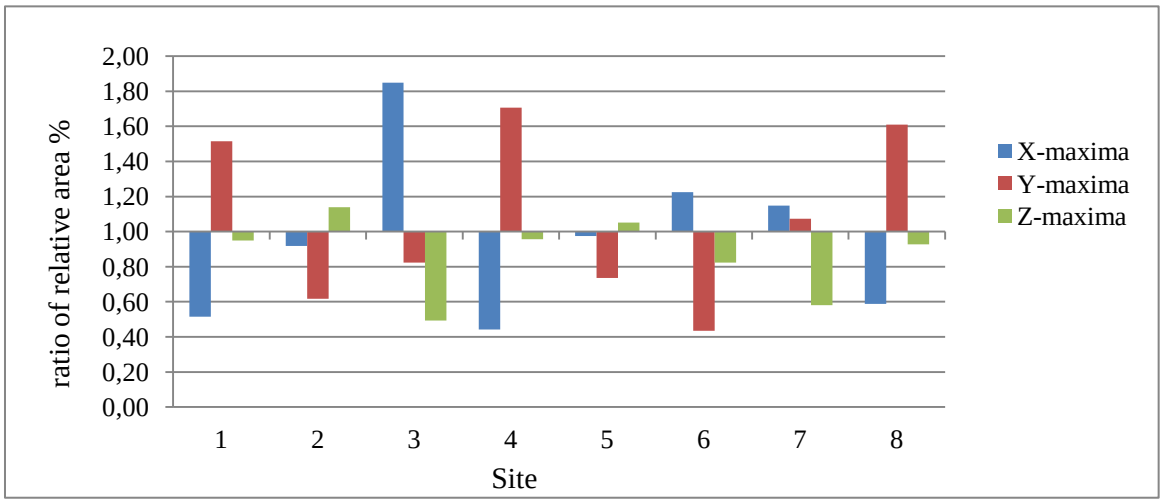

Figure 3.6-3: For each site, the ratio of area distribution of populations in relation to the expected area distribution given a random distribution of c-axis orientations is presented. For a random distribution of c-axis orientations, Y- and Z- maxima are calculated to give values of 13.6 area % and the X-maxima ~39 area %. The values have been adjusted so that 1 indicates c-axis orientations equivalent of a random distribution. All sites except 06 show peaks in area % in at least one of the populations. The X-maxima shows high values in site 03, 06, and 07. Y-maxima shows high values in site 01, 04 and 08. Z-maxima shows high values in site 02. Site 05 does not have any peaks, but show a low Y-maxima value.

3.6.2 Grain size and -shape

As a part of the CIP analysis, grain boundary maps of each site were produced. These maps were used during further investigations of grain size and –shape. In total, 3245 grains from the three different pole maxima populations were used in a grain size analysis. The results are presented in figures 3.6-4 to 3.6-6.

The results indicate that grains with CPOs close to the Y-direction tend to have a narrower- and finer grain size distribution than the grains with their CPOs close to either the X- or the Z direction. Although the grains are differently distributed, they all have dominant grain size at ~40μm (fig. 3.6-4).

The volumetric grain size distribution (fig.3.6-5) obtained using the StripStar software [2] confirms that the Y-maxima population is dominated by a finer grain size than that of the X- and Z-maxima populations. All populations show a sub-uniform distribution, with a slight peak at Dequ = ~180 μm for the X-maxima, Dequ = ~60 μm for Y-maxima and Dequ = ~120 μm for Z-maxima.

The aspect ratio distribution (fig. 3.6-6) gives nearly identical results for all three populations.

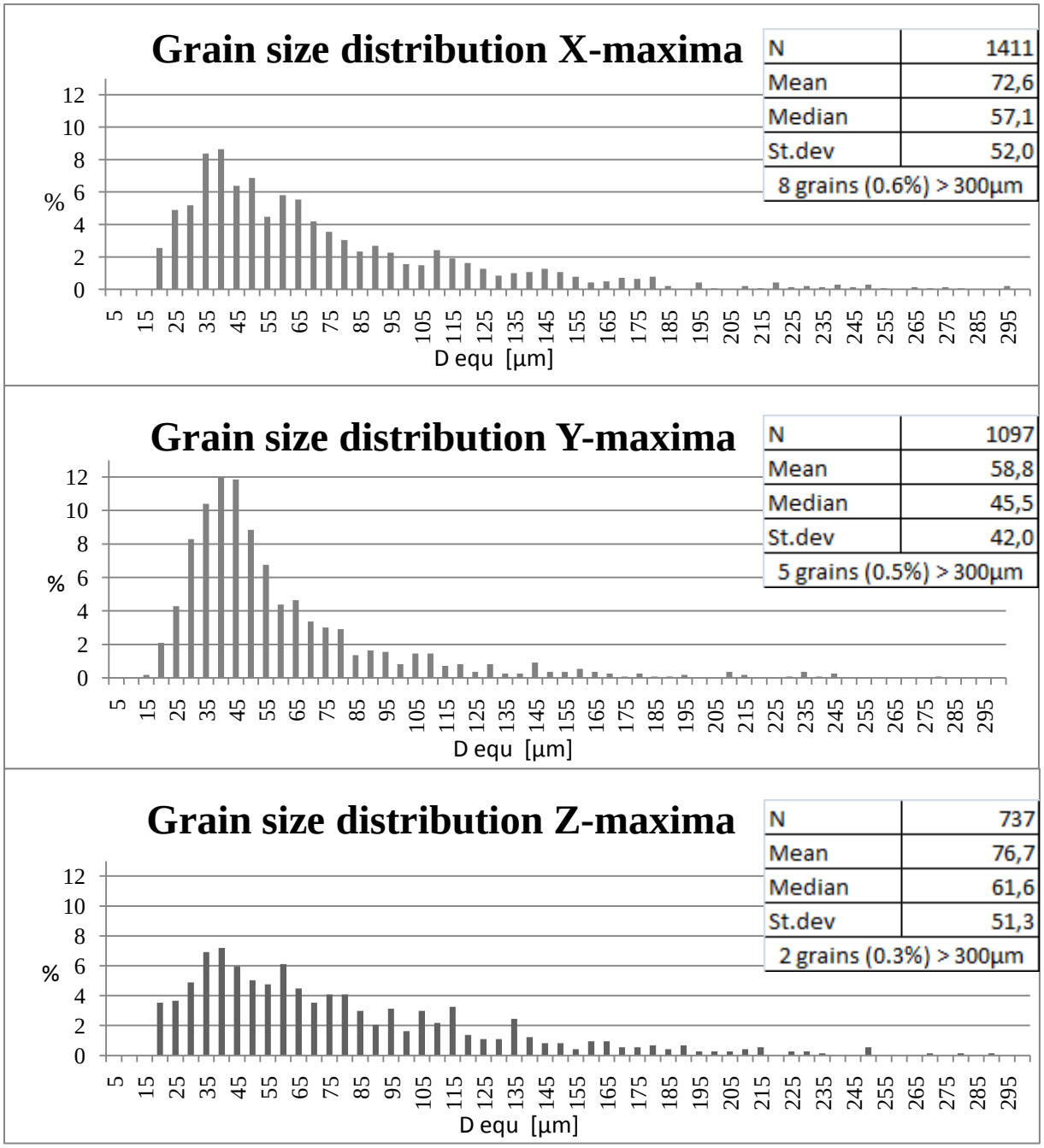

Figure 3.6-4: Histograms of the grain size distribution for the three different populations. Average recrystallized grain size is calculated as the diameter of a circle with the equivalent area of the individual grains. The average recrystallized grain size peaks at about 40µm. Grains with CPO close to the Y-direction have a more distinct normal distribution peaking at about 40µm. Grain size distribution from grains with CPO close to the Z- or X-directions is more distributed, but still peaking at about 40µm.

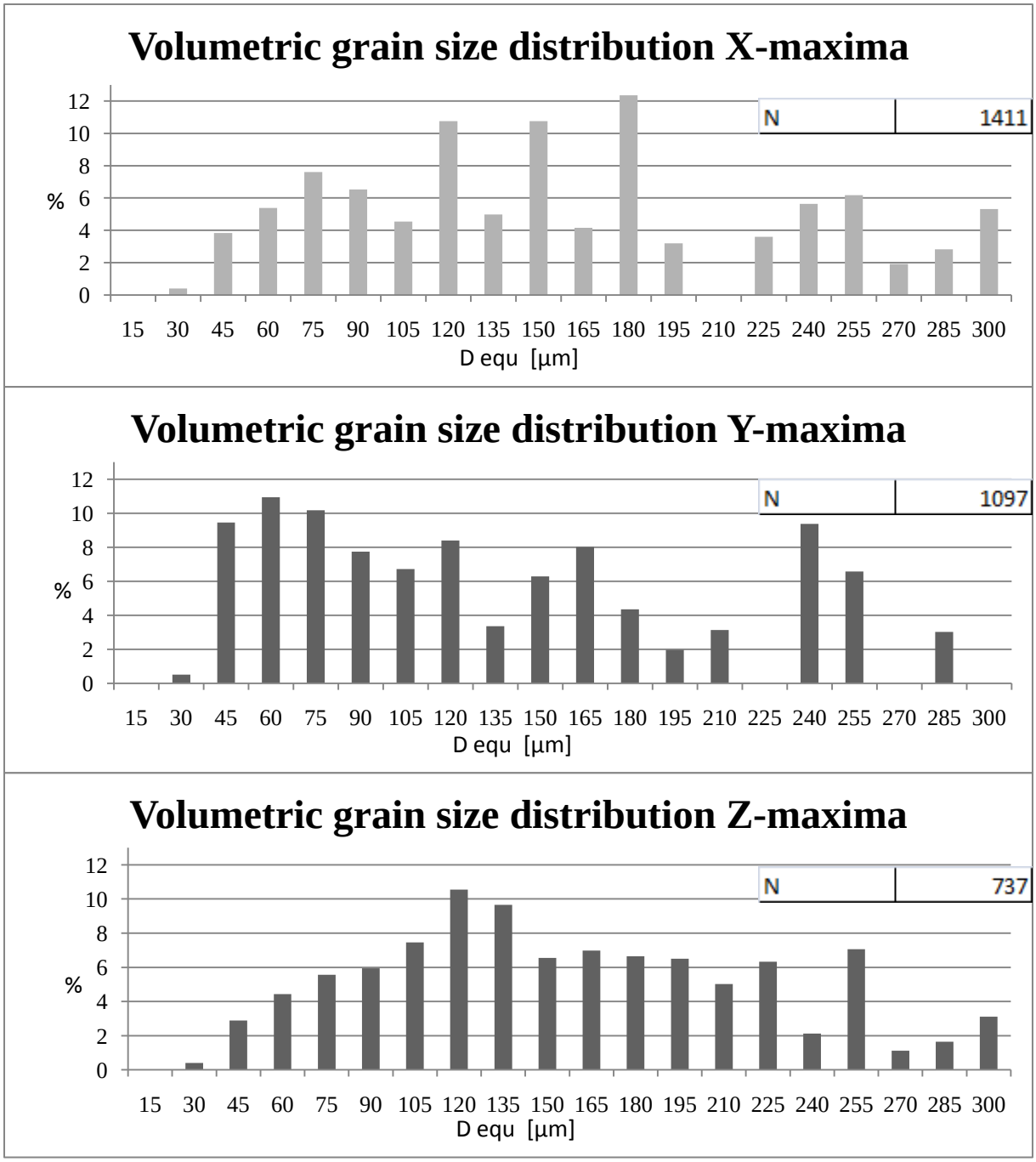

Figure 3.6-5: Histograms showing volumetric grain size distribution for each population. The distribution is relatively uniform and as with the 2D grain size distribution, the grains with CPO close to the Y-maxima are dominated by smaller grains than the grains with CPO close to the X- or Z-direction. The volumetric grain size distribution is calculated using StripStar [2].

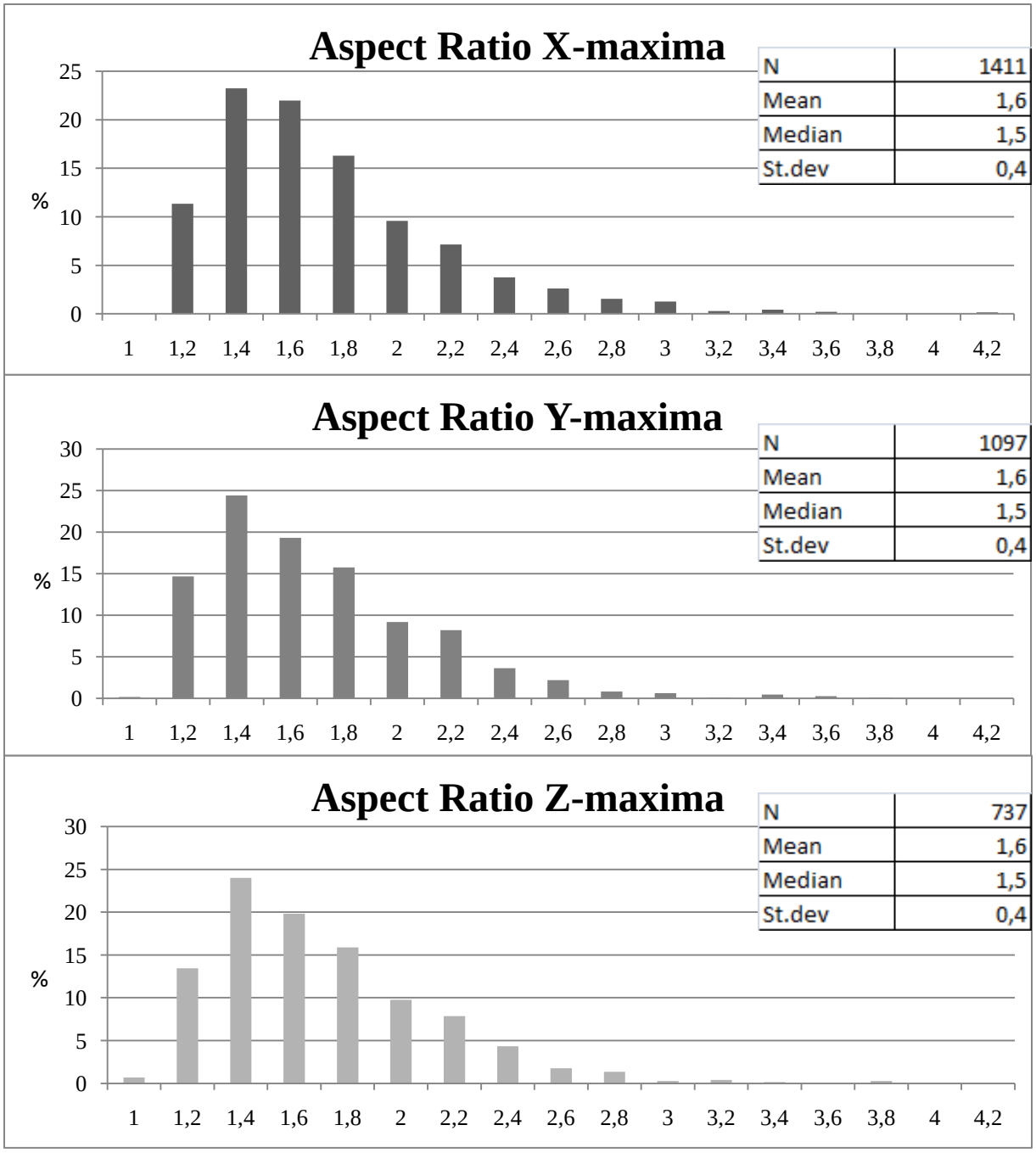

Figure 3.6-6: Histograms showing aspect ratio distribution of grains from the different populations. The distribution is close to identical for all three populations.

The grain shape analysis was applied on 1306 grains and the results are presented in fig. 3.6-7. A strong grain shape fabric with sinistral shear sense (e.g. Simpson & Schmid, 1983) is visible. The grain long axes distribution for the Y-maxima population is lesser aligned than that of the X- and Z-maxima populations and the median angle is slightly different in all three populations. The X- and Z maxima show a strong grain shape fabric with grain long axes orientation maximum at 130/310 and 110/290 degrees, respectively. The Y maxima shows several peaks at 130/310, 110/290 and 70/250 degrees, but still a clear grain shape fabric.

The grain boundary orientation indicates that grain shapes are preferably rhomb like with orientations at a small angle to the foliation and a sub-maxima at a high angle to the foliation for the X- and Z-maxima populations. The grains from the Y-maxima population tend to have a squared shape.

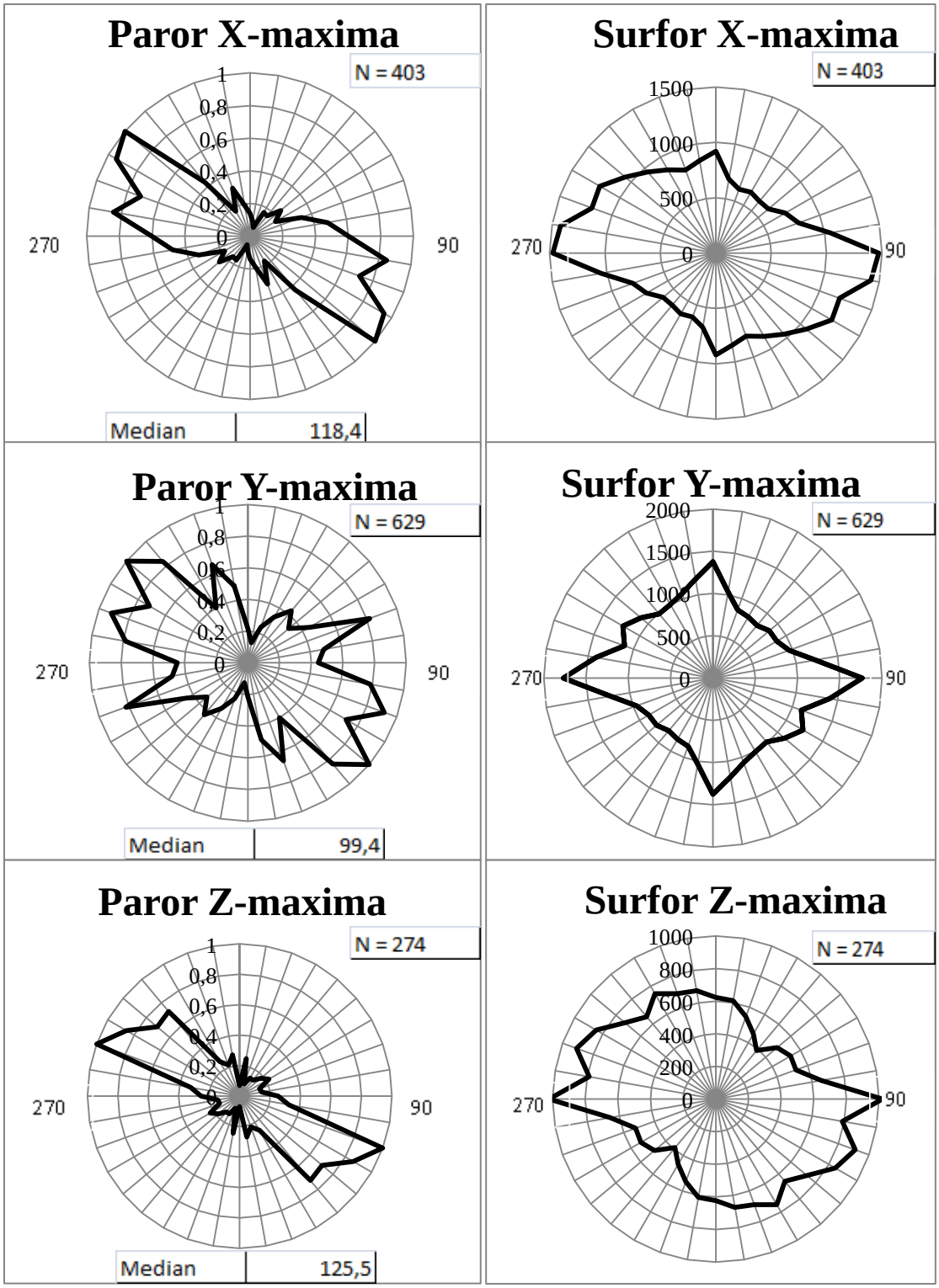

Figure 3.6-7: Grain long axes- (PAROR) and grain boundary orientations (SURFOR) presented in rose diagrams. Foliation is horizontal (90/270). A preferred shape fabric with sinistral shear sense is clearly evident in all three populations (Simpson & Schmid, 1983). The X- and Z maxima show a strong grain shape fabric with grain long axes orientation maximum at 130/310 and 110/290 degrees, respectively. The Y maxima shows several peaks at 130/310, 110/290 and 70/250, but still a clear grain shape fabric. In grains with CPO close to either X- or Z-direction, grain boundary diagrams indicate that grain shapes are preferably rhomb like with orientations at a small angle to the foliation and a sub-maxima at a high angle to the foliation. Grain boundary orientation of the Y-direction shows that grains of this population tend to be square.

3.7 STRENGTH OF CPO, STRESS AND STRAIN RATE ESTIMATION

The strength of CPO, flow stress estimation and strain rate estimation has been calculated using the equations presented in ch. 2.5. The flow stresses has been calculated for each of the c-axis pole figure maxima populations in addition to all grains combined using both the median and the mean recrystallized grain size calculated in the previous chapter (fig. 3.6-4).

The strain rate has been calculated using the minimum and maximum results from the flow stress calculation (bold numbers, table 3.7-2) for each population and all grains combined using two different sets of constants given in table 3.7-1.

	A [$MPa^{-n}s^{-1}$]	n	Q [kJ mol^{-1}]
a) Gleason & Tullis (1995)	$1.1*10^{-4}$	4	223
b) Rutter & Brodie (2004)	$300*10^{-4.93}$	2.97	242

Table 3.7-1: The constants used in the calculations of strain rate in table 3.7-2.

	Equation	X-maxima	Y-maxima	Z-maxima	All grains
Strength of CPO	1	0.26	0.09	0.23	0.19
Flow stress mean [MPa]	2	**22**	**26**	**21**	**23**
Flow stress median [MPa]	2	27	32	25	29
Flow stress mean [MPa]	3	25	29	24	26
Flow stress median [MPa]	3	**30**	**36**	**28**	**32**
Flow stress mean [MPa]	4	24	28	23	25
Flow stress median [MPa]	4	29	35	27	31
Strain rate min. estimate [s^{-1}]	5 (a)	$1.5*10^{-11}$	$3.0*10^{-11}$	$1.3*10^{-11}$	$1.8*10^{-11}$
Strain rate max. estimate [s^{-1}]	5 (a)	$5.3*10^{-11}$	$\mathbf{1.1*10^{-10}}$	$4.1*10^{-11}$	$6.9*10^{-11}$
Strain rate min. estimate [s^{-1}]	5 (b)	$1.9*10^{-12}$	$3.1*10^{-12}$	$\mathbf{1.6*10^{-12}}$	$2.1*10^{-12}$
Strain rate max. estimate [s^{-1}]	5 (b)	$4.7*10^{-12}$	$8.0*10^{-12}$	$3.8*10^{-12}$	$5.7*10^{-12}$

Table 3.7-2: Results from calculations of the strength of CPO, stress flow and strain rate for each population in addition to all grains combined. The flow stress is calculated for both the mean and median value of the grain size. The strain rate estimates are calculated using the minimum and maximum values from the flow stress. Equations and constants used are presented in chapter 2.5.

The calculated strength of CPO (table 3.7-2) shows that the X- and Z-maxima have a stronger CPO than the Y-maxima. The weaker strength of CPO for Y-maxima is supported by the PAROR analysis, which indicates a weaker grain shape fabric for the Y-maxima population.

The flow stresses calculated for the different populations varies some with the use of the different paleopiezometer. Still, it is evident that the Y-maxima population was subjected to higher flow stresses (average: 31 MPa) than the X- and Z-maxima (average: 26 and 25 MPa, respectively). This is a direct result of the finer grain size measured in the Y-maxima population compared to the X- and Z-maxima populations.

The strain rate estimation varies from $1.6*10^{-12}$ and $1.1*10^{-10}$ for the different populations. The average bulk strain rate is calculated to $2.4*10^{-11}$, which is an expected value at the given temperature (Stipp et al., 2002a).

4. DISCUSSION

4.1 LITHOLOGIES

This section will discuss the characteristics of the lithologies and their relations to the Caledonian Orogeny. Many of the observations made in this thesis fit well with previous studies in the area (Gee, 1975; Roberts & Gee, 1985; Krogh et al., 1990; Rindstad, 1992; Zwaan et al., 1998; Selbekk et al., 2000; Selbekk & Skjerlie, 2002; Roberts, 2003; Ravna & Roux, 2006; Roberts et al., 2007; Corfu et al., 2003; 2007) and will not be discussed in detail. Observations which are not previously described or that are contradictory to previous studies will be discussed.

4.1.1 LITHOLOGIES WITHIN THE NAKKEDAL NAPPE COMPLEX

The lithological characteristics of the SMC in the mapped area agree well with previous descriptions. Even so, variations within the unit are observed which have not been described in the literature.

The non-layered unit within the SMC is distinguished from the more common type of the SMC by being richer in Ca and showing a "salt and pepper"-texture in its melanosome. Locally, the "salt and pepper"-texture seems to be due to partial anatexis without any drainage of melt. This has created a random distribution of felsic melt pockets. The higher Ca-content could possibly be explained by metasomatosis in connection with the activation of the tectonic contact. As the non-layered unit in the SMC is not observed along the tectonic contact in the northern part of the mapped area, the unit as a whole is more likely a lens which has its origin due to magmatic layering in connection with the intrusion of the SMC protolith.

In addition, Ca-rich minerals also occur in felsic dykes that can be distinguished from oligoclase dykes in the field by their hardness. These Ca-rich dykes, showing a greenschist facies mineral assemblage, have been found close to-, and on both sides of the tectonic contact. They are interpreted to reflect a late stage movement and fluid infiltration along the tectonic contact.

4.1.2 LITHOLOGIES WITHIN THE TROMSØ NAPPE

The Tromsø Nappe commonly shows amphibolite facies mineral assemblages, but traces of an earlier high pressure metamorphic event are still present. The frequent bodies of eclogites reported in the literature, e.g. the Tromsdalstind eclogite, are spectacular examples and leads

to the question whether neighboring amphibolite bodies in the Tromsø Nappe show traces of eclogitization aswell. The Tromsø Nappe amphibolite occurs locally with residual clinopyroxene, indicative of an earlier higher pressure and temperature event, possibly granulite at facies conditions, but no eclogite is found in the mapped area.

The cpx-garnet amphibolite body of Langlitind, however, shows interesting petrological and textural properties that differentiate it from other amphibolites of the Tromsø Nappe and which give traces of a high pressure metamorphic event:

Thin sections of the cpx-garnet amphibolite show finer equigranular symplectites of cpx + plagioclase ± amphibole with rims of coarser grained amphibole. Similar symplectites are reported from retrograded omphacite in eclogites within the Tromsø Nappe (Ravna & Roux, 2006; Krogh et al., 1990; Broks, 1985). The similarities between the reported symplectites after omphacite in Krogh et al. (1990) and the observed symplectites in this thesis are striking (fig. 4.1-1) and leads to the interpretation that the Langlitind body reached eclogite facies metamorphism, later being overprinted by amphibolite facies metamorphism. Residual garnet in the cpx-garnet amphibolite may originate from the eclogite facies metamorphism, but this difficult to confirm with the investigations done in this thesis.

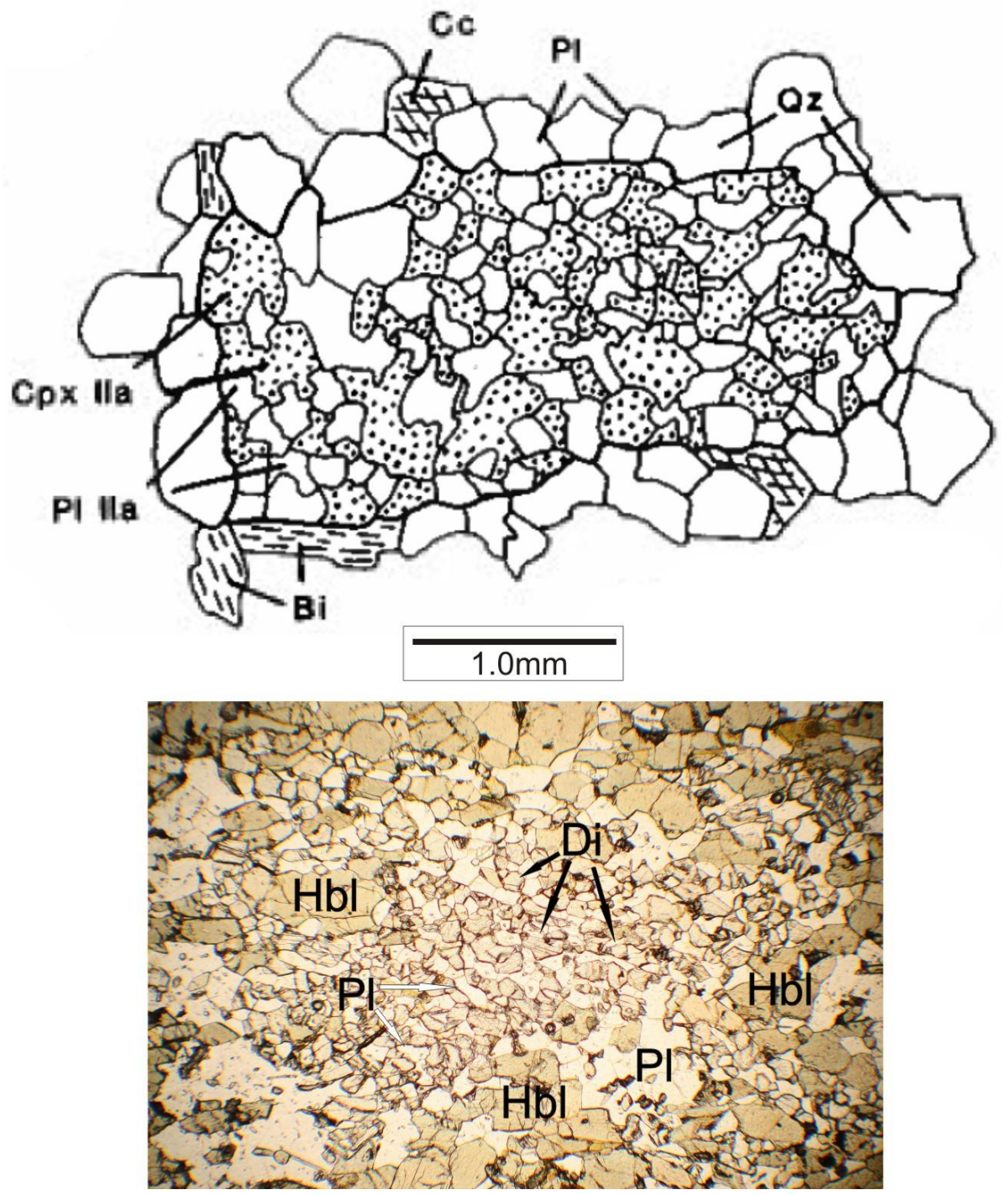

Figure 4.1-1: Comparison of symplectite development after secondary alteration of high pressure clinopyroxene. Top: Aggregate of recrystallized low-Al Na-augite (Cpx IIa) + plagioclase probably pseudomorphing an earlier high-Al Na-augite. From Krogh et al. (1990). Bottom: Fine grained symplectites with recrystallized diopside, plagioclase and hornblende found in the cpx-garnet amphibolite in the Tromsø Nappe. From this work. The textural similarities between the two examples are striking.

Other amphibolite layers and lenses do not show petrological and textural features similar to the Langlitind body, but residual clinopyroxene may be traces from post-eclogite-, pre-

amphibolite, metamorphic conditions in connection with D^T_1 and partial melting. This will be discussed further in chapter 4.3.1.

Another high pressure indicator from the Tromsø Nappe is the presence of rutile as inclusion in secondary titanite. This has previously been reported from eclogites in the Tromsø Nappe (Krogh et al., 1990; Ravna & Roux, 2006; Lucassen et al., 2010). Inclusions of rutile in titanite are found throughout the Tromsø Nappe and have been used as a criterion when differentiating between amphibolites of the SMC and the Tromsø Nappe. This criterion indicates that the Tromsø Nappe as a whole suffered higher pressure conditions prior to the amphibolite overprint and that the SMC suffered different metamorphic conditions.

Phengite has been reported from the garnet-mica schist of the Tromsø Nappe (Krogh et al., 1990), but only biotite and secondary muscovite have been observed in the mapped area. This, together with the lack of preserved eclogites, may be explained by the area being subjected to a more thorough amphibolite overprint than other parts of the nappe.

4.2 Structural and kinematic analysis

4.2.1 Mesoscale

When plotted in stereonets; lineations, fold axes and axial planes from the Tromsø Nappe fit nicely into two populations; one weak population with stretching lineations trending SW-NE and fold axes and axial planes trending SE-NW and one strong population with stretching lineations trending SE-NW and fold axes and axial planes trending SW-NE (fig 3.1-1 and 3.1-2). Orientation of foliation consistent with the strong population of structures confirms the observations of folding in the field. A scattering of the data may be explained by the effect of both the Tromsdalstind and Langlitind bodies acting as competent bodies within a weak matrix comprised of the garnet-mica schist and calc-silicates during deformation. This interpretation is supported by the deflection of foliation within the garnet-mica schist around the two bodies (fig 3.1-1). Such bodies could also develop pressure shadows, and together with any relative movement of the two bodies, these processes may create local structural elements which are not representative for the regional structural pattern. As the structural elements of the populations can be found independently of their relative position to the major bodies it is assumed that this effect was only local and that the structural data gathered in the area are representative for the region. The two populations are interpreted to reflect two directions of nappe movement, which in the Tromsø Nappe reflects D^T_1 and D^T_2. This will be discussed further in chapter 4.2.2.

The structural data from the Nakkedal Nappe Complex indicates that there are at least two populations of lineations within the uppermost parts of the SMC aswell. The two populations of lineation show nearly identical orientation to the two populations in the Tromsø Nappe. Both populations in the SMC are defined by amphibole and found on the S_3-foliation close to the contact. Based on the similarities in orientation of the two populations in the two nappes and that the the two sets of lineations are only found in the upper 10-15m of the SMC, it is interpreted that the lineations in the SMC is a result of a change in shear direction along the tectonic contact. Thus must the change in movement have occurred after the SMC and the Tromsø Nappe came into contact.

4.2.2 MICROSCALE

From chapter 3.4.1, it is evident that the shear sense indicators are abundant, especially in the garnet-mica schist. The movement of the upper block groups into two populations, fitting the structural data from chapter 3.1. One population is weak and connected with D^T_1, indicating a relatively early movement of the upper block towards either S-SW or N-NE direction. Unfortunately, as the only two thin sections showing the D^T_1 -population give opposite movement directions, the definitive direction of movement of this population cannot be obtained from this thesis. The second population, connected with D^T_2, is strong, show consistent shear senses and leaves little doubt that the movement of translation was top towards SSE. In general, the expected direction of movement in the Caledonian nappes is ESE (Binns, 1978; Zwaan et al., 1998). The results obtained here fit relatively well and indicates that minor local variations in the direction of the main nappe movement may have occured.

The occurrence of two structural populations at ~90° to each other as seen in the area of investigation has been reported in regions with oblique plate convergence where deformation is partitioned into strike-slip and contractional components. (e.g. Tikoff & Teyssier, 1994; Bergh et al., 2000). Roberts (2003) states that the Caledonian Orogeny evolved through a gradual, oblique convergence and hence, this possibility must be considered. However, as the two structural populations in this case are defined by minerals belonging to different metamorphic facies, they are clearly separated in time and conditions of deformation. Thus, the observed variations in orientation are difficult to explain by partitioning during deformation. When considering (1) that the deformation is suggested to have been continuous for a considerable amount of time and strain and (2) the complexity of the Caledonian Orogeny reported in the litterature, involving several subduction zones and exotic terrains, it

is much more likely that the two directions of movement reflect two seperate kinematic events. An adjustment in the stress pattern may have caused a change in direction of nappe translation from either SW or NE to SSE during uplift and retrograde metamorphism.

4.3 Evidence for partial melting

Indications of partial melting have been found in:

(1) the occurrence of meso- and microscale quartzo-feldspathic leucosomes (ch. 3.1 and 3.2),

(2) P-T pseudosection melt ratio estimation (ch. 3.3),

(3) micro-scale, melt-indicative pseudomorphs (ch. 3.4.3).

It is therefore concluded that the Tromsø Nappe suffered at least one event of partial melting. Due to the overprint of SGR and BLG in the leucosomes, the partial melting is interpreted to have happened early in a post-Scandian uplift, possibly in connection with D^{T}_{1}, and later being overprinted by D^{T}_{2}-recrystallization microstructures. This event of partial melting is believed to correspond to the second event of partial melting described by Stevenson (2005; 2006) based on the similarities in obtained P-T conditions.

4.4 Deformation microstructures in quartz

4.4.1 Recrystallized grains

From table 3.4-2 (chapter 3.4.2), it is evident that all of the recrystallization mechanisms in quartz are represented in thin sections. This indicates that deformation took place over a large span of temperatures and/or strain rate, in order to produce such diversity of mechanisms (Stipp et al., 2002a). The relationship between dislocation creep mechanisms, strain rate and temperature is given in fig. 4.4-1.

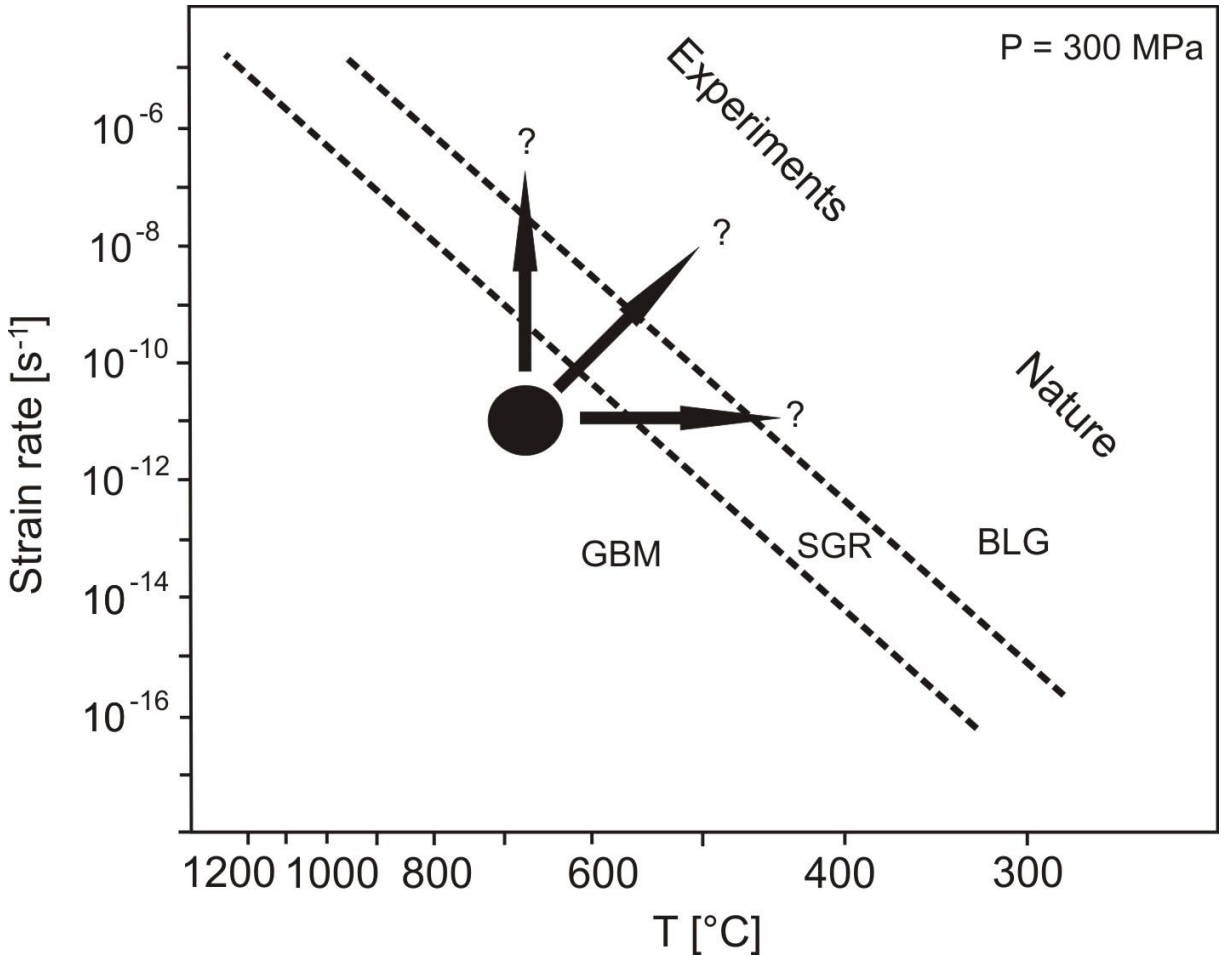

Figure 4.4-1: Strain rate versus temperature diagram with microstructural correlations. Black field indicates conditions of deformation in the garnet-mica schist as calculated from pseudosection and strain rate calculation (chapter 3.3 and 3.5.3), respectively. Black arrows indicate possible change of conditions to produce microstructures as observed in sample T8.6. The confining pressure used in the figure is not consistent with the pressure of deformation obtained from the Tromsø Nappe (e.g. Ravna & Roux, 2006), but the figure is adequate to demonstrate the effect of changing temperatures and strain rate on deformation mechanisms in quartz. Modified from Stipp et al. (2002a).

In sample T8.6 for example, chessboard patterns occur in coarse grained quartz in leucosomes, overprinted by BLG along grain boundaries. As shown in figure 4.2-1, such an overprint may be produced by (1) an increase in strain rate, (2) a decrease in temperature, or (3) a combination of both. As the strain rates needed to produce such an overprint are rarely seen in naturally deformed rocks (eg. Stipp et al. 2002a; b), it is more likely that this overprint was largely caused by a decrease in temperature. Applying this assumption, figure 4.4-1 indicates that the temperature must have decreased from more than ~700°C to less than 400°C during deformation. The chessboard patterns will be discussed further in chapter 4.4.2.

Based on the dominating recrystallization mechanisms, the overall temperature of deformation of the preserved microstructures seems to be in the range between SGR and

GBM, i.e. ~500°C. This temperature, together with the inferred pressure conditions fits well with the wide distribution of amphibolite facies rocks in the area.

When considering the dominant recrystallization mechanism with respect to the distance from the tectonic contact from which the samples were collected, it is difficult to see any systematic differences or relationship. This indicates that the Tromsø Nappe as a whole was subjected to high temperatures during deformation. This fits well with the previous understanding of the Caledonian nappes, where metamorphism is common throughout the nappes and not only limited to the nappe contacts (chapter 1.4).

4.4.2 C-AXIS PREFERRED ORIENTATION

CPO patterns as presented in chapter 3.6 are interpreted to be caused by the glide of dislocations along crystallographic controlled slip-systems (Trépied et al., 1980) according to fig. 4.4-2 (Lister and Dornsiepen, 1982; Schmid and Casey, 1986; Blumenfeld et al., 1986; Mainprice et al., 1986; Stipp et al., 2002b).

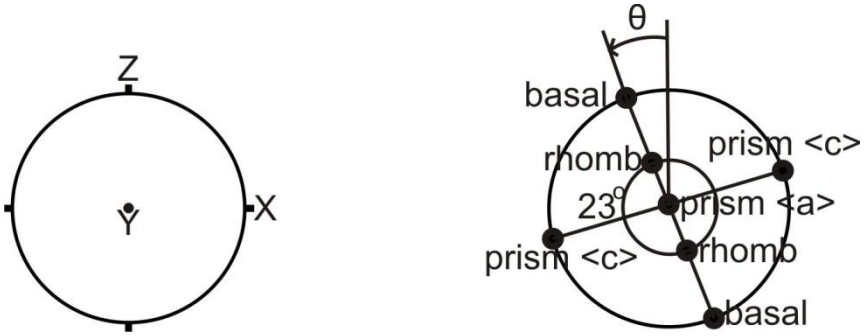

Figure 4.4-2: Left: A diagram of the upper hemisphere pole figure and the orientation of its reference directions. X is parallel to lineation, Y is parallel to foliation, but perpendicular to foliation and Z is perpendicular to foliation. Right: A diagram of the upper hemisphere pole figure with the interpreted areas of which different slip systems produce CPO maxima. The angle θ increases with increased sinistral shear strain (Lister and Dornsiepen, 1982; Blumenfeld et al., 1986; Schmid and Casey, 1986; Mainprice et al., 1986; Stipp et al., 2002b) Figure modified from Heilbronner & Tullis (2006).

The pole figures (fig. 3.6-2) show that basal <a>-, rhomb <a>-, prism <a>- and prism [c]-slip have been activated during deformation of the quartz vein. The apparent rotation, θ, of the basal <a>- and prism [c] pole figure clusters are indicative of a sinistral shear sense (Simpson & Schmid, 1983).

The activation of the different slip systems is partly temperature dependent (e.g. Lister and Dornsiepen, 1982; Blumenfeld et al., 1986; Mainprice et al., 1986; Stipp et al., 2002b; Heilbronner & Tullis, 2006). At low-grade conditions (300-400°C) dislocation creep along the basal- and rhomb- planes is common. At medium temperatures (400-500°C), prism <a>

slip starts to dominate. Above 600-700°C, prism [c]-slip gets activated and a combination of basal <a>- and prism [c]-slip produce an approximately square subgrain structure, known as chessboard patterns (Kruhl, 1996; 1998). Chessboard patterns are observed in coarse grained leucosomes in the amphibolite and garnet-mica schists of the Tromsø Nappe. In the quartz vein subjected to the CIP analysis, CPOs indicate prism [c]-slip in more or less all pole figures. Here, the chessboard pattern has been completely recrystallized (with the exception of a few larger grains) so that the evidence of the former presence of chessboard patterns is exclusively preserved by prism [c]- and basal <a>-slip indicative CPOs of the recrystallized quartz.

Prism [c]-slip has previously been reported in the literature from (1) granulite facies terrains with either orogenic-, or syndeformational contact metamorphic origin and (2) in subsolidus deformation of granites. Independent of the deformation conditions, the presence of prism [c]- and basal <a>-slip from the same microstructure has been restricted to large, submagmatic grains (e.g. Gapais & Barbarin, 1986; Mainprice et al, 1986; Kruhl, 1996; 1998; Zibra et al. 2009). However, to this author's knowledge, prism [c]- and basal <a>-slip pole figures from the same microstructure in completely recrystallized quartz has not been previously documented.

To reach such complete recrystallization with chessboard pattern-indicative CPOs, the metamorphic conditions must have been favorable for prism [c]-slip for an adequate amount of time and strain. According to Kruhl (1996; 1998), this indicates that the α-β quartz transition was reached. The P-T conditions needed to reach the α-β quartz transition at the obtained pressure conditions of the Scandian deformation for the Tromsø Nappe lies well within the granulite facies stability field (fig. 4.4-3). As the Tromsø Nappe shows a pervasive amphibolite overprint, it is contradictory to the assumption that prism [c]-slip was activated and held activated at the α-β quartz transition as the microstructures indicate. The evidence of residual clinopyroxene found in amphibolite of the Tromsø Nappe could be traces of such a granulite facies event. Still, if Kruhl (1996; 1998) is correct, one should expect a more widespread distribution of granulites.

Also, if assuming that the onset of chessboard patterns is controlled by the α-β quartz transition, the presence of prism [c]-slip does not correlate with the minimum P-T condition obtained in chapter 3.3. This may indicate either that the α-β quartz transition was reached at a different mineral assemblage equilibrium, or that the actual P-T conditions were not at the

minimum P-T condition, but higher. As seen in figure 4.4-3, the α-β quartz transition does truncate the stability field of the applied mineral assemblage, indicating that if prism [c]-slip was activated according to Kruhl (1996; 1998) in association with the inferred equilibrium mineral assemblage, the temperature may have been peaking at >800°C.

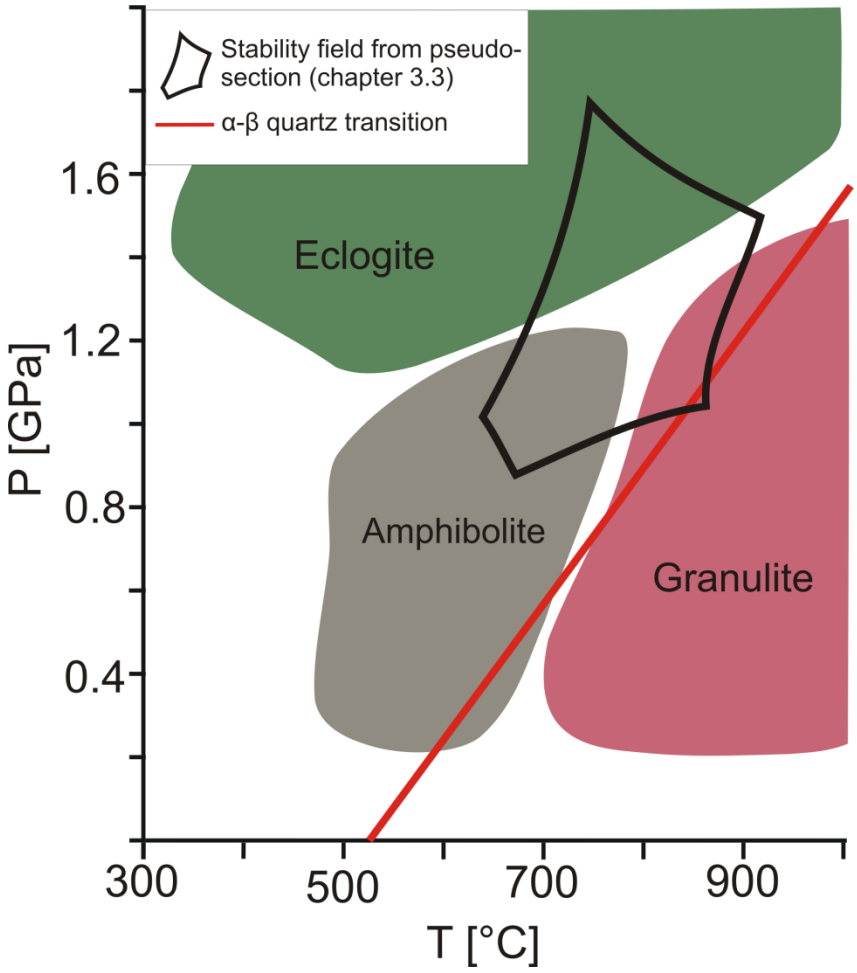

Figure 4.4-3: Overview of fields of metamorphic facies with the field of stability for the Scandian prograde mineral assemblage from the pseudosection analysis given in chapter 3.3. The field has been recalculated to show its topological extent at higher P-T conditions using Perple_X 07 [1]. The α-β quartz transition is marked.

Based on the poor correlation of temperatures expected according to Kruhl (1996; 1998) and the obtained P-T conditions favorable for α quartz obtained here and in previous work from the Tromsø Nappe (e. g. Krogh et al., 1990; Stevenson, 2005; 2006; Ravna & Roux, 2006, see fig. 4.5-1), it is suggested that prism [c]-slip may be active under amphibolite facies conditions, regardless of wether the α-β quartz transition was reached. The evidence of partial melting during deformation (ch 3.4) is more supportive of Mainprice et al. (1986) which states that the onset of prism [c]-slip is controlled by the occurence of partial melting and wet conditions rather than the α-β quartz transition.

Structural observations indicate that the Tromsø Nappe was subjected to two deformation events, D^T_1 and D^T_2. The thin section that was subjected to the CIP analysis is cut along the lineation connected to the D^T_2. A certain interference of these two deformation events should be expected and could complicate the CPO-pattern. As the orientation of foliation connected to the two deformation events are identical, the pole figures can only be modified by the rotation of c-axis pole figures around the Z-axis. Any rotation of the pole figures around this axis will produce either prism [c]-slip indicative CPOs or theoretically unlike pole figures. The apparent prism [c]-slip is therefore concluded to be genuine. Still, it is speculated that any geometric effect of a ~90° rotation of principal axes of strain during deformation may cause the activation of slip systems that under normal circumstances would not have been activated. For example, D^T_1 may have formed a quartz fabric with grains suitably oriented for prism [c]-slip during D^T_2. Such possible geometric effects are largely hypothetical and will not be pursued here.

4.4.3 Grain size in connection with flow stress and strain rate

From both the area- and volumetric grain size distribution (ch. 3.6.2) it is evident that prism <a> slip produces a grain size that is finer than prism [c]- and basal <a>-slip. As the applied flow stress is directly tied to the recrystallized grain size through paleopiezometers (chapter 2.5 and 3.7), it is evident that grains with prism <a>-slip indicative CPO have been subjected to higher flow stresses (~30 MPa, compared to ~25 MPa for prism [c]- and basal <a>-slip, see table 3.7-2) and probably strain rate during deformation.

This may be explained by interpreting the prism <a>-slip as an overprint. However, the grains are clearly a part of the same microstructure regardless of which slip system indicative CPO the grains obtain. Thus, it is concluded that the prism <a>-slip is not an overprint.

A more likely explanation is that the properties of prism <a>-slip at the given conditions are slightly different than those of the other slip systems, requiring a higher flow stress at the given conditions to deform, i.e. a grain with the CPO suitable for prism <a> is more resistant towards deformation. Similar investigations on both experimentally- and naturally deformed quartzites have, in contrary, concluded that prism <a> slip produce coarser grain sizes than basal <a>-slip during dynamic recrystallization and constant temperatures (Heilbronner & Tullis, 2006; Mancktelow, 1987; Knipe and Law, 1986). The high-temperature prism [c]-slip is not reported in any of these papers and may be a key to understanding the conflicting results. It is suggested that the properties of glide along slip planes are controlled by a

complex balance between different parameter such as e.g. the starting grain size and water content during deformation.

The strain rates calculated in chapter 3.7 are relatively high for naturally deformed rocks (e.g. Stipp et al., 2002a), but still probable when considering that the nappe was subjected to a late- to post Scandian, rapid uplift (Ravna & Roux, 2006).

4.5 TECTONOMETAMORPHIC EVOLUTION

Applying the observations and assumptions mentioned above with previous work, the following tectonometamorphic evolution of the area of investigation is proposed.

The metamorphic elements have been divided into the following events:

M_1 - Eclogite facies metamorphism in the Tromsø Nappe, producing eclogites and high pressure minerals such as rutile.

M_1 is interpreted to be associated with the Taconian phase (Krogh et al., 1990; Corfu et al., 2003; Ravna & Roux, 2006; Ravna et al., 2006; Stevenson, 2005; 2006).

The SMC was subjected to extensive partial melting at ~1.0 GPa and ~900°C (Selbekk & Skjerlie, 2002) dated to 456 ± 4 Ma (Selbekk et al., 2000). Stevenson (2005; 2006) describes an event of partial melting in the Tromsø Nappe at 2.0-2.2 GPa and 762-844°C dated to 450.3 ± 0.9 Ma (Corfu et al., 2003). Based on the similarities in ages, both events are interpreted to be connected to the Taconian phase. Still, the differences in P-T conditions and age indicate that the two nappes were clearly separated in space and that their associated events of partial melting were separated in time. This, together with the observation that none of the leucosomes within the SMC are observed to cut the contact towards the Tromsø Nappe, leads to the conclusion that these events must have occurred prior to the juxtaposition of the two nappes.

M_2 - Scandian prograde upper amphibolite facies metamorphism with an obtained minimum P-T condition at 0.9 GPa and 680°C. The event was followed by partial melting and uplift in the Tromsø Nappe, which produced retrograde-indicative symplectites and overgrowth of M_1 minerals in addition to melt indicative pseudomorphs. The partial melting is believed to correspond with the second event of partial melting and uplift described by Stevenson (2005; 2006) on the basis that the obtained pressures and temperatures coincides well with those of this thesis (fig. 4.5-

1). M_2 is interpreted to be result of the Scandian phase (Krogh et al., 1990; Corfu et al., 2003; Ravna & Roux, 2006; Stevenson 2005; 2006). The movement is suggested to have been continuous during a considerable amount of cooling and uplift on the basis of the wide occurrences of different recrystallization microstructures and active slip-systems in quartz. D^T_1 and D^T_2 are interpreted to date from this metamorphic event indicating a change in movement direction during uplift. As the same indications of change in movement direction are found in the top ~15 m of the SMC, the change in movement direction is interpreted to have occurred after the two nappes came into contact. The D_3 - structures are interpreted to be late elements of the juxtapositioning.

M_3 - Greenschist facies, late stage movement and fluid infiltration along the tectonic contact affecting only rocks in the immediate vicinity. M_3 is interpreted to be the last recorded traces of movement along the contact during post-M_2 further cooling and uplift.

Based on previous work and results from this thesis a possible P-T path for the Tromsø Nappe has been obtained (fig 4.5-1). The data gathered from the SMC in this thesis is insufficient for producing a similar P-T path.

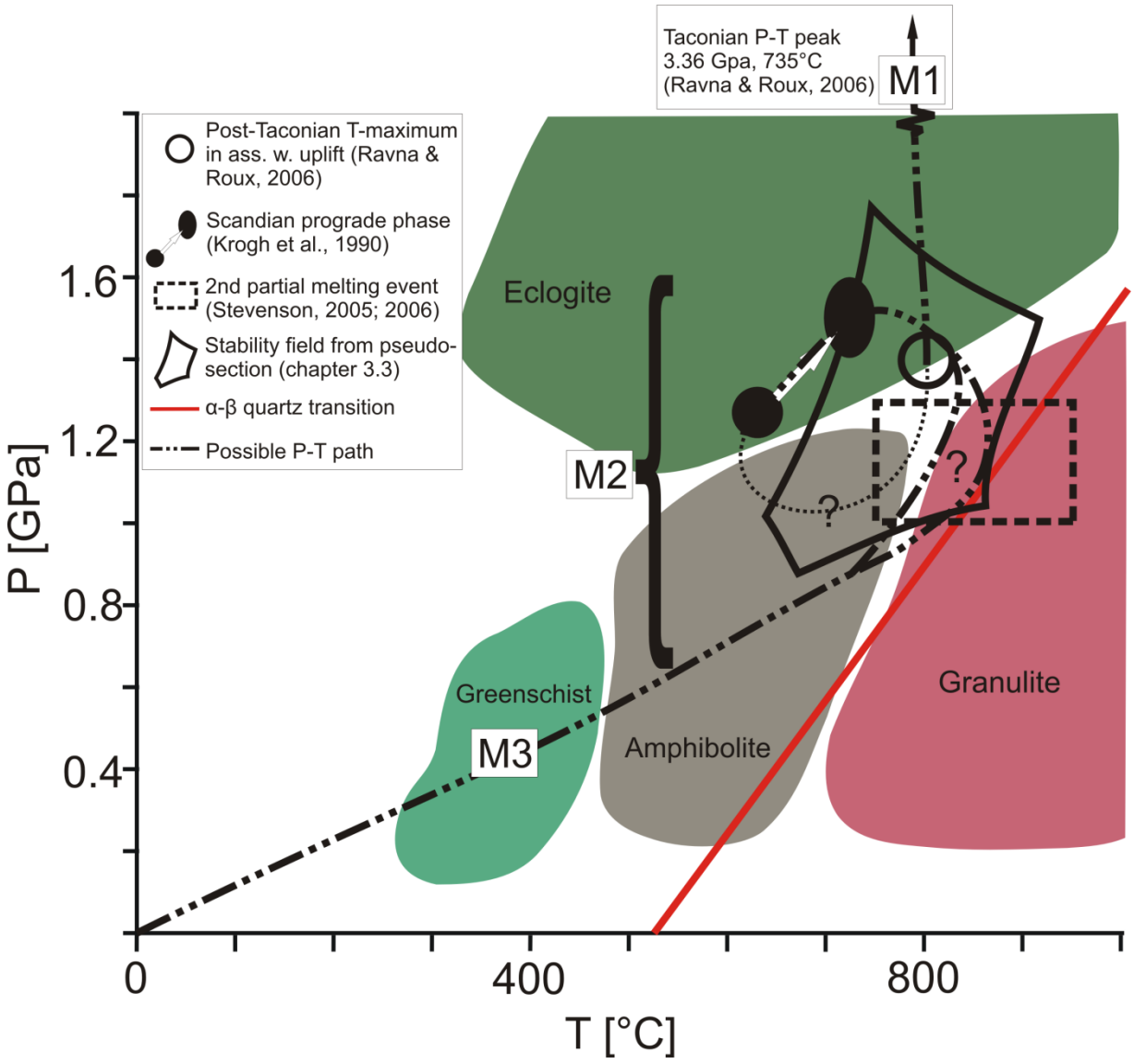

Figure 4.5-1: Overview of fields of metamorphic facies with plotted P-T estimates in the Tromsø Nappe based on previous work and results from this thesis. The field of stability for the Scandian prograde mineral assemblage from the pseudosection analysis given in chapter 3.3 has been recalculated to show its topological extent at higher P-T conditions using Perple_X 07 [1]. A possible P-T path is indicated. The major tectonometamorphic events discussed in this chapter (M_1 - M_3) are marked.

5. CONCLUSIONS

Through the investigations done in this thesis, the following conclusions are made:

- A new unit within the SMC is identified. The non-layered amphibolitic melanosome inhabits a "salt and pepper"-texture and is suggested to be of a magmatic origin.
- The cpx-garnet amphibolite, which constitutes the main parts of Langlitind, is concluded to be a retro-eclogite based on retrograde symplectites after omphacite.
- Analysis through pseudosections obtained a minimum P-T condition for a Scandian prograde mineral assemblage at 0.9 MPa and 680°C.
- A wide variety of recrystallization microstructures in quartz indicate that the deformation took place over a large span of temperatures, possibly from more than 700°C to less than 400°C.
- No relation between recrystallization mechanism in quartz and the distance from the tectonic contact is found. This indicates that the Tromsø Nappe as a whole was subjected to high temperatures and strain.
- The Tromsø nappe underwent partial melting during uplift in a late stage of the Scandian phase. The amount of melt at the minimum P-T condition obtained from the pseudosections is calculated to 13 vol%.
- The presence of chessboard subgrain patterns in quartz indicates that prism [c]-slip was activated during deformation. Because of the occurrence of completely recrystallized quartz with chessboard-indicative CPOs in amphibolite facies rocks, it is suggested that the activation of prism [c]-slip may not be controlled by the α-β quartz transition, but by the presence of partial melting and wet conditions during deformation (Mainprice et al., 1986).
- The bulk strain rate of the garnet-mica schist of the Tromsø Nappe is calculated to be in the order of 10^{-11} s^{-1} during higher temperatures of deformation.
- The SMC was subjected to a high degree of partial melting in connection with the Taconian phase. The later juxtaposition of the two nappes influenced only the top 10-15 meters of the SMC.
- The Tromsø Nappe was subjected to the following metamorphic events:
  (1) Eclogite facies metamorphism as a part of the Taconian phase.
  (2) A prograde metamorphic event interpreted to be connected to the Scandian phase, followed by partial melting. The nappe translation and associated deformation is

suggested to have been continuous during a considerable amount of cooling and uplift. Shear sense indicator suggest that a change in movement direction from either SW or NE to SSE occurred after the Tromsø Nappe and the Nakkedal Nappe Complex came into contact.

(3) Greenschist facies Ca-rich dykes are interpreted as fluid infiltration as a part of the last recorded traces of movement along the tectonic contact during further cooling and uplift.

6. REFERENCES

Andréasson, P.G., Svenningsen, O.M., Albrecht, L., 1998. Dawn of Phanerozoic orogeny in the North Atlantic tract: evidence from the Seve–Kalak superterrane, Scandinavian Caledonides. Geol. Fören. Stockh. Förh. 120, 159–172.

Andersen, T.B., 1993. The role of extensional tectonics in the Caledonides of south Norway: Discussion. Journal of Structural Geology **15**. p. 1379–1380.

Andresen, A., Fareth, E., Bergh, S., Kristensen, S. E., Krogh, E.J., 1985. Review of the Caledonian lithotectonic units in Troms, North Norway. The Caledonian Orogen – Scandinavia and Related Areas. Pp. 569-578. Wiley & Sons, Chichester.

Andresen, A., Steltenpohl, M. G., 1994. Evidence for ophiolite obduction, terrane accreation and polyorogenic evolution of the north Scandinavian Caledonides. Tectonophysics, v. 231, p. 59-70.

Barker, A.J., 1989. Metamorphic evolution of the Caledonian nappes of north central Scandinavia. In: R.A. Gayer (Editor), The Caledonide Geology of Scandinavia, Graham and Trotman, London, pp. 193-204.

Barrett S. D., 2002. Software for scanning microscopy. Proc. Roy. Microsc. Soc., v.37, pp.167-174.

Bergh, S. & Andresen, A., 1985. Tectonometamorphic Evolution of the Allochthonous Caledonian Rocks between Malangen and Balsfjord, Troms, North Norway. Norges geologiske undersøkelse Bulletin. 401, 1-34.

Bergh S., G., Maher, H., D., & Braathen, A., 2000. Tertiary divergent thrust directions from partitioned transpression, Brøggerhalvøya, Spitsbergen. Norsk Geologisk Tidsskrift, Vol. 80-2, p.63-81.

Berthé, D., Choukroune, P & Jegouzo, P., 1979. Orthogneiss, mylonite and non-coaxial deformation of granites: The example of the South Armorican Shear Zone. Journal of Structural Geology 1, p. 31-42.

Binns, R., 1978. Caledonian nappe correlation and orogenic history in Scandinavia north of lat 67°N. Geological Society of America, Bulletin 89.

Binns, R.E. & Gayer, R. 1980. Silurian or Upper Ordovician fossils at Guolasjávri Troms, Norway. Nature 284, 53–55.

Bjørlykke, A. & Olaussen, S., 1981. Silurian sediments, volcanics and mineral deposits in the Sagelvvatn area, Troms, Northern Norway. Norges geologiske undersøkelse. 365, 39-54.

Blumenfeld P, Mainprice D, Bouchez J. L., 1986. C-slip in quartz from subsolidus deformed granite. Tectonophysics 127:97–115.

Bucher, K. & Frey, M., 1994. Petrogenesis of Metamorphic Rocks. 6th ed. Springer-Verlag: Germany.

Broks, T. M., 1985. Berggrunnsgeologiske undersøkelser innen Tromsø dekkekompleks i området Tromsdalen-Ramfjord-Breivikeidet, Troms. Unpubl. Cand. scient. oppgave, Universitetet i Tromsø, 104 s.

Brueckner, H.K., Medaris, L.G., 2000. A general model for the intrusion and evolution of 'mantle' garnet peridotites in highpressure and ultra-high-pressure metamorphic terranes. Metamorph. Geol. 18, 123–133.

Cladouhos, T. T., 1999. Shape preferred orientations of survivor grains in fault gouge. Journal of Structural Geology 21, 419–436.

Connolly J. A. D., 2005. Computation of phase equilibria by linear programming: a tool for geodynamic modeling and its application to subduction zone decarbonation. Earth Planet. Sci. Lett. 236, p. 524-541.

Corfu, F., Roberts, R. J., Torsvik, T. H., Ashwal, L. D. and Ramsay, D. M., 2007. Peri-Gondwanan elements in the Caleonian Nappes of Finnmark, Northern Norway: implications for the paleogeographic framework the Scandinavian Caledonides, Am. J. Sci. 307 (Part 2) (2007), pp. 434–458.

Corfu, F., Ravna, E. J. K. & Kullerud, K., 2003. A Late Ordovician U-Pb age for the Tromsø Nappe eclogites, Uppermost Allochton of the Scandinavian Caledonides. Contributions to Mineralogy and Petrology. 145, 502-513.

Cuthbert, S., Carswell, D. A., Krogh-Ravna E. J. and Wain, A., 2000. Eclogites and eclogites in the Western Gneiss Region, Norwegian Caledonides, Lithos 52, pp. 165–195.

Dallmeyer, R. D. & Andresen, A., 1992. Polyphase tectonothermal evolution of exotic Caledonian nappes in Troms, Norway: Evidence from 40Ar/39Ar mineral ages. Lithos. 29, 19-42.

Eide, E. A. & Lardeaux, J.-M., 2002. A relict blueschist in meta-ophiolite from the central Norwegian Caledonides - discovery and consequences. Lithos. 60, 1-19.

Gapais, D. & Barbarin, B., 1986. Quartz fabric transition in a cooling syntectonic granite (Hermitage Massif, France). Tectonophysics 125. 357-370.

Gee, D.G., 1975. A tectonic model for the central part of the Scandinavian Caledonides. Am. J. Sci. 275A, 468– 515.

Gleason, G.C., Tullis, J., 1995. A flow law for dislocation creep of quartz aggregates determined with the molten salt cell. Tectonophysics 247, 1–23.

Heilbronner, R., 2000a. Optical Orientation Imaging. In: Stress, Strain and Structure, A volume in honour of W. D. Means. Eds: M.W. Jessell and J.L.Urai. Volume 2, Journal of the Virtual Explorer.

Heilbronner, R., 2000b. Automatic grain boundary detection and grain size analysis using polarization micrographs or orientation images. Journal of Structural Geology 22, p. 969-981.

Heilbronner, R. & Tullis, J., 2006. Evolution of c axis pole figures and grain size during dynamic recrystallization: Results from experimentally sheared quartzite. Journal of Geophysical Reasearch, Vol. 111.

Holland, T. J. B. & Powell, R., 1998. An internally-consistent thermodynamic dataset for phases of petrological interest. Journal of Metamorphic Geology 16, p. 309-344.

Knipe, R. J., and Law, R. D., 1987. The influence of crystallographic orientation and grain boundary migration on microstructural and textural evolution in an SC mylonite, Tect

Kohlstedt, D. L., Evans, B. & Mackwell, S. J., 1995. Strength of the lithosphere: Constraints imposed by laboratory experiments. J. Geophys. Res., Vol. 100, 17,587-17,602.

Krogh, E. J., Andresen, A., Bryhni, I., Broks, T. M. & Kristensen, S. E., 1990. Eclogites and polyphase P-T cycling in the Caledonian Uppermost Allochton in Troms, northern Norway. Journal of Metamorphic Geology. 8, 289-309.

Kruhl J. H., 1996. Prism- and basal-plane parallel subgrain boundaries in quartz: a microstructural geothermobarometer. J. Metamorphic Geol., 14: 581-589.

Kruhl J. H., 1998. Reply: Prism- and basal-plane parallel subgrain boundaries in quartz: a microstructural geothermobarometer. J. Metamorphic Geol., 16: 141-146.

Landmark, K., 1973. Beskrivelse til de geologiske kart "Tromsø" og "Målselv". II. Kaledonske bergarter. Tromsø Museum Skrifter. 15, 1-263.

Landmark, K., 1951. Dykes of oligoclase in amphibolite near Tromsø. Acta Borealia A. Scientia, 1.

Law, R.D., 1990. Crystallographic fabrics: a selective review of their applications to research in structural geology. In: R.J. Knipe and E.H. Rutter, Editors, Deformation Mechanisms, Rheology and Tectonics, Geological Society of London, Special Publication vol. 54 (1990), pp. 819–834.

Lindahl, I., Stevens, B. P. J. & Zwaan, K. B., 2005. The geology of the Váddás area, Troms. A key to our understanding of the Upper Allochthon in the Caledonides of northern Norway. Norges geologiske undersøkelse Bulletin. 445, 5-43.

Lindstrøm, M. & Andresen, A., 1992. Early Caledonian high-grade metamorphism within exotic terranes of the Troms Caledonides? Norsk Geologisk Tidsskrift. 72(4), 375-379.

Lister, G. S. & Dornsiepen, U. F., 1982. Fabric transitions in the Saxony granulite terrain. J. Structural Geology 4, 81-92.

Lister, G. S. & Snoke, A. W., 1984. S-C-mylonites. Journal of Structural Geology 6. P. 617-638.

Lucassen, F., Franz, G., Dulski, P., Romer, R. L., & Rhede, D., 2010. Element and Sr isotope signatures of titanite as indicator of variable fluid composition in hydrated eclogite. Lithos, 121 (2011) p. 12-24.

Mancktelow, N. S., 1987. Quartz textures form the Simplon Fault Zone, southwest Switzerland and north Italy, Tectonophysics, 135, 133– 153.

Marchildon, N. & Brown, M., 2002. Grain-scale melt distribution in two contact aureole rocks: implications for controls on melt localization and deformation. Journal of Metamorphic Geology 20, p. 381-396.

Mainprice, D., Bouchez, J. L., Blumenfeld, P. & Tubià, J. M., 1986. Dominant <c>-slip in naturally deformed quartz: implications for dramatic plastic softening at high temperature. Geology 14, 819-822.

Medaris, L.G., 2000. Garnet peridotites in Eurasian high-pressure and ultrahigh-pressure terranes: a discovery of origins and thermal histories. In: Ernst, W.G., Liou, J.G. (Eds.), UHP Metamorphism and Geodynamics in Collision Type Orogenic Belts. Boulder, CO: Geol. Soc. Am., p. 57–73.

Menegon, L., Pennacchioni, G., Heilbronner, R., Pittarello, L., 2008. Evolution of quartz microstructure and c-axis crystallographic preferred orientation within ductilely deformed granitoids (Arolla unit, Western Alps). Journal of Structural Geology 30, 1332 – 1347.

Mikkelsen, O. A., 2011. Kontakten mellom Tromsødekket og Skattøra Migmatitt Kompleks (Nakkedalsdekket) NØ for Tromsdalstinden: Kinematiske indikatorer og metamorfose. Mastergradsoppgave, IG, Universitetet i Tromsø.

Okudaira, T., Takeshita, T. & Toriumi, M., 1998. Prism-and basal-plane parallel subgrain boundaries in quartz: a microstructural geothermobarometer. Journal of Metamorphic Geology 16, p. 141.

Oliver, G. J. H. & Krogh, T., 1995. U-Pb zircon age of 469 +- 5 Ma for the Kjosen unit of the Lyngen magmatic complex, northern Norway. Norges geologiske undersøkelse Bulletin. 428, 27-33.

Panozzo, R., 1983. Two-dimensional analysis of shape-fabric using projections of digitized lines in a plane. Tectonophysics 95, 279e294.

Panozzo, R., 1984. Two-dimensional strain from the orientation of lines in a plane. Journal of Structural Geology 6 (1/2), 215e221.

Panozzo Heilbronner, R. & Pauli, C., 1993. Integrated spatial and orientation analysis of quartz c-axes by computer-aided microscopy,Journal of Structural Geology 15, pp. 369–382.

Passchier, C. W. & Trouw, R. A. J. 2006. Microtectonics,. 2nd ed. Elsevier: Amsterdam

Pettersen, K., 1868. Geologiske Undersøgelser i Tromsø Omegn, i DKNVS Skr. i 19. Aarh., bd. 5, hf. 2, s. 113–240.

Pettersen, K., 1873. Geologiske Undersøgelser i Tromsø Amt, del 2–4, ibid., bd. 6, 1870, s. 39–165 og bd. 7. 1873, s. 97–176 og 257–444

Poirier, J.-P., 1985. Creep of Crystals. Cambridge University Press, Cambridge, 260 pp.

Ramsay, J. G., 1962. Interference Patterns Produced by the Superposition of Folds of Similar Type. The Journal of Geology Vol. 70, No. 4, p. 466-481.

Ravna, E. J. K., Kullerud, K., Davidsen, B. & Selbekk, R. S., 2008. Meta-silicocarbonatite or metasomatic calc silicate marble? REE-rich carbonate-rich rocks from the HP / UHP Tromsø Nappe. IGC 2008, 6 – 14th August.

Ravna, E. J. K. & Roux, M. R. M., 2006. Metamorphic evolution of the Tonsvika eclogite, Tromso Nappe - Evidence for a new UHPM Province in the Scandinavian Caledonides. International geology review. 48(10), 861-881.

Ravna, E. J. K., Kullerud, K. & Ellingsen, E., 2006. Prograde garnet-bearing ultramafic rocks from the Tromsø Nappe, northern Scandinavian Caledonides. Lithos. 92, 336-356.

Ravna, E. J. K., MacKenzie, J. R., Kullerud, K., Stunitz, H., Bergh, S. & Heilbronner, R., 2007. Prograde and retrograde evolution of ultrahigh-pressure rocks in the Tromsø Nappe - continuous shear over a broad P-T range? Poster presentert ved Vinterkonferansen i Stavanger, NGF.

Rindstad, L, 1992. Petrografiske, metamorfe og geokjemiske undersøkelser av Skattøragneisen på Tromsøya med særlig vekt på de leucosome gangenes opprinnelse. Cand. Scient. IBG, University of Tromsø.

Roberts, D., 2003. The Scandinavian Caledonides: event chronology, palaeogeographic settings and likely modern analogues. Tectonophysics 365, p. 283-299

Roberts, D., Gee, D.G., 1985. An introduction to the structure of the Scandinavian Caledonides. In: Gee, D.G., Sturt, B.A. (Eds.), The Caledonide Orogen—Scandinavia and Related Areas. Wiley, Chichester, pp. 55– 68.

Roberts, D., Nordgulen, Ø. & Melezhik, V.A. 2007. The Uppermost Allochthon in the Scandinavian Caledonides: from a Laurentian ancestry through Taconian orogeny to Scandian crustal growth on Baltica. Geological Society of America, Memoir 200.

Rutter, E.H., Brodie, K.H., 2004. Experimental grain size-sensitive flow of hotpressed Brazilian quartz aggregates. Journal of Structural Geology 26, 2011–2023.

Sawyer, E. W., 2001. Melt segregation in the continental crust: distribution and movement of melt in anatectic rocks. Journal of Metamorphic Geology 10, p. 291-309.

Schmid, S. M. & Casey, M., 1986. Complete fabric analysis of some commonly observed quartz [c]-axis patterns. In: B.E. Hobbs and H.C. Heard, Editors, Mineral and Rock Deformation: Laboratory Studies, American Geophysical Union, Geophysical Monograph vol. 36 (1986), pp. 263–286.

Selbekk, R. S., Furnes, H., Pedersen, R. B. & Skjerlie, K. P., 1998. Contrasting tonalite genesis in the Lyngen magmatic complex, north Norwegian Caledonides. Lithos. 42, 243-268.

Selbekk, R.S., Skjerlie, K.P., 2002. Petrogenesis of the anorthosite dyke swarm of Tromsø, North Norway: experimental evidence for hydrous anatexis of an alkaline mafic complex. J. Petrol. 43, 943–962.

Selbekk, R. S., Skjerlie, K. P. & Pedersen, R. B., 2000. Generation of anorthositic magma by H2O-fluxed anatexis of silica-undersaturated gabbro: an example from the north Norwegian Caledonides. Geological Magazine. 137(6), 609-621.

Shelley, D., 1993. Igneous and Metamorphic Rocks Under the Microscope. Chapman & Hall. London.

Shimizu, I., 2008. Theories and applicability of grain size piezometers: The role of dynamic recrystallization mechanisms. Journal of Structural Geology 30, p. 899-917.

Simpson, C & Schmid, S. M., 1983. An evaluation of criteria to determine the sense of movement in sheared rocks, Bulletin of the Geological Society of America 94 (1983), pp. 1281–1288

Stevenson, J. A., 2005. High pressure partial melting of eclogite and garnet amphibolites rocks during decompression and heating, Tromso Nappe, Norway: EOS (Transactions of the American Geophysical Union), v. 85 (47), Abstract T23C-03.

Stevenson, J. A., 2006. Partial melting of eclogite, Tromsø, Norway. Ph.D., Yale University, 323 s.

Stipp, M., Stünitz, H., Heilbronner, R. & Schmid, S. M., 2002a: Dynamic Recrystallization of quartz: Correlation between Natural and Experimental Conditions. In: S. de Meer, M. R. Drury, J. H. P. de Bresser & G. M. Pennock: Deformation Mechanisms, Rheology and Tectonics: Current Status and Future Perspectives. - Geological Society, London, Special Publications 200, 171-190.

Stipp, M. Stünitz, H. Heilbronner, R. & Schmid, S.M., 2002b: The eastern Tonale fault zone: a "natural laboratory" for crystal plastic deformation of quartz over a temperature range from 250 - 700°C. J. Struct. Geol. 24, p. 1861-1884.

Stipp, M. & Tullis, J., 2003. The recrystallized grain size piezometer for quartz. Geophysical Research Letters, Vol. 30, No. 21, 2088.

Stünitz, H., 1989. Partitioning of metamorphism and deformation in the boundary region of the "seconda zona diorite-kinzigitica", Sesia zone, Western Alps, PhD Thesis, ETH, Zurich.

Tikoff, B. & Teyssier, C., 1994. Strain modeling of displacement-field partitioning in transpressional orogens. Journal of Structural Geology Vol. 16, Issue 16, p. 1575-1588.

Torsvik, T.H., Smethurst, M., Meert, J., Van der Voo, R., McKerrow, W.S., Brazier, M., Sturt, B.A. & Walderhaug, H., 1996. Continental break-up and collision in the Neo-proterozoic and Palaeozoic—a tale of Baltica and Laurentia. Earth-Sci. Rev. 40, 229– 258.

Trépied, L., Doukhan, J. C. & Paquet, J., 1980. Subgrain boundaries in quartz: Theoretical analysis and microscopic observations. Physics and Chemistry of Minerals, v.5, p. 201-218.

Underwood, E.E., 1970. Quantitative Stereology. Addison-Wesley, London.

Vernon, R. H., 2004. A practical guide to Rock Microstructure. Cambridge University Press: New York.

Weertman, J., 1978. Creep laws for the mantle of the Earth. Philos. Trans. R. Soc. London A, 288, 9-26.

White, R. W., Powell, R. & Holland, T. J. B., 2001. Calculation of partial melting equilibria in the system Na2O–CaO–K2O–FeO–MgO–Al2O3–SiO2–H2O (NCKFMASH). Journal of Metamorphic Geology 19, p. 139-153.

Winter, J. D., 2001. An Introduction to Igneous and Metamorphic Petrology. Prentice Hall, New Jersey.

Zwaan, K.B. 2001. Berggrunnskart TROMSØ 1534 III, M 1:50.000. Norges geologiske undersøkelse.

Zwaan, K. B., Fareth, E. & Grogan, P. W., 1998. Geologisk kart over Norge, berggrunnskart TROMSØ, M 1:250.000. Norges geologiske undersøkelse.

APPENDIX

Results from the CIP analysis which has not been presented previously in this thesis. PAROR and SURFOR rose diagrams where not generated for site 03 and 05.